Investigation of the stimulatory effect of type 1 diabetes mellitus on the ion transport mechanisms of pancreatic ductal epithelial cells and a novel method for their study

Attila Ébert

Ph.D. thesis

Szeged

2024

Department of Pharmacology and Pharmacotherapy
Albert Szent-Györgyi Medical School, University of Szeged
Doctoral School of Theoretical Medicine

Investigation of the stimulatory effect of type 1 diabetes mellitus on the ion transport mechanisms of pancreatic ductal epithelial cells and a novel method for their study

Ph.D. thesis

Attila Ébert

Supervisor:

Viktória Venglovecz Ph.D., D.Sc.

Szeged, Hungary

2024

PUBLICATIONS

List of publications included in the thesis

I. **Ébert A**, Gál E, Tóth E, Szögi T, Hegyi P, Venglovecz V. Role of CFTR in diabetes-induced pancreatic ductal fluid and HCO_3^- secretion. *J Physiol*. 2024;602(6):1065-1083. doi:10.1113/JP285702.
IF: 5.5 (Q1)

II. Gál E, Dolenšek J, Stožer A, Pohorec V, **Ébert A**, Venglovecz V. A Novel in situ Approach to Studying Pancreatic Ducts in Mice. *Front Physiol*. 2019;10:938. doi:10.3389/fphys.2019.00938.
IF: 3.367 (Q2)

List of publications related to the subject of the thesis

III. Khan D., Kelsey R., Maheshwari R., Stone V.M., Hasib A., Manderson K. F., Watson A., Harkin S., Irwin N., Shaw J., McClenaghan N., Venglovecz V., **Ébert A**., Flodstrom T. M., White M., and Kelly C. Short-term CFTR inhibition reduces islet area in C57BL/6 mice. *Sci Rep*. 2019;9(1):11244. doi:10.1038/s41598-019-47745-w.
IF: 3.998 (Q1)

IV. Hegyi P.J., Soós A., Tóth E., **Ébert A**., Venglovecz V., Márta K., Mátrai P., Mikó A., Bajor J., Sarlós P., Vincze Á., Halász A., Izbéki F., Szepes Z., Czakó L., Kovács Gy., Papp M., Dubravcsik Zs., Varga M., Hamvas J., Németh B.C., Macarie M., Ince A.T., Bordin D.S., Dubtsova E.A., Kiryukova M.A., Khatkov I.E., Bideeva T., Mickevicius A., Ramírez-Maldonado E., Sallinen V., Erőss B., Pécsi D., Szentesi A., Párniczky A., Tiszlavicz L., Hegyi P. Evidence for diagnosis of early chronic pancreatitis after three episodes of acute pancreatitis: a cross-sectional multicentre international study with experimental animal model. *Sci Rep*. 2021;11(1):1367. doi:10.1038/s41598-020-80532-6.
IF: 4.997 (Q1)

V. Gál E, Dolensek J, Stozer A, Czako L, **Ébert A**, Venglovecz V. Mechanisms of post-pancreatitis diabetes mellitus and cystic fibrosis-related diabetes: A review of preclinical studies. Frontiers in Endocrinology 2021;12:715043. doi:10.3389/fendo.2021.715043.
IF: 6.055 (Q1)

VI. Marolt U, Paradiž Leitgeb E, Pohorec V, Lipovšek S, Venglovecz V, Gál E, **Ébert A**, Menyhárt I, Potrč S, Gosak M, Dolenšek J, Stožer A. Calcium imaging in intact mouse acinar cells in acute pancreas tissue slices. Rooman I, ed. *PLOS ONE*. 2022;17(6):e0268644. doi:10.1371/journal.pone.0268644.

IF: 3.7 (Q1)

Number of full publications: 6	**MTMT identifier: 10064633**
Cumulative impact factor: 27.617	

ABBREVIATIONS

AC – Adenylate cyclase

ANO – Anoctamin

AQP – Aquaporin

ATP – Adenosine triphosphate

BCECF-AM – 2,7-bis-(2-carboxyethyl)-5(6)-carboxyfluorescein acetoxymethyl ester

$[Ca^{2+}]_i$ – Intracellular calcium ion concentration

cAMP – Cyclic adenosine monophosphate

CCK – Cholecystokinin

CCKBR – Cholecystokinin B receptor

CFTR – Cystic fibrosis transmembrane conductance regulator

$[Cl^-]_i$ – Intracellular chloride ion concentration

DAPI – 4′,6-diamidino-2-phenylindole

DRA – downregulated in adenoma Cl^-/HCO_3^- exchanger

GAD – Glutamic acid decarboxylase

HCO_3^- – Bicarbonate

IRBIT – Inositol-1,4,5-triphosphate receptor binding protein released with inositol-1,4,5-triphosphate

IP_3R2 – Type 2 inositol 1,4,5-trisphosphate receptor

KO – Knock out

MQAE – N-(Ethoxycarbonylmethyl-6-Methoxyquinolinium Bromide) (MQAE)

$[Na^+]_i$ – Intracellular sodium ion concentration

NBCe1-B – electrogenic Na^+-HCO_3^- co-transporter variant B

NBD – Nucleotide binding domain

NHE – Na^+/H^+ exchanger

NHERF – Na^+/H^+ exchanger regulatory factor

NKCC – $Na^+/K^+/2Cl^-$ cotransporter

OSR1 – Oxidative stress responsive kinase 1

PDEC – Pancreatic ductal epithelial cell

PDZ – PSD95/Discs-large/ZO-1

PEI – Pancreatic exocrine insufficiency

PKA – Protein kinase A

SCT – Secretin

SCTR – Secretin receptor

Shank2 – SH3 and multiple ankyrin repeat domains 2

SLC4A4 – Solute carrier family 4 member 4 Na^+-HCO_3^- co-transporter (NBCe1-B)

SLC9A1 – Solute carrier family 9 member 1 Na^+/H^+ exchanger (NHE-1)

SLC26A3 – Solute carrier family 26 member 3 Cl^-/HCO_3^- exchanger (DRA)

SLC26A6 – Solute carrier family 26 member 6 Cl^-/HCO_3^- exchanger

SPAK – STE20/SPS1-related proline/alanine-rich kinase

STAS – Sulphate transporter and anti-sigma factor antagonist

T1DE – Type 1 diabetes mellitus endotype 1

T1DM – Type 1 diabetes mellitus

TMD – Transmembrane domain

TMEM16A – Transmembrane member 16A

TS – Tissue slice

VIP – Vasoactive intestinal peptide

VPAC1 – Vasoactive intestinal polypeptide receptor 1

WNK – With-no-lysine kinase 1

WT – Wild-type

TABLE OF CONTENTS

SUMMARY

Background: The prevalence and incidence of T1DM is steadily increasing world-wide. It is associated with reduced quality of life, severe long-term complications, and substantial costs for the health-care system and the individual. PEI is a complication affecting about 40% of T1DM patients, therefore, investigating the effect of T1DM on pancreatic exocrine functions is of crucial importance. Great amount of knowledge exists on how T1DM affects the endocrine and acinar cells of the pancreas, however, there is considerably less information regarding the effect of T1DM on pancreatic ductal epithelial cells (PDECs) despite their important protective function in the pancreas. Related studies have reported contradictory results and descriptions of the molecular mechanisms involved are few. Therefore, we investigated the effect of induced T1DM on ductal function and characterised the expression and activity of the key ion transporters of PDECs in mice. We also implemented the tissue slice technique to develop a new method for the structural and functional study of PDECs.

Methods: Diabetes was induced in wild-type and cystic fibrosis transmembrane conductance regulator (CFTR) knockout (KO) mice following i.p. administration of streptozotocin. Pancreatic ductal fluid secretion was measured both *in vivo* in anesthetised mice by cannulation of the common bile duct and *in vitro* in ductal segments. Ductal HCO_3^- secretion and the effect of high extracellular glucose was determined using microfluorimetry. The expression of ion transporters was measured by quantitative reverse transcription PCR and fluorescence immunolabelling. Transmission electron microscopy was used for the morphological characterization of the pancreas. Plasma secretin and cholecystokinin levels were measured by ELISA. Pancreatic tissue slices were prepared by retrograde injection of low-melting point agarose into the main pancreatic duct, followed by preparation of agarose-embedded tissue blocks and microtomy. The structural integrity of ducts within slices was assessed by Giemsa staining and fluorescence immunolabelling of CFTR.

Results: Ductal fluid and HCO_3^- secretion was increased in mice with T1DM. The activity and expression of CFTR was also significantly increased in diabetes, as well as the expression of the Na^+/H^+ exchanger-1 (NHE-1), anoctamine-1, and aquaporin-1. Acute or chronic glucose treatment did not affect HCO_3^- secretion, but increased alkalizing transporter activity. The absence of CFTR significantly reduced HCO_3^- secretion in both control and diabetic CFTR KO animals. Plasma levels of secretin and cholecystokinin were unchanged, but the expression of

secretin receptors was significantly upregulated in mice with T1DM. Immunolabelling of CFTR and Giemsa staining showed preserved structure and physiological conditions within pancreatic tissue slices, as well as appropriate filling of the ductal tree.

Conclusion: Diabetes increases fluid and HCO_3^- secretion in pancreatic ductal cells, which is associated with (i) the increased function of ion and water transporters, particularly CFTR, (ii) enhanced sensitivity of ductal cells to secretin, and (iii) glucose-stimulated NHE-1 activity. We also conclude that the tissue slice technique is suitable for the functional and morphological study of PDECs and their homotypical and heterotypical interactions.

1. INTRODUCTION

1.1. The pancreas

1.1.1. Anatomy of the pancreas

The pancreas is an accessory digestive organ, found retroperitoneally in the upper abdomen. It can be divided into the large head on the right, which is surrounded by the C-shaped curve of the duodenum and covers the bile duct, the neck, connecting the head with the body, which passes over the aorta and L2 vertebra and ends in the narrow tail on, which lies anterior to the left kidney, touching the splenic hilum and the left colic flexure. The pancreas is a dual gland, comprised of both an exocrine and an endocrine part. The endocrine part secretes hormones into the blood stream that regulate carbohydrate metabolism, while the exocrine part secretes and conveys digestive enzymes into the intestinal lumen.[1]

1.1.2. Innervation of the pancreas

Sympathetic catecholaminergic neurons innervate the pancreatic ganglia, islets, blood vessels, and to some extent, the ducts and acini. Their function is to maintain glycaemic levels during stressful conditions by decreasing insulin and increasing glucagon secretion, and fine-tuning hormone access to the circulation via vasoconstriction. In general, sympathetic nerves in the pancreas have a stimulatory effect through beta-adrenergic receptors and inhibitory effect through alpha-adrenergic receptors. Sympathetic activation inhibits exocrine secretion indirectly through the inhibition of intra-pancreatic ganglia and the reduction of fluid supply via vasoconstriction.[2,3]

Preganglionic parasympathetic fibres from the dorsal motor nucleus of the *vagus* act on post-ganglionic neurons in the pancreatic ganglia via nicotinic acetylcholine receptors. In humans, postganglionic fibres innervate acinar and ductal epithelial cells, the ductal vascular plexus and smooth muscle cells, and other ganglia, but scarcely provide input to islet endocrine cells.[4] Nevertheless, the *vagus* nerve modulates the intrinsic pacemaker activity of the pancreas, responsible for pulsatile insulin secretion. Parasympathetic activation stimulates secretion in acinar and ductal cells through muscarinic acetylcholine receptors, induces ductal constriction, and increases fluid supply by vasodilation.[3,5]

1.1.3. Structure and function of the endocrine pancreas

The endocrine part of the pancreas is unique in the way that it is dispersed and embedded into the exocrine tissue, rather than forming an anatomically separate gland. The functional unit of the endocrine pancreas is the islet of Langerhans, which is an ovoid aggregate of a few tens to thousands of cells. Islets are mainly composed of five secretory cell types, described below.

β-cells are usually most abundant, comprising ~55%[6,7] of islet cells. Their main role is insulin secretion, which is induced by post-prandial increase of blood glucose concentrations and further stimulated by amino acids and fatty acids. β-cells are electrically connected via gap junctions, which allow synchronised membrane potential and intracellular Ca^{2+} oscillations across all β-cells in the islet that result in pulsatile insulin release at glucose levels >∼7 mM.[8,9] Insulin lowers blood glucose level by inducing the uptake and storage of nutrients – primarily glucose – by other organs and reduces their *de novo* synthesis.

α-cells comprise ~35% of islet secretory cells. They principally secrete glucagon that is induced by hypoglycaemia and stimulated by amino acids and fatty acids. In the liver, glucagon induces glycogenolysis and gluconeogenesis – and ketogenesis during fasting – to increase and maintain blood glucose level inside a physiological range. In rodents, widely used as preclinical models, α-cells – along with δ-cells – are localized largely on the periphery of islets, with β-cells occupying most of the core. This structural organisation however, is absent in the human islet.[10,11]

δ-cells show a complex cellular morphology with neurite-like processes, forming an extensive paracrine network. They comprise ~5% of islet cells and secrete somatostatin, which in the islet is a potent paracrine inhibitor of insulin and glucagon release, although the overwhelming majority of total body somatostatin is produced in gastric and enteric D-cells, and in the central nervous system. The intrinsic regulation of δ-cell somatostatin secretion in response to post-prandial nutrients is similar to that of insulin.[12]

PP-cells – or F-cells – produce pancreatic polypeptide (PP) and comprise less than 1% of secretory cells in most islets; however, islets located in the posterior head region of the pancreas contain ~80% F-cells.[13,14] PP is released into the circulation after a meal in a biphasic manner, stimulated mainly by the *vagus* nerve, but also by amino acids and fatty acids. PP has effects on gastrointestinal motility, gastric acid production, glucose metabolism, and satiety.[15]

ε-cells comprise ~10% of islet cell volume during foetal development, but are reduced to ~0.15% in the adult human pancreas.[16] They secrete ghrelin, which is abundantly produced by endocrine cells in the gastrointestinal mucosa, mainly in the stomach. Ghrelin stimulates growth hormone release, appetite, energy storage, and gastrointestinal motility. In the islet of

Langerhans ghrelin released from ε-cells is proposed to suppress glucose-stimulated insulin secretion from β-cells and stimulate somatostatin secretion from δ-cells.[17,18]

Hypoglycaemia suppresses insulin release from β-cells and induces glucagon release from α-cells, while high blood glucose levels trigger insulin release from β-cells and suppress glucagon release from α-cells. The intrinsic response to glucose by these cells is further influenced by intra-islet paracrine and gut-derived factors, as well as sympathetic and parasympathetic modulation to fine-tune blood glucose levels and metabolism. The islets are well vascularized and directly receive 11-23% of the total pancreatic blood flow, despite amounting only ~1.5% to total pancreatic mass.[19] The thin endothelium of islet capillaries is richly fenestrated and allows direct accession of hormones to the circulation.[20] Through the microcirculation of the pancreas, the secretions are first drained to the acinar, then ductal cells, and eventually into the hepatic portal system.

1.1.4. Structure and function of the exocrine pancreas

The functional unit of the exocrine pancreas is the acinus, which consists of pyramidal acinar cells forming a central cavity, to where they secrete a fluid, rich in Cl^-, proteins, zymogens, and enzymes (i.e. trypsinogen, chymotrypsinogen, pancreatic amylase and lipase, phospholipase, sterol esterase, elastases, carboxypeptidases, and nucleases). These enzymes are drained from the central cavity to an intercalated duct, formed of flattened cuboidal epithelial cells. The acini are organized into larger lobules containing several intercalated ducts, which unite to form a main intralobular duct, characterised by typical cuboidal epithelium. Intralobular ducts from multiple lobules, then unite to form interlobular ducts, comprised of columnar epithelium. The interlobular ducts eventually combine to form the main pancreatic duct, which typically unites with the common bile duct before connecting to the duodenum through the papilla of Vater. An accessory branch of the main pancreatic duct, called the duct of Santorini, may also be present in some individuals.[5,21]

The digestive enzymes are stored in zymogen granules, located in the apical region of acinar cells, while the nucleus and endoplasmic reticulum are located in the basal region. The basolateral membrane contains receptors of hormones and neurotransmitters, such as insulin, cholecystokinin (CCK), secretin (SCT), vasoactive intestinal polypeptide (VIP), and acetylcholine. Interaction of these secretagogues with their specific surface receptors leads either to spikes of Ca^{2+} release from intracellular storages, causing the fusion of zymogen granules with the plasma membrane, or potentiation of exocytosis through protein kinase A (PKA) activation and the production of cyclic adenosine monophosphate (cAMP).[22]

The ductal epithelial cells play a key role in the production of pancreatic juice by adding water to dilute, and replacing Cl^- to HCO_3^- to alkalinize the secretions of acinar cells.[5] The key transporters of HCO_3^- secretion are most highly expressed in the intercalated ducts,[23–25] which are suggested to be the main sites of fluid and HCO_3^- secretion in the human pancreas. As the juice flows along the ductal tree, it is sequentially modified to obtain increasingly higher concentrations of HCO_3^-.[21] The alkaline juice functions to prevent premature activation of the digestive enzymes and to neutralize acid chyme entering the duodenum from the stomach.[26,27] About 2500 mL of fluid is secreted daily by the human pancreas, with HCO_3^- concentrations reaching 140 mM or higher. Peak secretion levels correspond to feeding.

1.1.5. Exocrine–endocrine crosstalk

Ductal and acinar cells affect the physiology of endocrine islet cells through intercellular connections and the secretion of cytokines and growth factors,[28–30] while endocrine islet cells control ductal and acinar cell exocrine activities by secreting their hormones into the insulo-acinar portal vasculature.[31] This system consists of an islet afferent vessel that branches off an intralobular artery and splits into a capillary glomerulus within the islet, from which multiple efferent vessels extend into the surrounding exocrine tissue.[32] Subsequently, venous blood from the acini supply the vascular plexus surrounding pancreatic ducts.[33] In this way, acinar and ductal cells are exposed to particularly high concentrations of islet hormones, the effect of which is most noticeable on peri-insular acinar cells that are larger and contain higher amounts of secretory proteins compared to tele-acinar cells.[20]

1.2. Functioning of pancreatic ductal epithelial cells (PDECs)

1.2.1. Ion transport mechanisms of pancreatic ductal epithelial cells

The ductal epithelium is comprised of functionally polarized cells. The transporters involved in fluid and HCO_3^- secretion are differentially expressed on the apical and basolateral membrane. Furthermore, ion transport mechanisms differ in cells located in the proximal versus the distal regions of the ductal tree. HCO_3^- can enter the cell via multiple ways through the basolateral membrane. One way is passive diffusion of CO_2 into the cell, where it is hydrated by intracellular carbonic anhydrase (CA), and the H^+ ions produced are exported through the basolateral membrane by the Na^+/H^+ exchanger (NHE-1). The electrochemical driving force of Na^+ is generated by the functioning of the Na^+/K^+ ATPase pump and K^+ channels. However, the overwhelming majority of HCO_3^- is actively transported into the cell by the $1Na^+/2HCO_3^-$

cotransporter, NBCe1-B. Secretion of HCO_3^- through the apical membrane and into the lumen occurs via the solute carrier family 26 member 6 (SLC26A6) $2HCO_3^-$ /$1Cl^-$ exchanger, with the cystic fibrosis (CF) transmembrane conductance regulator (CFTR) Cl^- channel providing the recycle of Cl^- ions. The transcellular movement of HCO_3^- generates a negative electrical potential in the lumen that drives the paracellular movement of Na^+ ions. Water follows Na^+ and HCO_3^- osmotically via both paracellular and transcellular routs, facilitated by aquaporin 1 and 5 (AQP1, -5). Because the poor basolateral and high apical permeability of duct cells to Cl^-, most of the luminal Cl^- is reabsorbed in proximal ductal segments due to Cl^-/HCO_3^- exchange activity. The remaining luminal Cl^- concentration is further diluted by the large fluid volume secreted.

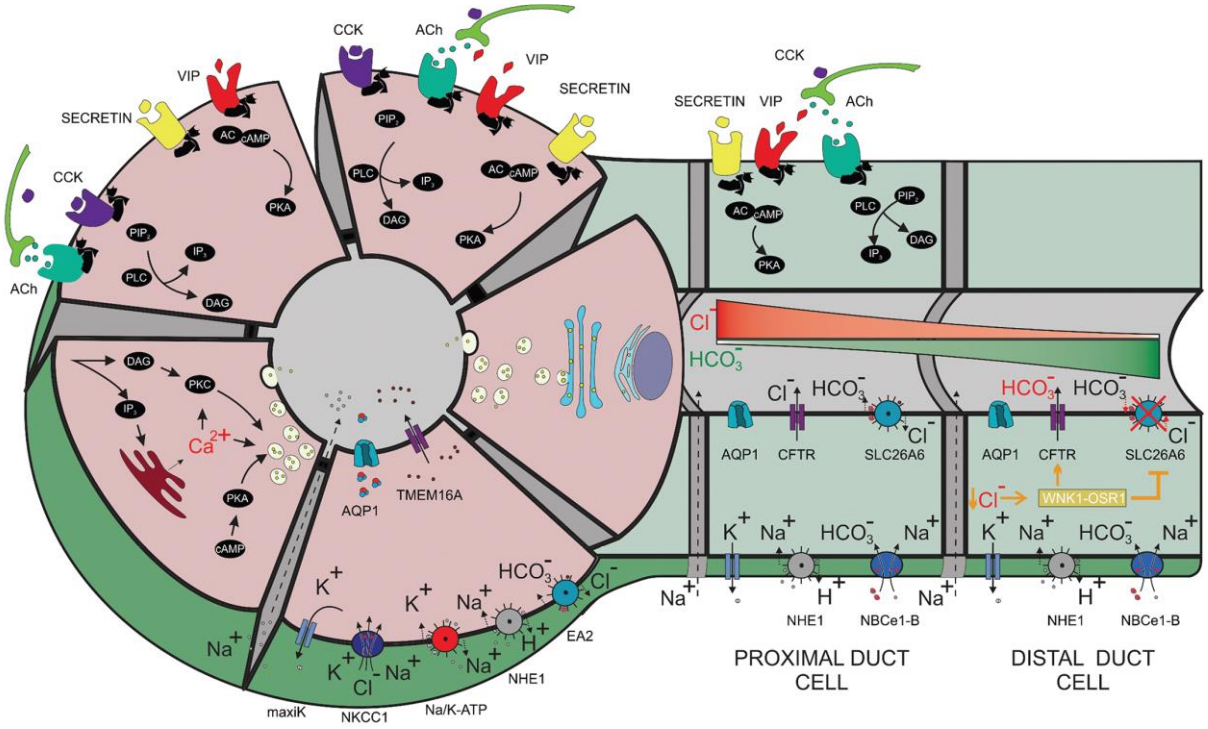

Figure 1. Molecular mechanisms and regulation of pancreatic exocrine secretion[5]
Image source: Jurij Dolensek et al. (2017). Pancreas Physiology. Challenges in Pancreatic Pathology. doi:10.5772/65895

In the distal duct, the decreased luminal Cl^- concentration results in rapid reduction of $[Cl^-]_i$. When $[Cl^-]_i$ drops under 10 mM, the Cl^--regulated kinase, with-no-lysine kinase 1 (WNK1) becomes activated and changes the pore size of CFTR, making it more permeable to HCO_3^-. At the same time, WNK1 inhibits apical SLC26 anion exchangers through the STE20/SPS1-related proline/alanine-rich and oxidative stress responsive kinase 1 (SPAK/OSR1) pathways,

preventing their activity in reverse mode, and thus, the reabsorption of luminal HCO_3^-. This mechanism enables 140 mM HCO_3^- concentration or higher in the final pancreatic juice.[5,34] There are, however, significant differences in ductal HCO_3^- output between species. Unlike in human, dog, cat, and guinea pig, secretion in the rat and mouse pancreas achieves a maximal HCO_3^- concentration of ~70 mM.[35] Nevertheless, experiments using mice offer the availability of knock out (KO) animals, which is why we have chosen the mouse as our experimental model.

1.2.2. Regulation of HCO_3^- secretion in pancreatic ductal epithelial cells

HCO_3^- secretion in PDECs is triggered via the cAMP/PKA pathway and potentiated by the Ca^{2+} signalling pathway. Upon entry of acidic chyme from the stomach into the proximal duodenum, neuroendocrine S-cells release SCT, which is the primary activator secretagogue of PDECs.[36] SCT binds to its G-protein coupled receptor, localized in the basolateral membrane of PDECs, which activates adenylate cyclase (AC). The generation of cAMP results in the activation of PKA, which phosphorylates and activates key mediators of HCO_3^- secretion, like CFTR. Activation of the cAMP/PKA pathway may also occur via the VIP receptor, VPAC1, and beta-adrenergic receptor activation. Other important agonists of PDECs are CCK and acetylcholine, which function to potentiate SCT-induced HCO_3^- secretion.[5] CCK-B and muscarinic M2, M3 receptors, localized in the basolateral membrane of PDECs, activate phospholipase C (PLC) to generate inositol 1,4,5-trisphosphate (IP_3), which triggers Ca^{2+} release from intracellular storages.[37] Intracellular Ca^{2+} levels are further amplified by Ca^{2+}-activated Ca^{2+} channels in the plasma membrane. The Ca^{2+} signalisation pathway may stimulate HCO_3^- secretion by activating the Ca^{2+}-dependent AC and Ca^{2+}-activated Cl^- channels.[38,39]

The synergism of the two molecular pathways in PDECs is mediated by the IP_3 receptor binding protein released with IP_3 (IRBIT). In the unstimulated state, IRBIT is bound to the IP_3 receptor (IP_3R) and prevents its association with IP_3. Phosphorylation of IP_3R serine residues by PKA increases the affinity of the receptor to IP_3 and reduces its affinity to IRBIT. When stimulation of Ca^{2+} signalisation produces IP_3, IRBIT becomes dissociated from the IP_3R and recruits protein phosphatase 1 (PP1) and calcineurin to dephosphorylate vesicular NBCe1-B, CFTR, and SLC26A6, promoting their translocation to the plasma membrane.[40] Furthermore, in the plasma membrane, IRBIT mediates the removal of specific inhibitory phosphate groups of CFTR and NBCe1-B,[41] enhancing their activity, while also reducing the inhibitory effect of intracellular Cl^- on NBCe1-B.[42]

Potential inhibitory factors of ductal HCO_3^- secretion include substance P, serotonin, arginine-vasopressin, and nucleotide phosphates; however, their mechanism of action is not yet fully understood.[21]

1.2.3. The cystic fibrosis transmembrane conductance regulator Cl^- channel

CFTR belongs to the ATP-binding cassette (ABC) transporter superfamily and conducts Cl^- and HCO_3^- along the electrochemical gradient. It is an essential component of epithelial HCO_3^- secretion in the pancreas, lung, lacrimal and salivary glands, and other organs. Mutations in the CFTR gene can impair functions of the channel, leading to dysregulation of epithelial secretion and the disease, CF.

1.2.3.1. The Structure of CFTR and activation via the cAMP/PKA pathway

CFTR consists of two transmembrane domains (TMD) that form the channel, two nucleotide binding domains (NBD), responsible for gating, and a regulatory domain (R), situated between the NBDs. Dislocation of the R domain enables ATP binding to both NBDs, triggering NBD dimerization and channel opening. ATP to ADP hydrolysis results in the disengagement of NBDs and closure of the channel. ADP replacement with ATP can restore the NBD dimer as long as the R domain is displaced. The displaced state of the R domain – that may be spontaneous and occurs with very low frequency – is stabilized via phosphorylation by PKA.[43]

1.2.3.2. Modulation of CFTR by WNK1

Modulation of CFTR by WNK1 at low $[Cl^-]_i$ was initially suggested to happen through complexes of WNK1 and the kinases OSR1 or SPAK; however, it has been shown that WNK1 alone was sufficient to increase the HCO_3^- permeability and conductance of CFTR.[44] WNK1 potentially binds to elbow helix 1 of CFTR TDM1 and changes the pore size of the channel from 4.8 Å to 5.7 Å. The increased pore size favours the passage of HCO_3^- versus the smaller Cl^- ion. Additionally, the lasso motif of TMD1 is proposed to affect channel gating by interaction with the R domain. Through binding to Elbow helix 1, which is closely connected to – and may able WNK1 interaction with – the lasso motif, WNK1 may also affect the gating of CFTR. [43,45]

1.2.3.3. Interactions of CFTR with other transporters

Besides mainly functioning as an anion channel, CFTR affects a multitude of other transporters through direct interaction. CFTR has a PDZ (PSD95/Discs-large/ZO-1) ligand at the C-terminus end of TMD2 that can bind to PDZ domains of other proteins. Such proteins include the Na^+/H^+ exchanger regulatory factor (NHERF) family of scaffold proteins and SH3 and multiple ankyrin repeat domains 2 (Shank2). Through these scaffolds, CFTR forms functional complexes with other transporters and regulates them through direct interaction. The R domain of CFTR interacts with the sulphate transporter and anti-sigma factor antagonist (STAS) domain of SLC26 anion exchangers, hence, the two transporters are mutually activated by PKA.[46–48] At the same time, PKA inhibits transporters involved in HCO_3^- salvation in the apical membrane of epithelial cells, i.e. NHE-3 and NBCn1. This process is also mediated by interaction with CFTR through NHERFs. Therefore, it has been proposed that HCO_3^- secretion and reabsorption is controlled by complex interactions between CFTR, SLC26 anion exchangers, NHE-3, and NBCn1, connected through their PDZ domains.[49–51] Interestingly, direct interaction with CFTR also might be necessary for the membrane deployment of CA IV. It has been shown that CA IV is decreased 8-fold in the plasma membrane of CFPAC-1 cells, characterised by expression of the mutant ΔF508 CFTR, which fails to reach the apical membrane. However, transfection with wild-type (WT) CFTR was able to restore membrane localization of CA IV.[52] Indeed, mutations in CFTR can affect its functions in diverse ways.[53] CFTR mutants that lack Cl^- channel activity, but are able to activate SLC26 anion exchangers retain most of epithelial Cl^-/HCO_3^- exchange. In contrast, the activity of SLC26A6 is markedly reduced in mice expressing the aforementioned ΔF508 CFTR.[54] Other mutants that reach the plasma membrane and are able to function as Cl^- channels may still be associated with pancreatic insufficiency.[53,55]

1.2.3.4. Effect of CFTR on the expression of ion channels

Among the numerous studies dedicated to investigate the ion transport mechanisms of epithelial cells, some have found that CFTR increased the expression of certain transporters. Shumaker *et al.* have shown that transfection of CFPAC-1 cells with WT CFTR upregulated the mRNA expression and activity of the basolateral Na^+-K^+-$2Cl^-$ cotransporter, NKCC1,[56] while Greeley *et al.* have shown the same for the apical anion exchangers, SLC26A6 and SLC26A3.[57] Additionally, our workgroup has shown that the expression of AQP1 – which co-localizes with CFTR in PDECs and is the main rout of water in pancreatic ductal epithelial secretion – is severely diminished in the pancreatic ducts of CFTR KO mice.[58] Although the

mechanism by which CFTR could affect the expression of other proteins on the mRNA level is not yet clear, it further supports the diverse and indispensable role of CFTR in pancreatic epithelial HCO_3^- secretion.

1.3. Type 1 diabetes mellitus

1.3.1. Development and aetiology of type 1 diabetes mellitus (T1DM)

T1DM is a chronic disease characterized by insulin deficiency due to autoimmune-induced pancreatic β-cell loss that leads to hyperglycaemia and related complications. Early immune responses include the activation of pattern recognition receptors by endogenous or exogenous (produced due to viral infection) ligands, which results in the production of type I interferons by β-cells. This initiates the recruitment of macrophages, which produce tumour necrosis factors and trigger β-cell apoptosis. Due to the inflammatory processes, the permeability of islet vasculature increases in later stages, facilitating the infiltration of lymphocytes, mainly CD8+ T-cells. Additionally, cytokines in the pro-inflammatory environment disrupt the metabolic and electrical activity, insulin synthesis, and gap junctions of β-cells, and induce excessive generation of reactive oxygen species (ROS) and activation of caspases. Stage 1 of T1DM is marked by the presence of more than one autoantibody against insulin, glutamic acid decarboxylase (GAD), protein tyrosine phosphatase IA-2 or IA-2β, or zinc transporter 8, while stage 2 is characterized by dysglycaemia or glucose intolerance. Since both stages are asymptomatic, patients usually present to the clinic at stage 3 with symptoms of hyperglycaemia, i.e. polyuria, polydipsia, enuresis, weight loss, and blurred vision. Long-term complications developed due to hyperglycaemia include microvascular (i.e. retinopathy, nephropathy, and neuropathy) and macrovascular (i.e. cardiovascular disease, cerebrovascular accidents, and peripheral vascular disease) defects, as well as pancreatic exocrine insufficiency (PEI). The aetiology of T1DM is influenced by various factors, including composition of the gut microbiome, diet, viral infections, and importantly, endogenous genetic predisposition. Two endotypes of T1DM can be differentiated: T1DE1, with disease onset occurring at young age, and T1DE2, with clinical manifestation later in life (>13 years). Patients with T1DE1 generally carry the DR4/DQ8 allele of the human leukocyte antigen (HLA) complex and develop insulitis with high level of $CD8^+$ T cells and $CD20^+$ B cells, and anti-insulin antibodies. Additionally, they show low number of insulin-containing islets and abnormal insulin processing in the remaining β-cells. In contrast, patients with T1DE2 generally carry the DR3/DQ2 allele of HLA, develop insulitis with low level of $CD8^+$ T cells and $CD20^+$ B cells, produce anti-GAD

antibodies, and have higher number of insulin-containing islets, with normal insulin processing.[59]

1.3.2. Pancreatic exocrine insufficiency (PEI) in T1DM

While on average, 10% of the global adult population is diabetic, and T1DM represents only ~10% of total diabetes cases, the prevalence and incidence of T1DM is steadily increasing world-wide.[60–62] It is associated with reduced quality of life, severe long-term complications, and substantial costs for the health-care system and the individual.[63] PEI is a complication affecting about 40% of T1DM patients.[64–66] Several factors are involved in the development of PEI in T1DM. (1) Enteropancreatic reflexes may become impaired due to autonomic diabetic neuropathy.[67] (2) Microvascular damage in the pancreas may lead to insufficient perfusion and ischemia, which contributes to the development of pancreatic atrophy and fibrosis.[68] (3) Hyperglycaemia was shown to inhibit SCT-induced pancreatic exocrine secretion.[69,70] (4) Oxidative stress, hyperglycaemia, and cytokines released from infiltrating immune cells activate pancreatic stellate cells, which play a central role in pancreatic fibrosis.[69,71] Lastly and most importantly, (5) the impaired insulin output from islets has a reduced trophic effect on the pancreatic parenchyma, which is physiologically accustomed to exceptionally high insulin levels.[72] Accordingly, reduced pancreatic volume and acinar atrophy has been shown in patients with T1DM,[73–77] and it has been demonstrated that the lack of insulin negatively affects acinar enzyme secretion.[72,78,79] In contrast to acinar cells, there is considerably less information regarding the effect of diabetes on PDECs.

1.3.3. Effect of T1DM on pancreatic ductal ion transport mechanisms

Research focused on pancreatic ductal ion transport mechanisms in diabetes is limited. In a few early clinical studies, ductal fluid and bicarbonate secretion was investigated in diabetic patients using the SCT-caerulein test and direct duodenal juice collection. While Aktan and Klotz found no significant difference, Vacca *et al*. have shown decreased HCO_3^- output in 73% of diabetic patients, compared to healthy volunteers.[80,81] However, *in vivo* and *in vitro* experiments using rats made somewhat contradictory results. Okabayashi *et al.* have found that the basal rate of pancreatic juice flow was significantly increased in the isolated pancreata of streptozotocin (STZ) induced diabetic rats, while the sensitivity to SCT of induced secretion was decreased.[82] In a separate study, the authors have also shown, that the sensitivity of pancreatic fluid secretion to the CCK receptor agonist caerulein was decreased, while enzyme and protein secretion, but not fluid output were more sensitive to carbachol (an acetylcholine

receptor agonist) in the isolated diabetic rat pancreas compared to controls.[83] Similarly, Patel *et al*. have demonstrated increased basal pancreatic juice flow in anesthetised diabetic rats. Interestingly, exogenous insulin stimulated pancreatic juice flow in healthy rats and stimulation could be abolished by the administration of atropine (a muscarinic acetylcholine antagonist). However, neither exogenous insulin, nor atropine had any effect on basal pancreatic juice flow in diabetic rats.[84] In an in-depth study, Futakuchi *et al*. have demonstrated that high extracellular glucose, present during hyperglycaemia, decreases luminal HCO_3^- secretion of PDECs via the activity of the sodium-dependent glucose co-transporter-1 (SGLT1). Reabsorption of Na^+ and glucose by SGLT1 increases $[Na^+]_i$ and apical membrane depolarization, reducing the electrochemical driving force for HCO_3^- efflux via CFTR.[85] Although this study might partly explain some of the inhibitory effect of diabetes on ductal HCO_3^- secretion, it does not explain the increased basal secretory rate observed in other experiments.

1.4. Experimental systems for the functional study of PDECs

1.4.1. Cell cultures

The greatest feature of cell cultures is the convenient use of genetic manipulation (e.g. transfection and heterologous expression, overexpression, deletion, mRNA silencing, etc.) to study the functions and interactions of one or multiple proteins. For example, the ability of CFTR to activate the anion exchangers SLC26A3 and SLC26A6 was demonstrated by co-expression of the transporters in HEK293 cells[48]. Ion transport activities in cells can be detected real-time with patch-clamp technique, or with the use of intracellular fluorescent indicators of pH, Na^+, Cl^-, and Ca^{2+}.[86] The most widely used cell lines include those derived from human ductal adenocarcinomas, like CAPAN-1, CFPAC-1, PANC-1, MIAPACA-2, BxPC, etc. Because the CAPAN-1 cell line expresses WT CFTR, it is considered the most suitable one for ion transport studies. However, most human cell lines are likely derived from distal parts of the ductal tree and therefore may not represent well the cellular phenotype responsible for the bulk of fluid secretion in the proximal ducts. Because of the low heterogeneity of cell cultures, experimental results obtained from them may lack physiological relevance. Additionally, the gene expression pattern of cells becomes altered when their original intercellular connections are disrupted due to isolation,[87–90] and with increasing number of passages.

1.4.2. Isolated ductal segments

Most early *in vitro* studies used isolated perfused whole pancreas preparations from rat, cat, or rabbit to examine pancreatic functions, however, whole pancreas preparations do not allow direct examination of ductal cells. The advent of the technique to isolate intact intra-interlobular pancreatic ducts from the pancreas of rodents, developed by Argent *et al*. signified an important milestone in pancreas research and opened the way to specifically detect the cellular mechanisms of PDECs.[91] After enzymatic digestion and microdissection, the isolated ductal segments are cultured for 6–12 h, during which their ends spontaneously fuse, resulting in a closed tube or bubble-like structure. Ion transport mechanisms can be triggered by superfusion of ductal segments and subsequent modification of bath composition. Fluid secretory rate can be measured through recording the changes in luminal volume by videomicroscopy. Intracellular changes in pH or ion concentration can be detected using microfluorimetric dyes. Membrane impermeable versions of these dyes can be injected into the lumen to monitor luminal pH and ion concentration. Alternatively, the lumen can be cannulated and perfused to specifically trigger apical transport activities. Our workgroup has been reliably utilizing this technique for more than a decade to produce novel and relevant results in the field of pancreatic pathophysiology, further confirming the diverse utility of isolated ductal segments.[58,92,93]

Although isolated ductal segments are one of the most valuable tools in exocrine pancreas research, they also have limitations. Similarly to islets of Langerhans and acinar cells, isolation of ducts require enzymatic digestion and relatively long duration of culturing, which may result in functional changes.[88,90,94] At the same time, they can only be maintained for up to about 48 h, which make them unsuitable for experiments that require long durations of treatment. Additionally, since the connections between ductal and other pancreatic cell types are disrupted, ductal segments are not suitable to use for investigating endocrine–exocrine interactions.

1.4.3. Pancreatic ductal organoids

Another *in vitro* model increasingly used in pancreas research is the organoid cell culture (OC). Organoids are 3D cell cultures grown from tissue stem cells in extracellular matrix-based hydrogels by artificial activation of the Wnt/β-Catenin signal transduction cascade. They can be maintained for several months and are therefore a valuable tool for maximizing the use of rare patient samples in both research and clinical applications. In contrast to 2D cell cultures, pancreatic ductal OCs maintain the original intercellular connections

characteristic of epithelial cells. In contrast to isolated ductal segments, OCs do not contain any components of the surrounding connective tissue (e.g. fibroblasts), which may interfere with protein or mRNA expression assays. Most tests used to investigate epithelial functions in isolated ductal segments are well applicable in OCs as well.[95] However, similarly to any isolated and cultured specimen, pancreatic ductal OCs also carry the possibility of non-physiological genetic and functional changes.

1.4.4. Pancreatic tissue slices

The acute tissue slice technique is an *in situ* experimental system that is widely used in research investigating the structure and function of the brain, as well as the liver, adrenal gland, and retina.[96–99] The technique was first optimized by Speier and Rupnik to study β-cells[100] and it was thereafter successfully used in the structural and functional study of both acinar and β-cells.[101–104] In contrast to the experimental systems detailed above, the preparation of tissue slices (TSs) does not require enzymatic digestion. Direct intercellular junctions and interactions are involved in maintaining pancreatic development, cellular differentiation and functional regulation.[87–90,105,106] Since tissue architecture is well preserved in the slice, this technique is suitable for both morphological and functional imaging, without the risk of phenotypic changes. Electrophysiological studies using patch-clamp or microfluorimetric measurements can be conveniently implemented to TSs. Additionally, the TS technique may allow investigation of the interactions between cells of the exocrine and endocrine component of the pancreas, a field of increased focus in our workgroup.

Noticing the clear advantages of TSs, we aimed to adopt and optimize this technique for the functional and structural study of PDECs. Because the tissue of the murine pancreas is exceptionally soft, the injection of agarose is a critical step in the preparation of TSs. Filling the ductal tree by retrograde injection of 37◦C low melting point agarose into the common bile duct serves as a scaffold that stabilized the tissue during cutting. However, this raises concerns regarding the structural and functional integrity of the ducts, and raises the question that how far up the ductal tree is the agarose able to penetrate?

2. AIMS OF THE STUDY

T1DM is associated with reduced quality of life, severe long-term complications, and substantial costs for the health-care system and the individual.[63] The prevalence of T1DM is steadily increasing world-wide,[60,61] however, our knowledge on the mechanisms of the disease and our ability to reduce disease-associated complications like PEI are still incomplete. Some of the few available studies on pancreatic ductal ion transport mechanisms in T1DM are outdated, or have yielded conflicting results. Because PDECs play an essential role in the maintenance of pancreas integrity, identification of the mechanism through which ductal fluid secretion is altered in diabetes may bring us closer to understanding the pathogenesis of exocrine insufficiency. Furthermore, the experimental systems widely used to study ductal secretion do not enable examination of PDECs in their physiological environment.

Therefore, our aims in the **first** part of this thesis were

I. to determine the effect of T1DM on the activity and expression of the main ductal ion transporters,
II. to define the role of CFTR in the changes of ductal ion transport in T1DM,
III. to study the underlying mechanisms in the changes of ductal ion transport in T1DM,

and our aim in the **second** part of this thesis was

IV. to investigate whether TSs are suitable for the functional examination of the pancreatic ducts.

3. MATERIALS AND METHODS

3.1. Ethical approval

Animal experiments were conducted in accordance with the Guide for the Care and Use of Laboratory Animals (Department of Health and Human Services, USA). The experimental protocol was approved by the local Ethical Board of the University of Szeged, Hungary, and by the Public Health and Food Chain committee, Csongrad County Government Office, Hungary (XI./128/2019).

3.2. Transgenic mice

CFTR KO mice on an FVB/N background were kindly provided by Dr Ursula Seidler (Hannover Medical School, Hannover, Germany). Standard plastic cages were used to house the animals with a 12:12 h light-dark cycle at a room temperature of 23± 1°C. Standard or CFTR-specific laboratory chow and drinking solutions were freely accessible. 8–12 weeks old male mice were genotyped using genomic DNA isolated from tail tip and homozygous animals (WT and CFTR KO) were used for functional experiments.

3.3. Chemicals and solutions

The composition of the solutions used for microfluorimetry and video microscopy measurements are shown in Table 1. For the standard HEPES-buffered solution the pH was adjusted to 7.5 with NaOH. Standard HCO_3^-/CO_2-buffered solutions were gassed with a mixture of 95% O_2 and 5% CO_2. The solutions were heated to 37°C prior to perfusion.

	Standard HEPES	**Standard HCO_3^-**	**NH_4^+ in HCO_3^-**	**Cl^--free HCO_3^-**
NaCl	140	115	95	
KCl	5	5	5	
$MgCl_2$	10	1	1	
$CaCl_2$	1	1	1	
HEPES	1			
D-glucose	10	10	10	10
$NaHCO_3$		25	25	25
NH_4Cl			20	
Na-gluconate				115
KNO_3				5
Ca-gluconate				6
Mg-gluconate				1

Table 1. Composition of solutions. Values are concentrations in mM.

2,7-bis-(2-carboxyethyl)-5(6)-carboxyfluorescein acetoxymethyl ester (BCECF-AM, 2 mM) and N-(Ethoxycarbonylmethyl-6-Methoxyquinolinium Bromide (MQAE, 1 mM) were prepared in dimethyl sulfoxide (DMSO) and stored at −20°C. All chemicals and reagents used are shown in Table 2.

Reagent name	Cat. No.	Manufacturer
2,7-bis-(2-carboxyethyl)-5(6)-carboxyfluorescein acetoxymethyl ester (BCECF-AM)	1932864	Invitrogen (Eugene, OR, USA)
N-(Ethoxycarbonylmethyl-6-Methoxyquinolinium Bromide (MQAE)	ENZ-52156	
Collagenase	LS005273	Worthington (Lakewood, NJ, USA)
Secretin (SCT)	1919	Tocris (Bristol, UK)
Forskolin	1099	
Mouse Secretin ELISA Kit	NBP2-82434	Biotechne (Minneapolis, USA)
Mouse CCK EIA Kit	EIAM-CCK-1	Ray Biotech (Peachtree Corners, GA, USA)
Anti-CFTR Antibody	ACL-006	Alomone Labs (Jerusalem, Israel)
Anti-Na+/H+ Exchanger 1 (NHE-1) Antibody	ANX-010	
Anti-TMEM16A (ANO-1) Antibody	ACL-011	
Anti-Aquaporin 1 Antibody	AQP-001	
cOmplete™, EDTA-free Protease Inhibitor Cocktail	4693132001	Roche (Budapest, Hungary)
Cryomatrix	6769006	Thermo Scientific (Waltham, MA, USA)
Hoechst33342	2086723	
Diamidino-2-phenylindole (DAPI)	62248	
Secretin receptor Antibody	BS-0089R	
beta Actin Loading Control Antibody (BA3R)	MA5-15739	
Goat anti-Mouse IgG Secondary Antibody, Alexa Fluor™ Plus 488	A-32723	
Goat anti-Rabbit IgG Antibody, Alexa Fluor™ 647	A-21244	
Goat anti-Rabbit IgG Antibody, Alexa Fluor™ 488	A-11008	

All other chemicals were obtained from Merck (Budapest, Hungary).

Table 2. Chemicals and reagents.

3.4. Induction of diabetes

Type 1 diabetes was induced using the low-dose STZ protocol of the Diabetic Complications Consortium.[107] Briefly, 50 μg/bwkg STZ, dissolved in citrate buffer (pH 4.5) was administered daily to 8–12 weeks old male mice for 5 consecutive days, while control animals received citrate buffer only. STZ injections were preceded by a 6 h fasting period. 4

weeks after the first injection, the fasting blood glucose level (BGL) was measured using a blood glucose meter (77 Elektronika, Budapest, Hungary) and animals with a BGL of ≥12.0 mmol/L were considered diabetic. The mice were then sacrificed by i.p. 200 mg/bwkg pentobarbital overdose and exsanguinated through cardiac puncture. The pancreas was immediately removed, trimmed from fat and lymphatic tissue, and a portion was fixed in 6% neutral formaldehyde solution, embedded in paraffin blocks, cut into 3 μm thick sections, stained with hematoxylin/eosin, and observed by light microscopy. Small pieces of the pancreas were fixed in 3% glutaraldehyde for transmission electron microscopy. The other portion of the pancreas was used for the isolation of ducts. Microvette CB300 fluoride/heparin-coated capillaries (Sarstedt, Nümbrecht, Germany) were used to collect and centrifuge blood samples at 2500 RCF for 15 min at 4°C. Plasma samples were stored at −20°C until use.

3.5. Isolation of pancreatic ducts and measurement of intracellular pH

The pancreas of WT and CFTR KO mice was used for the isolation of intra/interlobular ducts by enzymatic digestion and microdissection as described previously.[91] Changes in intracellular pH (pH_i) were measured using the pH-sensitive fluorescence dye, BCECF, and the alkaline load technique. Pancreatic ducts were incubated with 2 μM BCECF-AM for 1 h at 37°C, then attached to a cover glass, which formed the base of a perfusion chamber and was mounted on the stage of an IX71 live cell imaging fluorescence microscope (Olympus, Budapest, Hungary). The cells were excited at 440 and 490 nm and emission was monitored at 530 nm. Ten to fourteen regions of interest (ROIs) were marked for each experiment and one measurement per second was obtained. The 490/440 fluorescence ratio was calibrated to pH_i using the high K^+-nigericin technique as previously described.[108,109]

3.6. Measurement of HCO_3^- secretion

To estimate HCO_3^- efflux, the activity of the Cl^-/HCO_3^- exchanger was measured by the NH_4Cl pre-pulse technique and the Cl^- withdrawal technique. For the NH_4Cl pre-pulse technique, ducts were exposed to 20 mM NH_4Cl in HCO_3^-/CO_2-buffered solution, which resulted in an immediate increase in pH_i resulting from the influx of NH_3 across the membrane. After maximal alkalization, the pH_i began to recover. Under these conditions, the initial rate of pH_i ($\Delta pH/\Delta t$) recovery (over the first 30 seconds) reflects the rate of HCO_3^- secretion (base efflux).[110,111] After the removal of NH_4Cl, the pH_i suddenly decreases because of the dissociation of intracellular NH_4^+ to H^+ and NH_3. In HCO_3^-/CO_2-buffered solution, the initial

rate of recovery from the acid load **(**over the first 60 seconds) reflects the activity of NHEs and the NBC.

In the Cl^- withdrawal technique, Cl^- is removed from the external solution that causes alkalization of pH_i, which results from the reverse operation of the Cl^-/HCO_3^- exchanger. In the absence of Cl^-, the exchanger operates in reverse mode and absorbs HCO_3^- in exchange for Cl^-. The absorbed HCO_3^- binds free protons and induces alkalosis. The initial rate of alkalization and the rate of recovery from alkalosis (over the first 60 seconds) directly reflects the activity of the exchanger in reverse and normal mode respectively. Transmembrane base flux [$(J(B^-)$] was calculated using the following formula: $J(B^-) = \Delta pH/\Delta t \times \beta_{total}$, where $\Delta pH/\Delta t$ is the initial rate of recovery and β_{total} is the total buffering capacity.[112,110]

3.7. Measurement of CFTR activity

CFTR activity was analysed by measuring intracellular Cl^- concentration using MQAE fluorescent dye and forskolin. Because of the quenching effect of Cl^- on the dye, the fluorescence intensity of MQAE is inversely proportional to Cl^- concentration. Pancreatic ducts were incubated with MQAE (5 μM) for 1 h at 37°C, then perfused with HCO_3^-/CO_2-buffered solution containing 20 μM forskolin. Excitation was set to 350 nm and emission was monitored at 510 nm. Ten to twelve ROIs were marked for each experiment and one measurement per second was obtained. The readings were displayed as fluorescence ratio (F/F0) and a linear trend line was plotted on the curve for the first two min (120 sec) of forskolin stimulation. The area under the plotted curve was calculated using the definite integral of the equation.

3.8. Measurement of pancreatic fluid secretion

To estimate the rate of ductal fluid secretion, we measured the swelling of the intra-interlobular ducts using the video microscopy technique described previously.[113] Briefly, intra-interlobular pancreatic ducts were attached to the cover glass of a perfusion chamber and mounted on the stage of an IX71 live cell imaging fluorescence microscope. To stimulate fluid secretion, the ducts were perfused with forskolin (5 μM) and low magnification, bright-field images were captured at 1-min intervals using a CCD camera (Hamamatsu ORCA-ER, Olympus, Budapest, Hungary). The integrity of the ductal wall was confirmed at the end of each experiment using a hypotonic solution. Changes in relative luminal volume were analysed using Image J software.[113,114]

Pancreatic fluid secretion was assessed *in vivo* as well, using a protocol based on the work of Perides *et al*.[115] Briefly, mice were anesthetized with the combination of ketamine (100

mg/kg, i.p.) and xylazine (12.5 mg/kg, i.p.), and a single injection of buprenorphine (0.1 mg/kg, i.p.) was administered for the relief pain. To maintain body temperature, animals were kept on a heating pad (37°C) during the entire experiment. After median laparotomy, the lumen of the common biliopancreatic duct was cannulated using a 30-gauge needle with its end filed down. To prevent contamination with bile, the hepatic duct was occluded with a microvessel clip. Pancreatic fluid secretion was stimulated by i.p. administration of secretin (1 CU/kg) and the pancreatic juice was collected through a polyethylene tube over 60 min.

3.9. Immunolabelling of frozen tissue sections

Isolated pancreatic ducts were embedded in cryomatrix, snap-frozen in liquid nitrogen, stored at -20°C, and cut into 10 μm-thick sections. Immunofluorescence labelling was done based on the protocol provided at www.novusbio.com. Briefly, tissue sections were fixed with 4% para-formaldehyde in PBS for 15 min and permeabilized by washing twice with phosphate-buffered saline (PBS) containing 1% goat serum (GS) and 0.4% Triton X-100 for 10 min. Blocking was done for 30 min in PBST containing 5% GS, followed by incubation with primary antibodies overnight on 4°C. The sections were then incubated with Hoechst33342 for 15 min followed by a washing step and incubation with secondary antibodies for 1 h. After a washing step, the sections were covered with Fluoromount mounting medium and allowed to dry for 12 h under aluminium foil. Primary (2 μg/mL for CFTR, ANO-1, and NHE-1 antibodies; 2.5 μg/mL for anti-AQP1; 4 μg/mL for anti-β-actin) and secondary (5 μg/mL for goat anti-rabbit Alexa Fluor 647; 8 μg/mL for goat anti-mouse Alexa Fluor 488) antibodies and Hoechst 33342 (20 μg/mL) were diluted in PBS supplemented with 1% GS. All steps were done at room temperature unless specified otherwise. Images were captured using an LSM 880 confocal microscope (Carl Zeiss Technika Kft., Budaörs, Hungary). An optimal pinhole size and laser intensity was defined for every target antigen and the same settings were used to record all samples.

3.10. Quantitation of immunostainings

The images were evaluated using Image J software. The measured area was restricted to the layer of epithelial cells and to a constant threshold value of intensity. The average intensity in the green and red channels was then determined. Red intensity values marking the antigens of interest were normalized to the green intensity values representing β-actin.

3.11. Quantitative reverse transcription PCR (RT-qPCR)

Intra-interlobular pancreatic ducts were isolated from 6 normal and 6 diabetic mice and pooled for total RNA extraction with a NucleoSpin RNA Kit (Macherey-Nagel, Düren, Germany) according to the manufacturer's instructions. Total RNA (2 μg) was reverse-transcribed using the High-Capacity cDNA Reverse Transcription Kit (Applied Biosystems, Foster City, USA). qPCR was performed on a Light Cycler 96 instrument (Roche Magyarország Kft., Budaörs, Hungary) using TaqMan probe sets for specific genes (Thermo Fisher Scientific, Darmstadt, Germany). RT-qPCR reactions were prepared as previously described.[116] The results were expressed as fold-changes calculated by the $2^{-\Delta\Delta CT}$ method. Genes with expression values ≤0.5 were considered downregulated, whereas values ≥2 were considered upregulated. Values ranging from 0.51 to 1.99 were not considered significant. TaqMan assays applied are provided in Table 3.

Gene symbol	Official full name	GenBank Ref. No.	Taqman assay ID
CFTR	Cystic fibrosis transmembrane conductance regulator	NC_000072	Mm00445197_m1
TMEM16A (ANO-1)	Anoctamin-1	NC_000073.7	Mm00724407_m1
AQP-1	Aquaporin-1	NC_000072.7	Mm01326466_m1
AQP-5	Aquaporin-5	NC_000081.7	Mm00437578_m1
AQP-8	Aquaporin-8	NC_000073.7	Mm00431846_m1
SLC9A1 (NHE-1)	Solute carrier family 9 (Na^+/H^+ exchanger) member A1	NC_000001.11	Mm00444270_m1
SLC9A2 (NHE-2)	Solute carrier family 9 (Na^+/H^+ exchanger) member A2	NC_000067.7	Mm01237129_m1
SLC26A3 (DRA)	Solute carrier family 26 (Cl^-/HCO_3^- exchanger), member 3	NC_000078.7	Mm00445313_m1
SLC26A6	Solute carrier family 26 (Cl^-/HCO_3^- exchanger), member 6	NC_000075.7	Mm00506742_m1
SLC4A4 (NBCe1-B)	Solute carrier family 4 (Na^+/HCO_3^- co-transporter), member 4	NC_000071.7	Mm01347935_m1

Table 3. Taqman assays used to investigate the expression of ion transporters.

3.12. Transmission electron microscopy

For post-embedding transmission electron microscopy, small pieces of the pancreas were fixed in 3% glutaraldehyde. The tissues were rinsed with PBS and further fixed for 1 h in 2% OsO_4. The samples were then dehydrated in increasing concentrations of ethanol, rinsed with uranyl acetate and acetone, and embedded in Embed812 (Electron Microscopy Sciences, Hatfield, PA, USA). The embedded blocks were used to prepare ultrathin (70 nm) sections

(Ultracut S ultra-microtome (Leica, Wetzlar, Germany), which were mounted on copper grids. The grids were counterstained with uranyl acetate and lead citrate (Merck Millipore, Darmstadt, Germany) and examined and imaged using a JEOL JEM 1400 transmission electron microscope (JEOL; Tokyo, Japan). Five digital photographs of the cells were captured at a magnification of 5000X and 8000X using TEM Center software (JEOL; Tokyo, Japan).

3.13. ELISA

Plasma samples obtained by cardiac puncture were transferred to fluoride/heparin-coated capillaries and centrifuged at 2500 ×g for 20 min at 4°C. The samples were stored at −20°C and thawed on ice before use. Pancreas homogenates were prepared by grinding 100 mg tissue in liquid nitrogen using a mortar and pestle and dissolving it in 1 mL ice-cold protease inhibitor cocktail. The SCT and CCK assays were performed following the manufacturer's instructions.

3.14. Preparation of serial tissue sections from Giemsa-injected whole mouse pancreas

10% Giemsa dissolved in 1.5% low-melting-point agarose was injected into the common bile duct of the mice. The pancreas was removed, cleaned, and the divisions of head, body, and tail were cut into three separate pieces. Each pieces were subsequently embedded in cryomatrix and cut into 15 μm sections using a CM1800 cryostat (Leica Biosystems, Wetzlar, Germany). Giemsa staining was analysed using an Axio Scope.A1 light microscope (Carl Zeiss Technika Kft., Budaörs, Hungary).

3.15. Immunolabelling of acute pancreas tissue slices

The slices were fixed in 4% (v/v) paraformaldehyde for 20 min at room temperature, washed in PBS 3 times for 10 min, permeabilized with 0.05% TritonX-100 in PBS for 30 min and blocked with the mixture of 1% BSA and 1% goat serum in PBS. Incubation with rabbit anti-CFTR polyclonal antibody (2 μg/mL) was done overnight at 4°C. The slices were next washed 3 times with PBS for 15 min and incubated with Alexa fluor 488-conjugated goat anti-rabbit IgG secondary antibody (1 μg/mL) for 3 h. Nuclei were stained with 4′,6-diamidino-2-phenylindole (DAPI, 2 μg/mL) for 15 min and three final washes were made for 20 min is PBS. All steps were performed at room temperature and with applying gentle agitation, unless specified otherwise. Slices were covered using Fluoromount and analysed using a LSM 880 confocal laser scanning microscope (Carl Zeiss

Technika Kft., Budaörs, Hungary). Pancreas slices were excited at 405 and 488 nm and emissions were collected at 453 and 516 nm.

3.16. Statistical analysis

Prism, version 9.5.1. (GraphPad Software, San Diego, CA, USA) was used to produce graphs and images. Data are presented as the mean ± S.D and box and whisker plots showing the median, quartiles, and extremes. The Shapiro-Wilk and Kolmogorov-Smirnov tests were used to analyse data distribution. The equality of variances was analysed using F-test. One-way ANOVA (with Tukey's multiple comparisons test), Student's *t*-test (with Welch's correction as needed), the Kruskal–Wallis test (with Dunn's multiple comparisons test), and the Mann–Whitney test were used to determine statistical significance.

4. RESULTS

4.1. Morphology of the exocrine pancreas in diabetes

The number and size of islets decreased by the destruction of insulin-producing beta cells due to STZ treatment (Fig. 2A). Additionally, low levels of fibrosis, acinar atrophy, and leukocyte infiltration, were developed. In contrast, the structure of the ducts was preserved. Electron microscopic examination of the pancreas showed enlarged mitochondria and a fragmented mitochondrial internal membrane structure in the acini (Fig. 2B). To a lesser extent, enlargement of the mitochondria was also observed in ducts and islets.

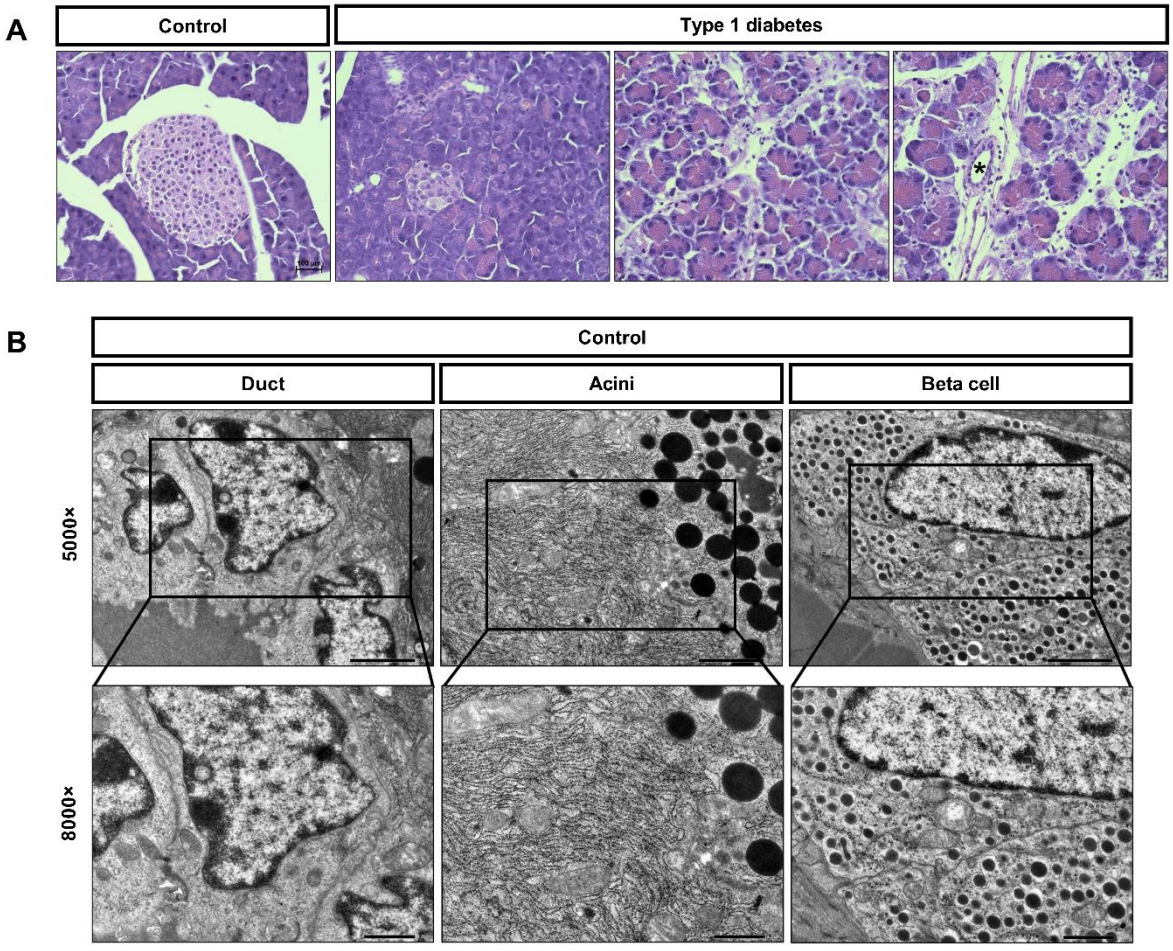

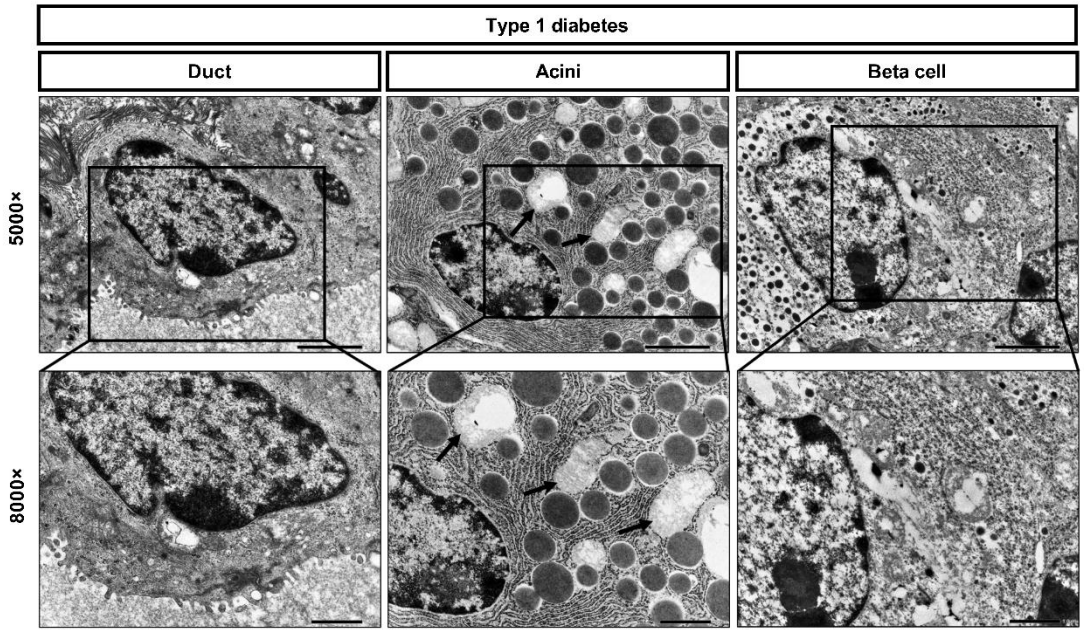

Figure 2. Effect of type 1 diabetes mellitus (T1DM) on pancreatic morphology**.** (**A**) Haematoxylin and eosin staining of the pancreas from normal and T1DM mice. An asterisk shows the pancreatic duct. Scale bar represents 100 μm. (**B**) Representative electron micrograph images of pancreatic duct, acini, and β cells from control and T1DM mice. Black arrows on the upper (magnification, X 5000) and lower (magnification, X 8000) panels indicate mitochondria.

4.2. Pancreatic ductal fluid secretion increases in diabetes

The volume of fluid secreted by ductal cells is an important indicator of ductal function. Therefore, the rate of fluid secretion was determined under *in vitro* and *in vivo* conditions. For the *in vitro* measurements, the rate of fluid secretion was estimated from the change of luminal volume of isolated ductal segments (Fig. 3A, B). Following stimulation with forskolin, the amount of fluid secreted by the diabetic ducts was significantly higher than that of non-diabetic ducts (13.2 ± 2.14 vs. 9.29 ± 0.51). *In vivo* fluid secretion studies revealed similar results. Both basal and secretin-stimulated (1 CU/kg) fluid secretion were significantly increased in diabetic mice, compared to normal mice (0.73 ± 0.12 vs. 1.15 ± 0.08 μl/h/BWg basal secretion and 1.48 ± 0.24 vs. 2.48 ± 0.25 μl/h/BWg stimulated secretion; Fig. 3C).

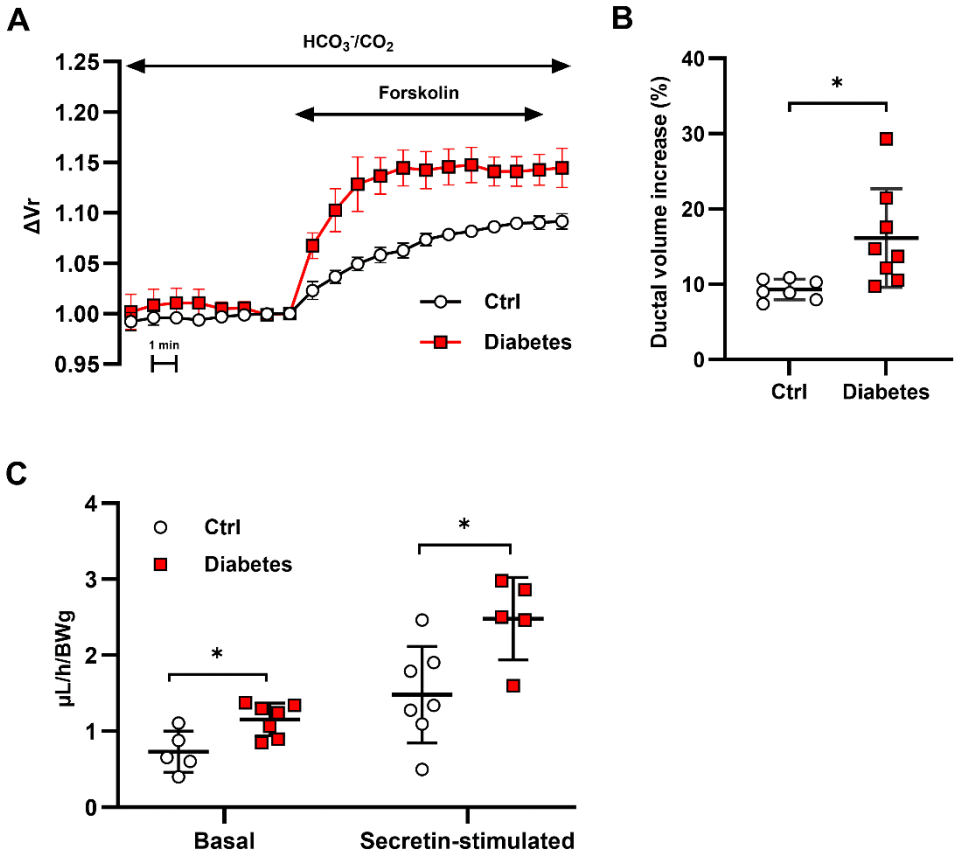

Figure 3. Effect of diabetes on ductal fluid secretion**.** (**A**) Pancreatic ductal fluid secretion was measured in pancreatic ductal segments isolated from control (black line) and diabetic (red line) mice using video microscopy and Image J software. (**B**) Ductal volume increase was measured during forskolin (5 µM) stimulation (between time points 8 and 18) and expressed as percentage. Data are shown as means ± SD. n = 7–8 ducts/3 mice/groups. *: p = 0.021 vs. Control using Welch's *t*-test. (**C**) Scatter plot showing the rate of *in vivo* pancreatic fluid secretion under basal and secretin-stimulated (1 CU/kg) conditions in control and diabetic mice. Data are shown as means ± SD. n = 5–7 mice/groups. *: p = 0.013 vs. Control for basal and 0.0174 for secretin-stimulated, using Student's *t*-test.

4.3. The activity and expression of ductal acid/base transporters is increased in diabetes

Intra-interlobular ducts were isolated from normal and diabetic mice and the alkaline load method was used to measure the activity of acid–base transporters in the ductal cells. In previous studies, we found that the degree of regeneration from alkalosis in HCO_3^-/CO_2–containing extracellular solution reflects the activity of the Cl^-/HCO_3^- exchanger, whereas the regeneration from acidosis indicates the activity of NHEs and NBC.[110] Both alkali and acid regeneration were increased in diabetic mice compared with control mice [rate of alkali regeneration: 3.2 ± 0.09 vs. 4.86 ± 0.14 $-J(B^-/min)$; rate of acid regeneration 7.25 ± 0.3 vs. 11.45 ± 0.34 $-J(B^-/min)$], indicating that diabetes increases the activity of these transporters

(Fig. 4A a–c). To confirm this result, the Cl^- withdrawal method was used (Fig. 4B a–c). The removal of extracellular Cl^- in the presence of HCO_3^- induces a robust alkalosis, because of the reverse mode of the exchanger. During the re-administration of extracellular Cl^-, the pH_i is regenerated and the rate of regeneration reflects the activity of the Cl^-/HCO_3^- exchanger. Similarly to the alkaline load method, the exchanger showed increased activity in diabetes (Fig. 4B b), although no difference in pH_i change was observed (Fig. 4B c).

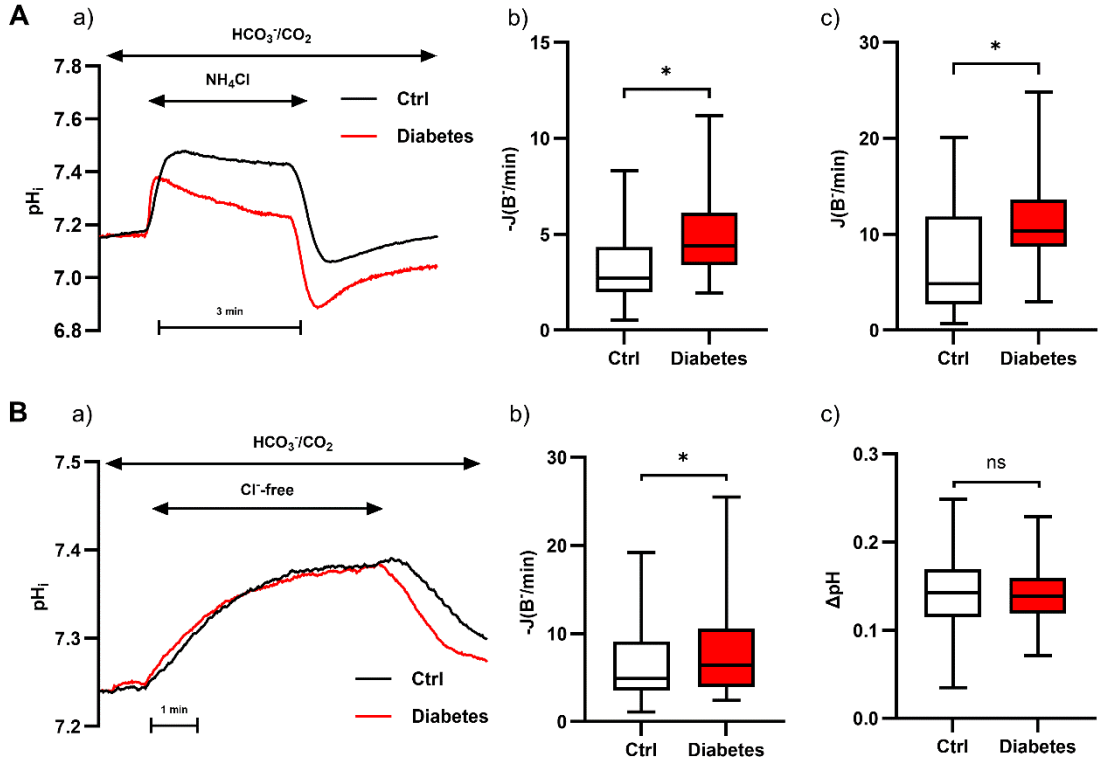

Figure 4. Effect of T1DM on the activity of ion transporters in isolated murine pancreatic ductal segments. (**A**) Ion transporter activity was examined using the alkaline load technique. **(a)** Representative pH_i traces showing the effect of diabetes (red line) on the activity of acid/base transporters in HCO_3^-/CO_2-buffered solution. The rate of regeneration from alkalosis **(b)** reflects the activity of the Cl^-/HCO_3^- exchanger, whereas regeneration from acidosis **(c)** reflects the activity of the Na^+/H^+ exchanger and the Na^+/HCO_3^- cotransporter. $-J(B^-/min)$ and $J(B^-/min)$ were calculated from the $\Delta pH/\Delta t$ obtained by a linear regression analysis of pH_i measurements made over the first 30 or 60 sec, respectively. n = 172–274 ROIs/14–24 ducts/4–5 mice/groups. *: $p < 0.0001$ vs. Control using Mann–Whitney test. (**B**) Activity of the Cl^-/ HCO_3^- exchanger was measured using the Cl^- withdrawal technique. **(a)** Representative pH_i traces show the effect of extracellular Cl^- removal on control (black line) and diabetic (red line) pancreatic ducts in HCO_3^-/CO_2-buffered solution. Box and whisker plots show the rate of regeneration from alkalosis after re-administration of extracellular Cl^- **(b)** and the maximal pH_i change **(c)**. $-J(B^-/min)$ was calculated from the $\Delta pH/\Delta t$ obtained by linear regression analysis of pH_i measurements made over the first 60 sec. n = 219–230 ROIs/21 ducts/4 mice/groups. *: $p = 0.0002$ vs. Control using Mann–Whitney test, ns: $p = 0.2687$ vs. Control using Welch's *t*-test.

Next, we examined mRNA and protein expression of the major acid–base transporters using RT-qPCR and immunohistochemistry. Intra-interlobular pancreatic ducts were isolated from normal and diabetic mice and the expression of CFTR, anoctamin 1 (ANO-1), NHE-1 and -2, SLC26A3 and SLC26A6, NBCe1-B, and aquaporin 1, 5, and 8 (AQP1, -5, and -8) were measured (Fig. 5A). Among the transporters, the expression of CFTR, ANO-1, NHE-1, and AQP-1 mRNA was significantly increased in diabetes; however, no differences were observed in the expression of the other transporters. The results obtained by PCR were confirmed on the protein level (Fig. 5B and C) using fluorescence immunolabelling, which showed increased expression of CFTR, ANO-1, NHE-1 and AQP-1 in diabetic mice.

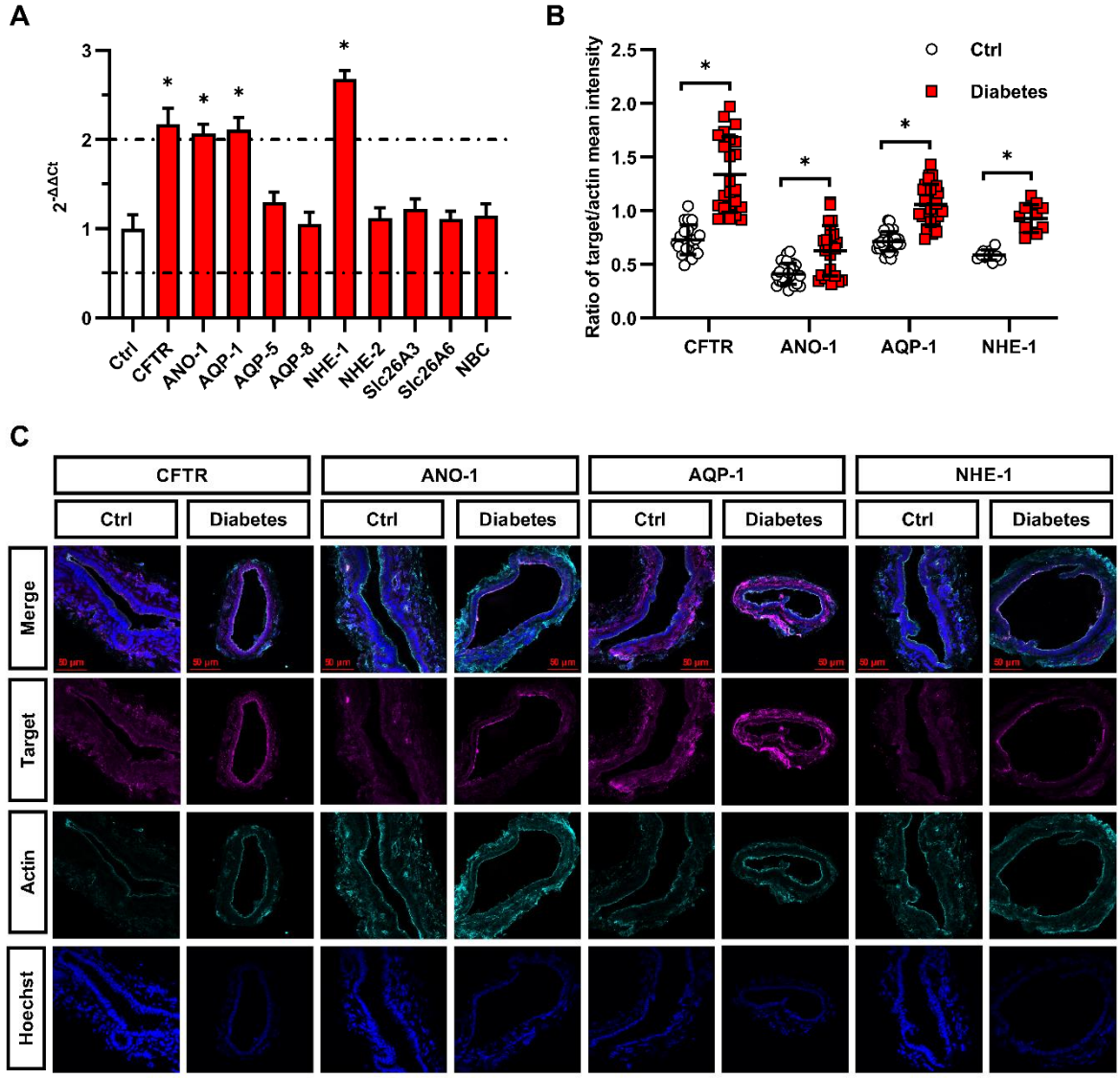

Figure 5. Effect of diabetes on the mRNA and protein expression of pancreatic ductal ion transporters. (**A**) Bars showing mRNA expression of ductal acid–base transporters. Genes with expression values ≤0.5 were considered to be downregulated, whereas values ≥2

were considered to be upregulated. (**C**) Representative images of fluorescence immunolabelling of pancreatic ducts showing the expression of CFTR, ANO-1, AQP-1, and NHE-1 (magenta), as well as beta-actin (cyan) in control and diabetic ducts. Nuclei (blue) were stained with Hoechst 33342. (**B**) Fluorescence signals were quantified and normalised to beta-actin as described in the Materials and Methods section. Data are shown as means ± SD. CFTR: n = 23 ROIs/8 ducts/4 mice/groups. *: $p < 0.0001$ vs. Control using Welch's *t*-test. ANO-1: n = 24–26 ROIs/6–7 ducts/3 mice/groups. *: $p < 0.0001$ vs. Control using Welch's *t*-test. AQP-1: n = 30–31 ROIs/8–9 ducts/3 mice/groups. *: $p = 0.0001$ vs. Control using Welch's *t*-test. NHE-1: n = 11 ROIs/3 ducts/2 mice/groups. *: $p < 0.0001$ vs. Control using Welch's *t*-test.

4.4. The central role of CFTR in diabetes-induced HCO_3^- secretion

The CFTR Cl^- channel plays an essential role in ductal HCO_3^- secretion. Its expression also increases in diabetes; thus we were curious how the activity of the channel changes under diabetic conditions. To estimate the activity of the channel, the Cl^--sensitive fluorescence dye, MQAE, and the specific CFTR activator, forskolin, were used (Fig. 6 A and B). Administration of 20 μM forskolin increased Cl^- efflux in the normal and diabetic mice; however, the increase was significantly higher in diabetes.

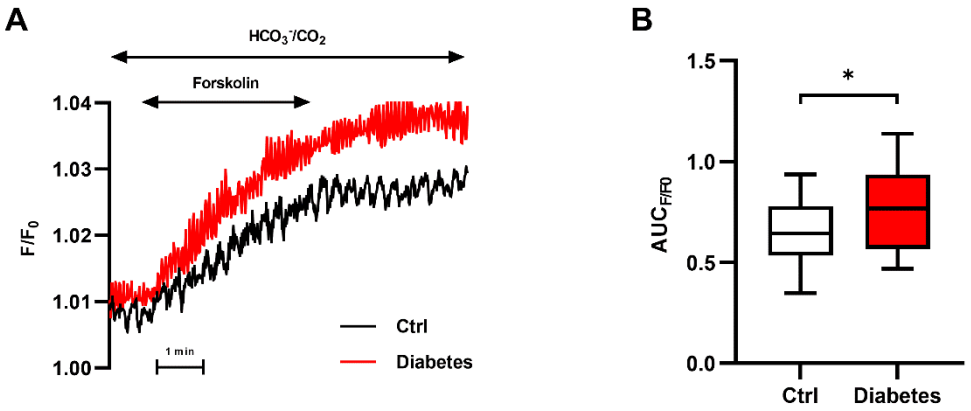

Figure 6. Effect of diabetes on the activity of CFTR. Intra-interlobular pancreatic ducts were isolated from control and diabetic mice and the rate of Cl^- efflux was estimated using a Cl^--sensitive fluorescence dye and the specific CFTR activator, forskolin (20 μM). (**A**) Representative fluorescence traces showing the effect of diabetes (red line) on the activity of CFTR in HCO_3^-/CO_2-buffered solution (**B**) The area under the curve was calculated for the first two minutes of forskolin stimulation. n = 42–77 ROIs/3–5 ducts/3 mice/groups. *: $p = 0.0053$ vs. Control using Mann–Whitney test.

To confirm the role of CFTR in diabetes-induced HCO_3^- secretion, we examined the activity of the Cl^-/HCO_3^- exchanger in the absence of CFTR, using CFTR KO mice. Diabetes was induced in both WT and CFTR KO mice, and the activity of the exchanger was assessed by the alkaline load technique (Fig. 7A). In the absence of CFTR, the rate of HCO_3^- secretion

was significantly reduced compared with the WT mice [3.2 ± 0.09 vs. 2.27 ± 0.1 $-J(B^-/min)$]. KO mice with induced diabetes also exhibited increased HCO_3^- secretion rates compared with their non-diabetic counterparts [3.01 ± 0.08 vs. 2.27 ± 0.1 $-J(B^-/min)$]; however, this increment fell short compared with that observed between diabetic and non-diabetic WT mice [3.01 ± 0.08 vs. 4.86 ± 0.14 $-J(B^-/min)$] and did not reach statistical significance. Interestingly, no difference was observed in the rate of regeneration from acidosis between WT and KO mice; however, in the absence of CFTR, the diabetes-induced activity of NHE and/or NBC was significantly decreased (11.4 ± 0.34 vs. 9.4 ± 0.32, Fig. 7B). Additionally, in CFTR KO mice, the rate of fluid secretion was far below that of WT (0.53 ± 0.08 vs. 1.19 ± 0.06, Fig. 7C). The presence of diabetes slightly increased the amount of fluid secretion in CFTR KO mice (0.84 ± 0.05 vs. 0.53 ± 0.17), but this did not reach statistical significance. Taken together, these results indicate that CFTR plays an important role in the increased fluid and HCO_3^- secretion induced by diabetes.

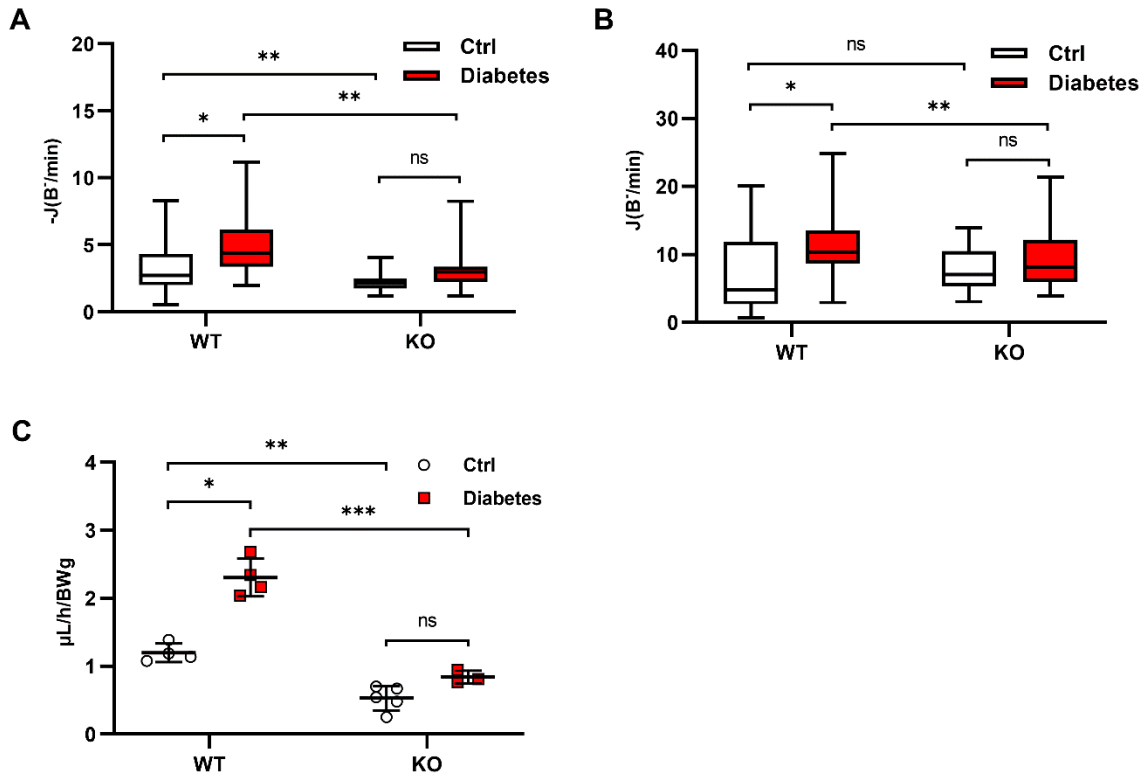

Figure 7. The role of CFTR in T1DM. Intra-interlobular pancreatic ducts were isolated from wild-type (WT) and CFTR knockout (KO) mice, both control and diabetic, and the activity of the acid/base transporters was measured by the NH_4Cl pre-pulse technique in HCO_3^-/CO_2-buffered solution. The rate of regeneration from alkalosis (**A**) reflects the activity of the Cl^-/HCO_3^- exchanger, whereas regeneration from acidosis (**B**) reflects the activity of the Na^+/H^+ exchanger and the Na^+/HCO_3^- cotransporter. n = 60–160 ROIs/5–13 ducts/3 mice/groups. *: $p < 0.0001$ vs. Control, **: $p \leq 0.0001$ vs. WT using Kruskal–

Wallis test. ns: p = 0.9799 vs. WT/Control and ns: p = 0.2723 vs. KO/Control. (**C**) Scatter plot showing the rate of *in vivo* pancreatic fluid secretion under secretin-stimulated (1 CU/kg) conditions in WT and CFTR KO mice, both control and diabetic. Data are shown as means ± SD. n = 3–5 mice/groups. *: p < 0.0001 vs. Control, **: p = 0.011 vs. WT, ***: p < 0.0001 vs. WT, using one-way ANOVA. ns: p = 0.1692 vs. KO/Control.

4.5. Effects of high glucose on the activity of acid/base transporters

The mechanism through which the functioning of transporters is increased in diabetes was examined. T1DM is often associated with hyperglycaemia; therefore, we determined the effect of acute and chronic glucose treatment on the activity of the transporters using the previously described alkaline load technique. During acute treatment, the isolated ducts were perfused with standard HCO_3^-/CO_2 solution containing 44.4 mM glucose, 8 minutes before the ammonia pulse, during the ammonia pulse, and 8 minutes after the ammonia pulse. During chronic treatment, the ducts were incubated in culture media supplemented with 44.4 mM glucose overnight and perfused only with solutions containing 44.4 mM glucose. Neither acute, nor chronic glucose administration showed difference in the rate of regeneration from alkalosis compared to control ducts (Fig. 8A a). However, chronic treatment increased the rate of recovery from acidosis, indicating that the activity of NHE-1 and/or NBCe1-B increases in response to chronic high glucose (Fig. 8A b). The activity of the Cl^-/HCO_3^- exchanger was also examined using the Cl^- withdrawal technique; however, neither the acute nor the chronic high glucose treatment caused any significant change in activity (Fig. 8B a) or maximal pH_i change (Fig. 8B b).

4.6. Plasma levels of secretin and cholecystokinin in diabetic mice

To determine whether hormonal effects are involved in the increased secretion observed, we measured the plasma levels of SCT and CCK (the main inducer hormones of pancreatic exocrine secretion) of diabetic mice. Secretin acts through the activation of the cAMP/PKA pathway and primarily targets PDECs, while CCK act through activating the Ca^{2+} signalisation pathway and primarily targets acinar cells. Neither plasma SCT nor CCK levels differed between the control and diabetic mice (Fig. 9A and B). Secretin was also examined in pancreatic homogenates, (Fig. 9C) in which we observed a slight, although not significant increase in diabetic animals. Finally, we examined whether there was a difference in the amount of ductal secretin receptors (SCTR). RT-qPCR revealed that the expression of SCTR was significantly increased in the intra-interlobular ducts isolated from diabetic mice compared with

the ducts isolated from control mice (Fig. 9D), however, we could not confirm this finding on the protein level using fluorescence immunolabelling (Fig. 9E and F).

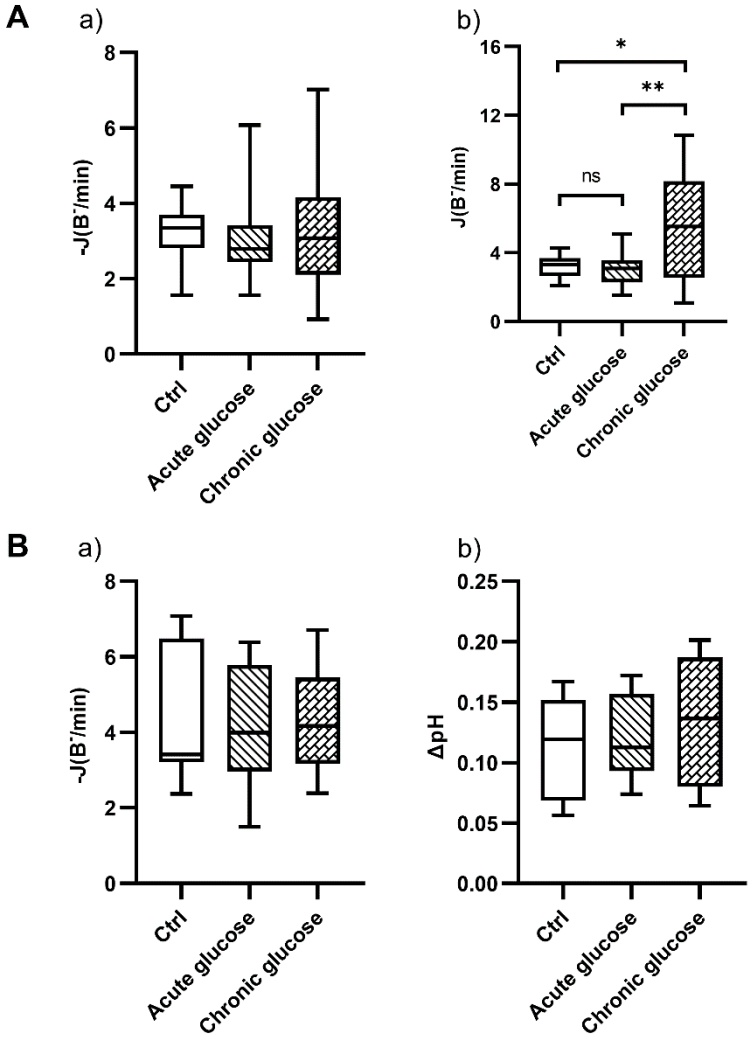

Figure 8. Effect of extracellular high glucose on the activity of ion transporters in isolated murine pancreatic ductal segments. Intra-interlobular pancreatic ducts isolated from WT mice were incubated with 44.4 mM glucose during the ammonia pulse (acute treatment) or overnight (chronic treatment). (**A**) Activity of the ion transporters was measured using the NH_4Cl pre-pulse technique. The rate of regeneration from alkalosis **(a**) reflects the activity of the Cl^-/HCO_3^- exchanger, whereas regeneration from acidosis **(b)** reflects the activity of the Na^+/H^+ exchanger and the Na^+/HCO_3^- cotransporter. n = 44–76 ROIs/3–5 ducts/3 mice/groups. For the regeneration from the alkaline load p = 0.2144 and 0.5524 vs. Control, p > 0.9999 vs. Acute glucose using Kruskal–Wallis test. For regeneration from the acidic load ns: p = 0.9702 and *: p = 0.0175 vs. Control, **: p < 0.0001 vs. Acute glucose using Kruskal–Wallis test. (**B**) Activity of the Cl^-/HCO_3^- exchanger was measured using the Cl^- withdrawal technique. Bar charts showing the rate of regeneration from alkalosis after re-administration of extracellular Cl^- **(a)** and the maximal pH_i change **(b)**. n = 44–60 ROIs/3–4 ducts/3 mice/groups. For the regeneration from the alkaline load

$p < 0.9999$. For pH_i change $p = 0.7677$ and 0.2583 vs. Control, $p > 0.9999$ vs. Acute glucose using Kruskal–Wallis test.

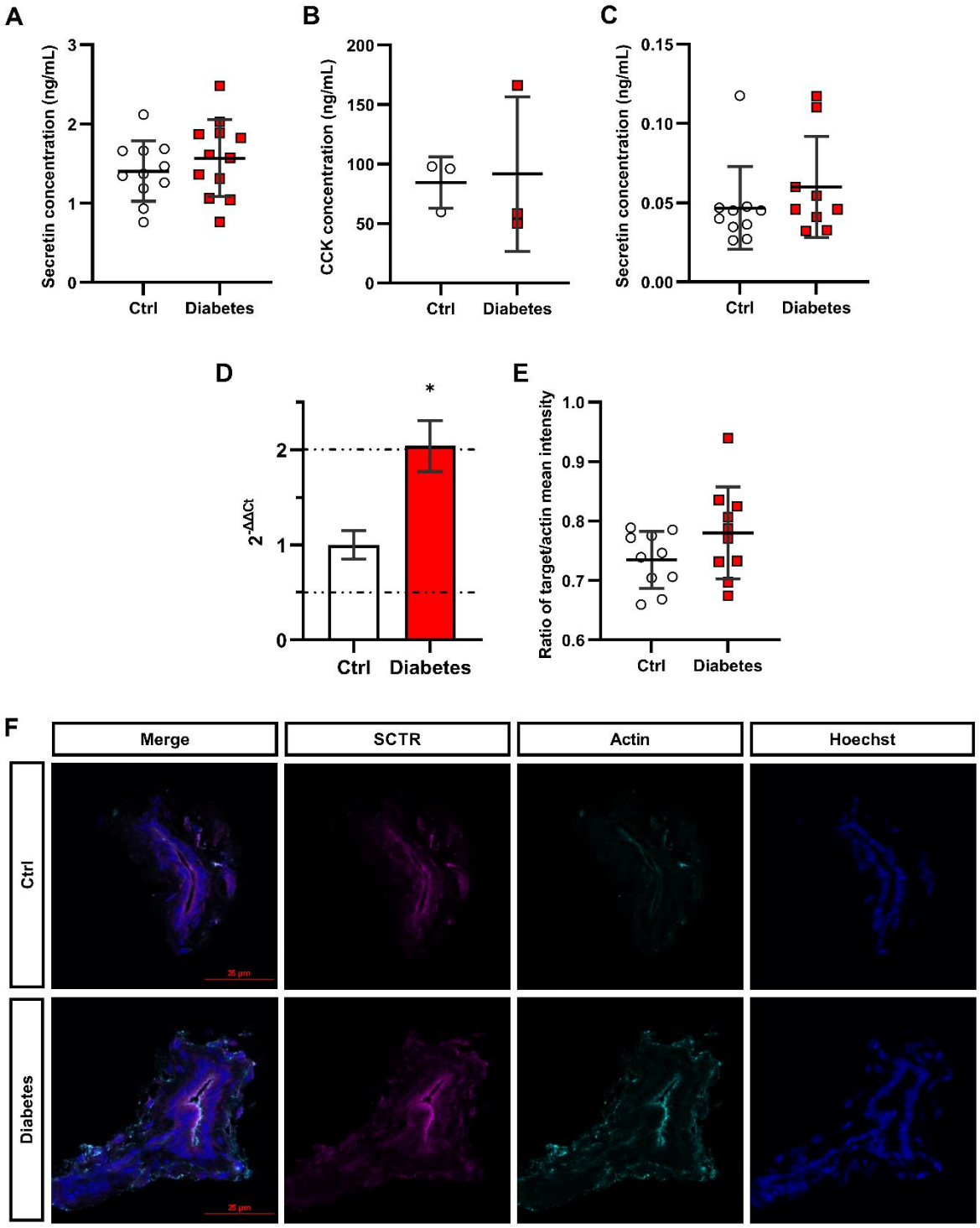

Figure 9. Effect of diabetes on secretin and cholecystokinin levels and the expression of secretin receptor. Plasma and pancreas homogenate were obtained from control and diabetic mice. The plasma levels of secretin (**A**) and cholecystokinin (**B**) and secretin content of the pancreas (**C**) were measured by ELISA. Data are shown as means ± SD. n = 3–12 mice/groups. $p = 0.3803$ for plasma secretin, $p = 0.3337$ for tissue secretin, and

p = 0.8689 for plasma cholecystokinin using two-sample t-test. Intra-interlobular pancreatic ducts were isolated from control and diabetic mice and the mRNA (**D**) and protein (**E** and **F**) expression of SCTR was measured by RT-qPCR and fluorescence immunolabelling respectively. mRNA expression values ≥2 were considered to be upregulated. Data are shown as means ± SD. For secretin protein expression n = 10 ROIs/4 ducts/2 mice/groups. p = 0.1311 using two-sample t-test.

4.7. Structural integrity of ducts in pancreatic TSs

Examination of sections from the head, body, and the tail of the pancreas revealed intact ductal morphology. Intra- and inter-lobular ducts of the head and the body (Fig. 10A and B) showed strong nuclear staining by Giemsa (Fig. 10), whereas weak or no staining was found in the tail (Fig. 10C). Blood vessels and acini remained unstained (Fig. 10E), indicating that injection of agarose affects only the ductal tree.

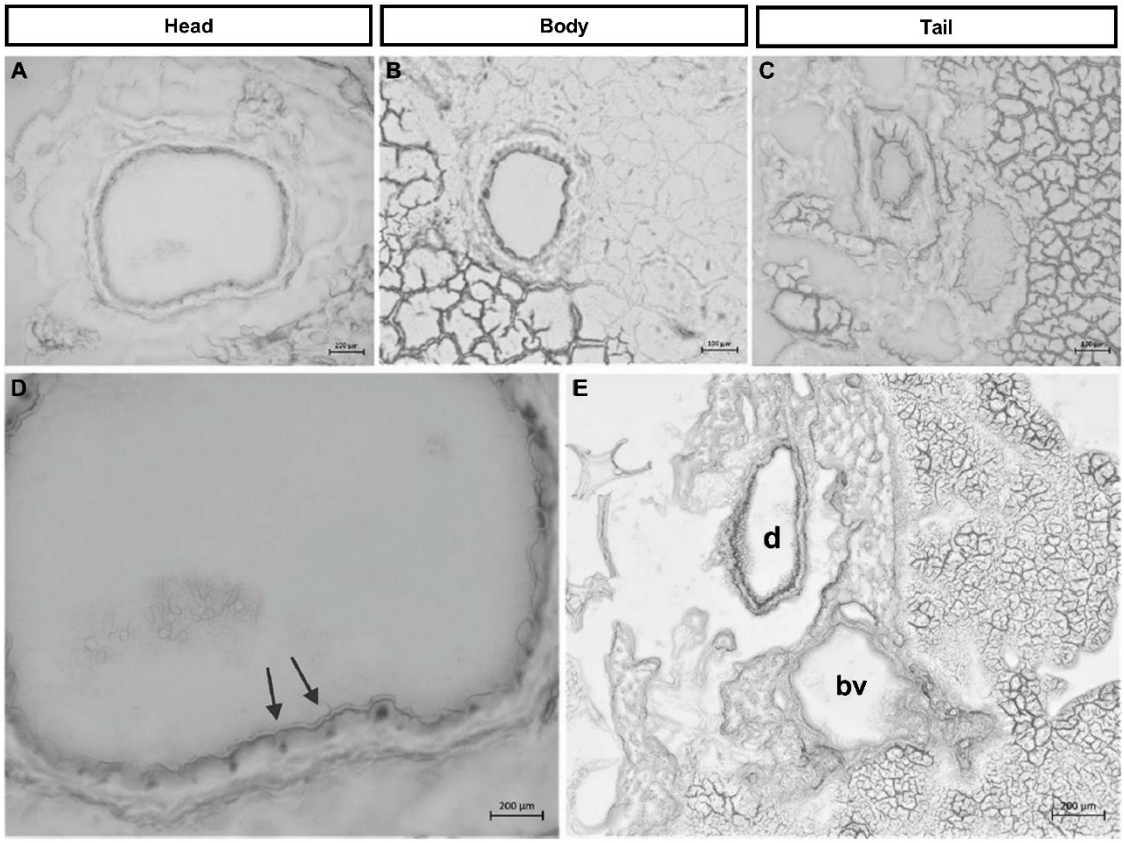

Figure 10. Examination of injection efficiency in agarose-injected pancreas tissue. (**A-C**) Serial sections of Giemsa-agarose injected pancreas, showing interlobular ducts from the head, body, and tail regions. (**D**) Arrows indicate strongly stained nuclei of PDECs. (**E**) Image showing Giemsa staining of a duct, but not blood vessel or surrounding acinar tissue.

Under normal conditions, CFTR is localized in the apical membrane of PDECs. Using fluorescence immunolabelling of CFTR, we were able to specifically stain the luminal

membrane of PDECs in the slice. As shown in Fig. 11, the luminal membrane showed strong CFTR staining and appeared structurally intact, suggesting normal functioning of PDECs.

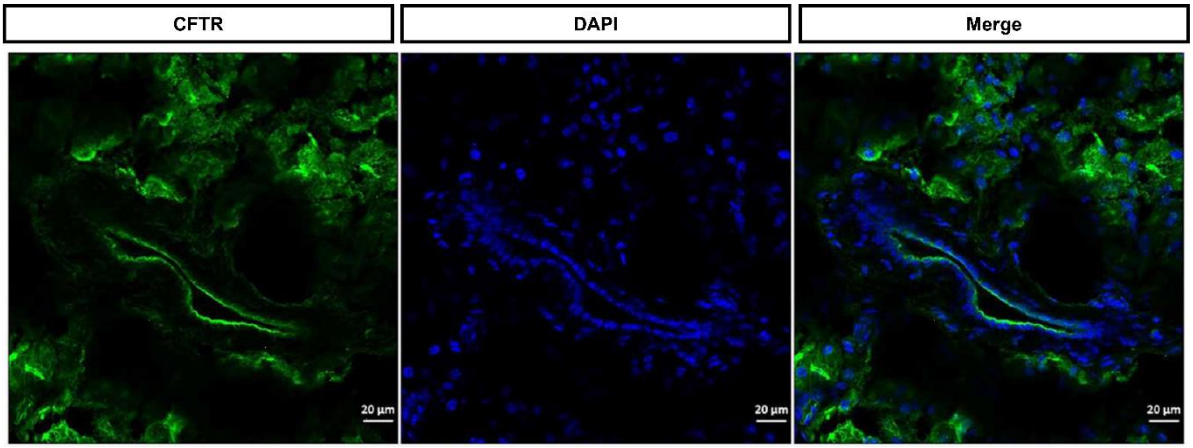

Figure 11. Investigation of ductal integrity in pancreas tissue slices. Fluorescence immunolabelling of CFTR (green) shows well defined apical localization. Nuclei were stained with DAPI (blue).

5. DISCUSSION

The negative long-term effects of diabetes on the exocrine pancreas are numerous; yet, our understanding of the underlying mechanisms is still incomplete, particularly regarding to PDECs. In the present study, we showed that the fluid and HCO_3^- secretion of ductal cells increases as a result of diabetes. This process likely involves activation and overexpression of CFTR, NHE-1, and possibly ANO-1.

First, we examined how T1DM affects the morphology of the exocrine and endocrine pancreas using electron microscopy. Acinar cells were identified by the presence of large, dark secretory granules and abundant endoplasmic reticulum and mitochondria. Islets were distinguished by the presence of cell clustering, smaller secretory granules and less endoplasmic reticulum. Ductal cells typically have large nuclei and the cells enclose a lumen, with cilia present on the apical membrane of the cells. The most characteristic difference between the normal and diabetic pancreas was the morphological change of mitochondria in acinar cells, which had a rounder, less elongated shape in diabetes. Additionally, enlargement of the mitochondria and disruption of the inner membrane structure were also observed. Similar results were observed in the intermediate cells (characterised by containing both zymogen and hormone storage granules) of T1DM patients and in the beta cells of T2DM patients.[117,118] In contrast to acini, ductal mitochondria remained mostly intact. Mitochondria play an important role in maintaining the normal energy production and balance of the cells, therefore, damage of acinar mitochondria probably contributes to the development of PEI. At the same time, the morphology of ductal cells remained largely unaltered, which suggests that ductal functions are preserved in T1DM.

The most important function of pancreatic ductal epithelium is the production a HCO_3^--rich luminal fluid, which conveys the digestive enzymes and counteracts the acid produced by the stomach and acini[26,27]. Using *in vivo* and *in vitro* approaches, we demonstrated that the amount of pancreatic fluid was significantly increased in streptozotocin-induced diabetic mice. This was observed under both basal conditions and under stimulation of the cAMP/PKA pathway by forskolin or SCT, suggesting an increased activation of CFTR, and suggesting that the sensitivity of stimulated ductal fluid secretion to SCT is also increased.

The rate of fluid secretion primarily depends on the rate of HCO_3^- secretion, and therefore, on the activity of ductal ion transporters. The major route for HCO_3^- secretion in the ductal cells is the apically localized Cl^-/HCO_3^- exchanger, SLC26A6, which mediates the electrogenic exchange of 1 Cl^- and 2 HCO_3^-.[119] Using the alkaline load method, we found that

the activity of the Cl^-/HCO_3^- exchanger is increased in diabetes. This was also confirmed by the Cl^- withdrawal technique, which allows for the direct measurement of exchanger activity. Similarly to the alkaline load method, the exchanger showed increased activity in diabetes, at least in normal mode. Interestingly, there was no difference in the degree of alkalosis, nor in the maximum pH_i change between control and the diabetic ducts, which suggests that the activity of the exchanger in reverse mode is not affected by diabetes. However, it is also possible that the increased HCO_3^- efflux, (but not influx) is mediated by CFTR, which becomes activated by WNK1 if $[Cl^-]_i$ drops under 10 mM.[44]

Because the CFTR Cl^- channel and the Cl^-/HCO_3^- exchanger interact with each other through NHERs and are mutually regulated, we measured the activity of CFTR using the Cl^- sensitive fluorescent dye, MQAE, and forskolin, which induces CFTR by activating AC. The increase in MQAE fluorescence intensity is inversely proportional to $[Cl^-]_i$, because the dye is quenched by Cl^-. We detected increased CFTR activity in diabetic ducts, which most probably contributes to the increased rate of HCO_3^- secretion.

The alkaline load technique also enables the investigation of alkalizing transporters by measuring the rate of regeneration from acidosis. We observed a significant increase in acidic recovery similarly to the alkaline recovery, indicating that the activity of alkalizing transporters was also increased as a result of diabetes. In ductal cells, the major alkalizing transporters are the basolateral NHE-1 and NBCe1-B. NHE-1 is an electroneutral transporter that mediates the exchange of intracellular H^+ to extracellular Na^+, whereas NBCe1-B is an electrogenic co-transporter, conveying 1 Na^+ and 2 HCO_3^-. Both transporters use the electrochemical driving force of Na^+ maintained by the Na^+/K^+ ATPase pump. During ductal HCO_3^- secretion, both transporters promote the intracellular accumulation of HCO_3^-. NBCe1-B transports HCO_3^- into the cell, whereas NHE removes H^+, a by-product of CA activity. Consequently, if the activity of the anion exchanger increases, it must be supported by the increased activity of NHE-1 and NBCe1-B, as confirmed by our experiments.

To identify the mechanism responsible for increased transporter activity in diabetes, we first tested the expression of the major acid–base transporters. We found that both the mRNA and protein expression of CFTR was significantly increased in diabetic ducts, which may partly explain increased CFTR activity. We also found that other acid–base transporters involved in ductal HCO_3^- secretion are overexpressed as well. Among the NHEs, increased NHE-1 expression was also observed in diabetic ducts, however, we did not find alterations in the expression of NBCe1-B. This may indicate that during increased secretion in diabetes, a substantial proportion of intracellular HCO_3^- is accumulated via the activity of CA and NHE-1,

rather than NBCe1-B; although, this rout is more ATP demanding, while at the same time, access to energy is more limited in diabetes due to hypoinsulinaemia.

Among the SLC26 anion exchangers, SLC26A3 and SLC26A6 isoforms are present in the apical membrane of PDECs and play major role in ductal HCO_3^- secretion.[120] Although our functional experiments revealed increased Cl^-/HCO_3^- exchange activity in diabetes, we found no difference in the expression of SLC26A3 and SLC26A6 compared to the control. This means that increased anion exchange activity probably occurs due to increased activation of SLC26A3 and SLC26A6 by CFTR, rather than overexpression of the exchangers.

We also examined AQP isoforms present in the pancreas (AQP-1, -5 and -8) and found that the expression of AQP-1 was also increased in diabetes. AQP-1 is a constitutively expressed water channel and its presence on the plasma membrane of centroacinar cells and interlobular ducts has been demonstrated.[23,58] AQP-1 facilitates transcellular water movement and, as the major water channel on ductal cells, it is responsible for most of the volume of the pancreatic juice.[120] The overexpression of AQP-1 in diabetes is probably a compensatory mechanism for increased anion secretion because transcellular ion movements are osmotically followed by water. Therefore, increased AQP-1 expression may partly explain increased volume of fluid secretion in diabetes.

An exciting finding of ours is that the Ca^{2+}-activated Cl^- channel, ANO-1, is also expressed in PDECs. ANO-1 exhibits multiple cellular functions in the body and its presence has been confirmed in salivary and pancreatic acini[121–123] Although, the presence of a Ca^{2+}-activated Cl^- current has been described in pancreatic ductal cells,[124,125] the molecular identity of this channel remained undetermined. Our study is the first to demonstrate the presence of ANO-1 on the luminal membrane of murine PDECs. The antibody we used is directed against the third extracellular loop of mouse ANO-1 and has been shown to be highly specific against the protein.[126] Activation of ANO-1 is triggered by divalent cations – mainly Ca^{2+} – which can be antagonized by Mg^{2+}.[127] Several signals have been described to activate the channel, such as extracellular ATP, decrease of pH_i, and heat stress.[121] Since increase in $[Ca^{2+}]_i$ leads to the activation of the channel in acinar cells and salivary ducts,[120] it is conceivable that the channel becomes activated in pancreatic ductal cells through the Ca^{2+}-signalisation pathway. Both murine and human PDECs show relatively large Ca^{2+}-activated Cl^- current density,[21,128] and some of the major secretagogues of PDECs (e.g. acetylcholine and CCK) act through the Ca^{2+}-signalisation pathway.[37] Furthermore, the ion selectivity ANO-1 can shift from Cl^- to HCO_3^- by modulation of its pore size, similarly to CFTR.[45,129] Therefore, we hypothesize that in addition to CFTR, ANO-1 also functions in close co-ordination with apical transporters and

acts as an alternative pathway for HCO_3^-, as has been shown in acinar cells.[129] We also found that diabetes increases the expression of ANO-1, therefore, it may also contribute to increased HCO_3^- secretion. In the end however, further functional studies are needed to clarify the role of ductal ANO-1 in pancreatic fluid secretion. Our results indicate that the increased expression of CFTR, ANO-1, and NHE-1 stimulates Cl^-/HCO_3^- exchange. This suggests that finding methods which induce upregulation of these transporters may prompt the development of new therapies in the treatment of CF or acute and chronic pancreatitis.

The central role of CFTR in the increased ductal secretory activity was further confirmed by our results produced in CFTR KO mice. As expected, both fluid and HCO_3^- secretion were significantly decreased in the ducts of CFTR KO mice. When diabetes was induced in KO mice, there was a small increase in both fluid and HCO_3^- secretion, but was not statistically significant. This indicates that the presence of functionally active CFTR is essential for the stimulatory effect of diabetes on ductal secretion. Yet, the small increase observed in diabetic CFTR KO animals may indicate that the activity of other apical transporters, like ANO-1 and the Cl^-/HCO_3^- exchangers, are also affected by diabetes.

In our subsequent experiments we sought to identify the stimuli responsible for the increased activity/expression of transporters observed in diabetes. A notable factor affecting ion transport mechanisms – in the renal proximal tubules and also in pancreatic ducts[85,130] – in T1DM is hyperglycaemia. Therefore, we tested the effect of acute introduction and 12 h incubation of high glucose treatment on transporter activity. The concentration of glucose was selected based on a previous report.[85] Using the alkaline load and Cl^--withdrawal techniques, we found that neither acute, nor chronic glucose treatment affected anion exchange activity. However, chronic glucose treatment did increase the rate of regeneration from acidosis, which suggests that hyperglycaemia directly increases the activity of NHE-1 and/or NBCe1-B. Previous studies showed that high extracellular glucose increases NHE-1 activity in distal nephron cells, vascular myocytes, and lymphoblasts of patients with diabetic nephropathy.[131–133] These studies suggest that glucose-induced NHE-1 activity regulated by protein kinase C or the Mek/Erk1/2/p90(RSK) and p38MAPK pathways, depending on the cell type. In the present study, we did not identify the mechanism by which high extracellular glucose stimulates NHE-1, although the results suggest that the stimulatory effect of diabetes on HCO_3^- secretion may involve increased NHE-1 activity. Somewhat paradoxically, the previous work of Futakuchi *et al*. showed that high extracellular glucose, present during hyperglycaemia, increases apical SGLT1 activity, which increases $[Na^+]_i$.[85] This in turn may inhibit efficient NHE function.

Another way by which ductal fluid and HCO_3^- secretion may increase in diabetes is the altered response to major secretagogues, like SCT and CCK. SCT is the primary hormone influencing the rate of HCO_3^- secretion in PDECs. Activation of basolateral SCTRs increases intracellular cAMP levels, which activate PKA. PKA subsequently activates CFTR and SLC26 anion exchangers and inhibits NHE-3 and NBCn1 within NHER-linked functional complexes, thereby inducing apical HCO_3^- transport in PDECs.[46–51] CCK, produced mainly by enteroendocrine I-cells, acts on CCKBR and induces elevation of intracellular Ca^{2+} levels in PDECs.[37] Through the Ca^{2+} signalisation pathway, CCK can potentiate SCT-induced HCO_3^- secretion mainly by activating IRBIT,[40,41] but also by potentially activating the Ca^{2+}-dependent AC and Ca^{2+}-activated Cl^- channels, like ANO-1.[38,39] We found no changes in plasma SCT and CCK levels, which suggest that T1DM probably does not affect the secretory activity of duodenal S-cells and enteroendocrine I-cells. However, we found that mRNA expression of SCTR is significantly increased in the ducts of diabetic mice. An increase was also observed on the protein level, but was not significant. We speculate that secretin exerts a greater stimulatory effect on ductal cells in mice with induced T1DM, however, further studies are needed to confirm this hypothesis.

In the second part of this thesis, we examined whether the acute pancreas slice technique is suitable for the functional examination of ductal cells. Giemsa staining of nuclei of PDECs, but not other structures within the pancreatic TS shows that the injected agarose gel is retained inside the ducts. Furthermore, based on the examination of pancreatic sections, the gel travels as far as the interlobular ducts of the body of the murine pancreas. The rupture of ducts and gel leakage would result agarose lumps in the tissue and would prevent appropriate gel distribution inside the ductal tree, ultimately resulting in poor tissue support during microtomy.

In a physiological state, CFTR is transferred to the apical membrane, indicated by well-defined apical staining of PDECs. The folding of CFTR is relatively complicated compared to other proteins and the maturation efficiency of even WT CFTR is only ~30%.[134] Due to toxic substances or pathological conditions like chronic pancreatitis, CFTR accumulates in the endoplasmic reticulum and shows cytoplasmic localization.[135,136] Therefore, the apical localization of CFTR on PDECs within the pancreatic TS is probably reflective of undisturbed cellular physiology, which was confirmed also by functional experiments.[137] Finally, we conclude that the structure and function of PDECs is preserved in the pancreatic TS and that this model is suitable for the study of PDECs and their interactions.

6. CONCLUSION AND NOVEL FINDINGS

In conclusion, our results demonstrate that the stimulatory effect of T1DM on ductal HCO_3^- secretion is a complex and multifactorial process. The activity of the SLC26 anion exchangers is enhanced by the upregulated expression of ductal acid–base transporters, particularly CFTR and NHE-1. Additionally, high extracellular glucose stimulates alkalizing transporters, such as NHE-1, which may also contribute to increased secretion. Furthermore, because ANO-1 is present in PDECs and its expression is upregulated in T1DM, it may also be involved in increased secretion. The role of increased ductal secretion in T1DM, and whether it is a temporary or permanent condition, is not known. Based on clinical studies, the most accepted view is that exocrine functions are mostly impaired by long-standing diabetes. An explanation for this is that the stimulatory effect of insulin is absent in T1DM. On the other hand, our study showed that ductal secretion increases as a result of diabetes, at least in the initial stage. This would not be unprecedented, since patients with diabetic kidney disease initially exhibit increased glomerular filtration rate to compensate for decreased Na^+ delivery due to hyperglycaemia. As the disease progresses over time, glomerular filtration rates slowly decline.[107,130,138–140] Therefore, we propose that increased ductal HCO_3^- secretion serves as a protective mechanism in T1DM and therefore represents a potential therapeutic target for the prevention or treatment of diabetes. Although this hypothesis is promising, further studies are needed in this area.

Our main novel findings are that

I. STZ-induced T1DM has a stimulatory effect on ductal fluid and HCO_3^- secretion,

II. the activity of the SLC26 anion exchangers is enhanced in T1DM due to upregulated expression of ductal acid–base transporters, mainly CFTR and NHE-1,

III. high extracellular glucose stimulates alkalizing transporters, such as NHE-1,

IV. ANO-1 is present in PDECs and its expression is upregulated in T1DM,

V. the acute pancreas tissue slice is a suitable model for the study of PDECs.

7. ACKNOWLEDGEMENTS

I would first like to express my gratitude to my supervisor, **Dr. Viktória Venglovecz**, for her exceptional guidance and support, and for giving me the opportunity to greatly expand my knowledge through a plethora of collaborations, conference meetings, and lab visits both abroad and within the country. To me, her ability to solve problems with great calmness stands as an extraordinary example to follow.

I thank to **Professor Dr. István Baczkó** and **Professor Dr. András Varró,** current and former head of department, the opportunity to acquire my PhD in the Department of Pharmacology and Pharmacotherapy of Albert Szent-Györgyi Medical School, University of Szeged.

I thank to **Professor Dr. Péter Hegyi** his professional support and advices throughout my work.

For the collaboration, I would like to express my great pleasure to all the co-authors of the published articles at the Department of Pharmacology and Pharmacotherapy, the Department of Internal Medicine, the Translational Pancreatology Research Group, Department of Pathology, and the Faculty of Medicine of the University of Maribor, with special thanks to **Emese Tóth** and **Eleonóra Gál**.

I would also like to thank to **Gabriella Fűr**, **Tünde Pritz**, **Miklósné Árva**, **Edit Magyarné Pálfi**, **Zsolt Tóth**, **Margaréta Korsós**, and all my colleagues their indispensable help and contribution.

I am grateful for the financial support of the CF-Trust CFRD-SRC Grant (No.: SRC 007), the National Research, Development, and Innovation Office (SNN134497) and EFOP 3.6.2-16-2017-00006).

I owe warm thanks to my parents, **Attila Ébert** and **Gabriella Godár**, and my grandparents, **Mária Kovács** and **József Ébert** for their teachings and support during my long years of work.

Lastly, I am most grateful to my wife, **Réka Molnár**, for her endless support and encouragement, and for accompanying me through both progress and throw-back. This thesis would have never been prepared without her.

8. REFERENCES

1. Talathi SS, Zimmerman R, Young M. Anatomy, Abdomen and Pelvis, Pancreas. In: *StatPearls*. StatPearls Publishing; 2024. Accessed May 7, 2024. http://www.ncbi.nlm.nih.gov/books/NBK532912/

2. Love JA, Yi E, Smith TG. Autonomic pathways regulating pancreatic exocrine secretion. *Auton Neurosci*. 2007;133(1):19-34. doi:10.1016/j.autneu.2006.10.001

3. Neural Control of the Pancreas. doi:10.3998/panc.2016.27

4. Rodriguez-Diaz R, Speier S, Molano RD, et al. Noninvasive in vivo model demonstrating the effects of autonomic innervation on pancreatic islet function. *Proc Natl Acad Sci U S A*. 2012;109(52):21456-21461. doi:10.1073/pnas.1211659110

5. Dolenšek J, Pohorec V, Rupnik MS, Stožer A. Pancreas Physiology. In: Seicean A, ed. *Challenges in Pancreatic Pathology*. InTech; 2017. doi:10.5772/65895

6. Brissova M, Fowler MJ, Nicholson WE, et al. Assessment of Human Pancreatic Islet Architecture and Composition by Laser Scanning Confocal Microscopy. *J Histochem Cytochem*. 2005;53(9):1087-1097. doi:10.1369/jhc.5C6684.2005

7. Suckale J. Pancreas islets in metabolic signaling - focus on the beta-cell. *Front Biosci*. 2008;Volume(13):7156. doi:10.2741/3218

8. MacDonald PE, Rorsman P. Oscillations, Intercellular Coupling, and Insulin Secretion in Pancreatic β Cells. *PLoS Biol*. 2006;4(2):e49. doi:10.1371/journal.pbio.0040049

9. Benninger RKP, Zhang M, Head WS, Satin LS, Piston DW. Gap Junction Coupling and Calcium Waves in the Pancreatic Islet. *Biophys J*. 2008;95(11):5048-5061. doi:10.1529/biophysj.108.140863

10. Briant L, Salehi A, Vergari E, Zhang Q, Rorsman P. Glucagon secretion from pancreatic α-cells. *Ups J Med Sci*. 2016;121(2):113-119. doi:10.3109/03009734.2016.1156789

11. Wendt A, Eliasson L. Pancreatic α-cells – The unsung heroes in islet function. *Semin Cell Dev Biol*. 2020;103:41-50. doi:10.1016/j.semcdb.2020.01.006

12. Rorsman P, Huising MO. The somatostatin-secreting pancreatic δ-cell in health and disease. *Nat Rev Endocrinol*. 2018;14(7):404-414. doi:10.1038/s41574-018-0020-6

13. Stefan Y, Orci L, Malaisse-Lagae F, Perrelet A, Patel Y, Unger RH. Quantitation of Endocrine Cell Content in the Pancreas of Nondiabetic and Diabetic Humans. *Diabetes*. 1982;31(8):694-700. doi:10.2337/diab.31.8.694

14. Rahier J, Goebbels RM, Henquin JC. Cellular composition of the human diabetic pancreas. *Diabetologia*. 1983;24(5). doi:10.1007/BF00251826

15. Pancreatic Polypeptide. doi:10.3998/panc.2014.4

16. Andralojc KM, Mercalli A, Nowak KW, et al. Ghrelin-producing epsilon cells in the developing and adult human pancreas. *Diabetologia*. 2009;52(3):486-493. doi:10.1007/s00125-008-1238-y

17. Tong J, Prigeon RL, Davis HW, et al. Ghrelin Suppresses Glucose-Stimulated Insulin Secretion and Deteriorates Glucose Tolerance in Healthy Humans. *Diabetes*. 2010;59(9):2145-2151. doi:10.2337/db10-0504

18. DiGruccio MR, Mawla AM, Donaldson CJ, et al. Comprehensive alpha, beta and delta cell transcriptomes reveal that ghrelin selectively activates delta cells and promotes somatostatin release from pancreatic islets. *Mol Metab*. 2016;5(7):449-458. doi:10.1016/j.molmet.2016.04.007

19. Lifson N, Kramlinger KG, Mayrand RR, Lender EJ. Blood flow to the rabbit pancreas with special reference to the islets of Langerhans. *Gastroenterology*. 1980;79(3):466-473.

20. Bendayan M. Morphometrical and immunocytochemical characterization of peri-insular and tele-insular acinar cells in the rat pancreas. *Eur J Cell Biol*. 1985;36(2):263-268.

21. Argent BE, Gray MA, Steward MC, Case RM. Cell Physiology of Pancreatic Ducts. In: *Physiology of the Gastrointestinal Tract*. Elsevier; 2012:1399-1423. doi:10.1016/B978-0-12-382026-6.00051-8

22. Petersen OH. Physiology of Acinar Cell Secretion. In: Beger HG, Warshaw AL, Hruban RH, et al., eds. *The Pancreas*. 1st ed. Wiley; 2018:41-55. doi:10.1002/9781119188421.ch4

23. Burghardt B. Distribution of aquaporin water channels AQP1 and AQP5 in the ductal system of the human pancreas. *Gut*. 2003;52(7):1008-1016. doi:10.1136/gut.52.7.1008

24. Marino CR, Jeanes V, Boron WF, Schmitt BM. Expression and distribution of the Na^+ - HCO_3^- cotransporter in human pancreas. *Am J Physiol-Gastrointest Liver Physiol*. 1999;277(2):G487-G494. doi:10.1152/ajpgi.1999.277.2.G487

25. Crawford I, Maloney PC, Zeitlin PL, et al. Immunocytochemical localization of the cystic fibrosis gene product CFTR. *Proc Natl Acad Sci*. 1991;88(20):9262-9266. doi:10.1073/pnas.88.20.9262

26. Hegyi P, Maléth J, Venglovecz V, Rakonczay Z. Pancreatic Ductal Bicarbonate Secretion: Challenge of the Acinar Acid Load. *Front Physiol*. 2011;2. doi:10.3389/fphys.2011.00036

27. Hegyi P, Pandol S, Venglovecz V, Rakonczay Z. The acinar-ductal tango in the pathogenesis of acute pancreatitis. *Gut*. 2011;60(4):544-552. doi:10.1136/gut.2010.218461

28. Kimura N, Yonekura H, Okamofo H, Nagura H. Expression of human regenerating gene mRNA and its product in normal and neoplastic human pancreas. *Cancer*. 1992;70(7):1857-1863. doi:10.1002/1097-0142(19921001)70:7<1857::AID-CNCR2820700708>3.0.CO;2-8

29. Bertelli E, Bendayan M. Association between Endocrine Pancreas and Ductal System. More than an Epiphenomenon of Endocrine Differentiation and Development? *J Histochem Cytochem*. 2005;53(9):1071-1086. doi:10.1369/jhc.5R6640.2005

30. Hayden MR, Patel K, Habibi J, et al. Attenuation of Endocrine-Exocrine Pancreatic Communication in Type 2 Diabetes: Pancreatic Extracellular Matrix Ultrastructural Abnormalities. *J Cardiometab Syndr*. 2008;3(4):234-243. doi:10.1111/j.1559-4572.2008.00024.x

31. Shiratori K, Shimizu K. Insulo–Acinar Relationship. In: Beger HG, Warshaw AL, Hruban RH, et al., eds. *The Pancreas*. 1st ed. Wiley; 2018:123-131. doi:10.1002/9781119188421.ch12

32. Murakami T, Hitomi S, Ohtsuka A, Taguchi T, Fujita T. Pancreatic insulo-acinar portal systems in humans, rats, and some other mammals: Scanning electron microscopy of vascular casts. *Microsc Res Tech*. 1997;37(5-6):478-488. doi:10.1002/(SICI)1097-0029(19970601)37:5/6<478::AID-JEMT10>3.0.CO;2-N

33. Lifson N, Lassa CV. Note on the blood supply of the ducts of the rabbit pancreas. *Microvasc Res*. 1981;22(2):171-176. doi:10.1016/0026-2862(81)90086-8

34. Molecular Mechanisms of Pancreatic Bicarbonate Secretion. doi:10.3998/panc.2020.06

35. Steward MC, Ishiguro H, Case RM. MECHANISMS OF BICARBONATE SECRETION IN THE PANCREATIC DUCT. *Annu Rev Physiol*. 2005;67(1):377-409. doi:10.1146/annurev.physiol.67.031103.153247

36. Schaffalitzky De Muckadell OB, Fahrenkrug J, Nielsen J, Westphall I, Worning H. Meal-Stimulated Secretin Release in Man: Effect of Acid and Bile. *Scand J Gastroenterol*. 1981;16(8):981-988. doi:10.3109/00365528109181015

37. Szalmay G, Varga G, Kajiyama F, et al. Bicarbonate and fluid secretion evoked by cholecystokinin, bombesin and acetylcholine in isolated guinea-pig pancreatic ducts. *J Physiol*. 2001;535(3):795-807. doi:10.1111/j.1469-7793.2001.00795.x

38. Jung J, Lee MG. Role of calcium signaling in epithelial bicarbonate secretion. *Cell Calcium*. 2014;55(6):376-384. doi:10.1016/j.ceca.2014.02.002

39. Willoughby D, Cooper DMF. Organization and Ca2+ regulation of adenylyl cyclases in cAMP microdomains. *Physiol Rev*. 2007;87(3):965-1010. doi:10.1152/physrev.00049.2006

40. Park S, Shcheynikov N, Hong JH, et al. Irbit Mediates Synergy Between Ca2+ and cAMP Signaling Pathways During Epithelial Transport in Mice. *Gastroenterology*. 2013;145(1):232-241. doi:10.1053/j.gastro.2013.03.047

41. Yang D, Shcheynikov N, Zeng W, et al. IRBIT coordinates epithelial fluid and HCO3-secretion by stimulating the transporters pNBC1 and CFTR in the murine pancreatic duct. *J Clin Invest*. 2009;119(1):193-202. doi:10.1172/JCI36983

42. Vachel L, Shcheynikov N, Yamazaki O, et al. Modulation of Cl^- signaling and ion transport by recruitment of kinases and phosphatases mediated by the regulatory protein IRBIT. *Sci Signal*. 2018;11(554):eaat5018. doi:10.1126/scisignal.aat5018

43. Liu F, Zhang Z, Csanády L, Gadsby DC, Chen J. Molecular Structure of the Human CFTR Ion Channel. *Cell*. 2017;169(1):85-95.e8. doi:10.1016/j.cell.2017.02.024

44. Kim Y, Jun I, Shin DH, et al. Regulation of CFTR Bicarbonate Channel Activity by WNK1: Implications for Pancreatitis and CFTR-Related Disorders. *Cell Mol Gastroenterol Hepatol*. 2020;9(1):79-103. doi:10.1016/j.jcmgh.2019.09.003

45. Jun I, Cheng MH, Sim E, et al. Pore dilatation increases the bicarbonate permeability of CFTR, ANO1 and glycine receptor anion channels. *J Physiol*. 2016;594(11):2929-2955. doi:10.1113/JP271311

46. Ko SBH, Zeng W, Dorwart MR, et al. Gating of CFTR by the STAS domain of SLC26 transporters. *Nat Cell Biol*. 2004;6(4):343-350. doi:10.1038/ncb1115

47. Lohi H, Lamprecht G, Markovich D, et al. Isoforms of SLC26A6 mediate anion transport and have functional PDZ interaction domains. *Am J Physiol-Cell Physiol*. 2003;284(3):C769-C779. doi:10.1152/ajpcell.00270.2002

48. Ko SBH. A molecular mechanism for aberrantCFTR-dependent HCO3- transport in cystic fibrosis. *EMBO J*. 2002;21(21):5662-5672. doi:10.1093/emboj/cdf580

49. Ahn W, Kim KH, Lee JA, et al. Regulatory Interaction between the Cystic Fibrosis Transmembrane Conductance Regulator and HCO 3 − Salvage Mechanisms in Model Systems and the Mouse Pancreatic Duct. *J Biol Chem*. 2001;276(20):17236-17243. doi:10.1074/jbc.M011763200

50. Park M, Ko SBH, Choi JY, et al. The Cystic Fibrosis Transmembrane Conductance Regulator Interacts with and Regulates the Activity of the HCO 3 − Salvage Transporter Human Na+-HCO 3 − Cotransport Isoform 3. *J Biol Chem*. 2002;277(52):50503-50509. doi:10.1074/jbc.M201862200

51. Luo X, Choi JY, Ko SBH, et al. HCO 3 − Salvage Mechanisms in the Submandibular Gland Acinar and Duct Cells. *J Biol Chem*. 2001;276(13):9808-9816. doi:10.1074/jbc.M008548200

52. Fanjul M, Salvador C, Alvarez L, Cantet S, Hollande E. Targeting of carbonic anhydrase IV to plasma membranes is altered in cultured human pancreatic duct cells expressing a mutated (ΔF508) CFTR. *Eur J Cell Biol*. 2002;81(8):437-447. doi:10.1078/0171-9335-00264

53. Choi JY, Muallem D, Kiselyov K, Lee MG, Thomas PJ, Muallem S. Aberrant CFTR-dependent HCO-3 transport in mutations associated with cystic fibrosis. *Nature*. 2001;410(6824):94-97. doi:10.1038/35065099

54. Lee MG, Choi JY, Luo X, Strickland E, Thomas PJ, Muallem S. Cystic Fibrosis Transmembrane Conductance Regulator Regulates Luminal Cl−/HCO3−Exchange in Mouse Submandibular and Pancreatic Ducts. *J Biol Chem*. 1999;274(21):14670-14677. doi:10.1074/jbc.274.21.14670

55. Lee MG, Wigley WC, Zeng W, et al. Regulation of Cl−/ HCO3−Exchange by Cystic Fibrosis Transmembrane Conductance Regulator Expressed in NIH 3T3 and HEK 293 Cells. *J Biol Chem*. 1999;274(6):3414-3421. doi:10.1074/jbc.274.6.3414

56. Shumaker H, Soleimani M. CFTR upregulates the expression of the basolateral Na^+-K^+-$2Cl^-$ cotransporter in cultured pancreatic duct cells. *Am J Physiol-Cell Physiol*. 1999;277(6):C1100-C1110. doi:10.1152/ajpcell.1999.277.6.C1100

57. Greeley T, Shumaker H, Wang Z, Schweinfest CW, Soleimani M. Downregulated in adenoma and putative anion transporter are regulated by CFTR in cultured pancreatic duct cells. *Am J Physiol-Gastrointest Liver Physiol*. 2001;281(5):G1301-G1308. doi:10.1152/ajpgi.2001.281.5.G1301

58. Venglovecz V, Pallagi P, Kemény LV, et al. The Importance of Aquaporin 1 in Pancreatitis and Its Relation to the CFTR Cl- Channel. *Front Physiol*. 2018;9:854. doi:10.3389/fphys.2018.00854

59. Melendez-Ramirez LY, Richards RJ, Cefalu WT. Complications of Type 1 Diabetes. *Endocrinol Metab Clin North Am*. 2010;39(3):625-640. doi:10.1016/j.ecl.2010.05.009

60. Maahs DM, West NA, Lawrence JM, Mayer-Davis EJ. Epidemiology of Type 1 Diabetes. *Endocrinol Metab Clin North Am*. 2010;39(3):481-497. doi:10.1016/j.ecl.2010.05.011

61. Gregory GA, Robinson TIG, Linklater SE, et al. Global incidence, prevalence, and mortality of type 1 diabetes in 2021 with projection to 2040: a modelling study. *Lancet Diabetes Endocrinol*. 2022;10(10):741-760. doi:10.1016/S2213-8587(22)00218-2

62. Mobasseri M, Shirmohammadi M, Amiri T, Vahed N, Hosseini Fard H, Ghojazadeh M. Prevalence and incidence of type 1 diabetes in the world: a systematic review and meta-analysis. *Health Promot Perspect*. 2020;10(2):98-115. doi:10.34172/hpp.2020.18

63. Ou HT, Yang CY, Wang JD, Hwang JS, Wu JS. Life Expectancy and Lifetime Health Care Expenditures for Type 1 Diabetes: A Nationwide Longitudinal Cohort of Incident Cases Followed for 14 Years. *Value Health*. 2016;19(8):976-984. doi:10.1016/j.jval.2016.05.017

64. Lewis DM. A Systematic Review of Exocrine Pancreatic Insufficiency Prevalence and Treatment in Type 1 and Type 2 Diabetes. *Diabetes Technol Ther*. 2023;25(9):659-672. doi:10.1089/dia.2023.0157

65. Zsóri G, Illés D, Terzin V, Iványi E, Czakó L. Exocrine pancreatic insufficiency in type 1 and type 2 diabetes mellitus: do we need to treat it? A systematic review. *Pancreatology*. 2018;18(5):559-565. doi:10.1016/j.pan.2018.05.006

66. Piciucchi M, Capurso G, Archibugi L, Delle Fave MM, Capasso M, Delle Fave G. Exocrine Pancreatic Insufficiency in Diabetic Patients: Prevalence, Mechanisms, and Treatment. *Int J Endocrinol*. 2015;2015:1-7. doi:10.1155/2015/595649

67. Hardt PD, Ewald N. Exocrine Pancreatic Insufficiency in Diabetes Mellitus: A Complication of Diabetic Neuropathy or a Different Type of Diabetes? *Exp Diabetes Res*. 2011;2011:1-7. doi:10.1155/2011/761950

68. Kakkar R, Mantha SV, Radhi J, Prasad K, Kalra J. Increased Oxidative Stress in Rat Liver and Pancreas during Progression of Streptozotocin-Induced Diabetes. *Clin Sci*. 1998;94(6):623-632. doi:10.1042/cs0940623

69. Nomiyama Y, Tashiro M, Yamaguchi T, et al. High Glucose Activates Rat Pancreatic Stellate Cells Through Protein Kinase C and p38 Mitogen-Activated Protein Kinase Pathway. *Pancreas*. 2007;34(3):364-372. doi:10.1097/MPA.0b013e31802f0531

70. Lam WF, Gielkens HAJ, Coenraad M, Souverijn JHM, Lamers CBHW, Masclee AAM. Effect of Insulin and Glucose on Basal and Cholecystokinin-Stimulated Exocrine Pancreatic Secretion in Humans: *Pancreas*. 1999;18(3):252-258. doi:10.1097/00006676-199904000-00006

71. Apte MV, Pirola RC, Wilson JS. Pancreatic stellate cells: a starring role in normal and diseased pancreas. *Front Physiol*. 2012;3. doi:10.3389/fphys.2012.00344

72. Cavalot F, Bonomo K, Perna P, et al. Pancreatic Elastase-1 in Stools, a Marker of Exocrine Pancreas Function, Correlates With Both Residual β-Cell Secretion and Metabolic Control in Type 1 Diabetic Subjects. *Diabetes Care*. 2004;27(8):2052-2054. doi:10.2337/diacare.27.8.2052

73. Gilbeau JP, Poncelet V, Libon E, Derue G, Heller FR. The density, contour, and thickness of the pancreas in diabetics: CT findings in 57 patients. *Am J Roentgenol*. 1992;159(3):527-531. doi:10.2214/ajr.159.3.1503017

74. Silva MER, Vezozzo DP, Ursich MJM, Rocha DM, Cerri GG, Wajchenberg BL. Ultrasonographic Abnormalities of the Pancreas in IDDM and NIDDM Patients. *Diabetes Care*. 1993;16(9):1296-1297. doi:10.2337/diacare.16.9.1296

75. Alzaid A, Aideyan O, Nawaz S. The Size of the Pancreas in Diabetes Mellitus. *Diabet Med*. 1993;10(8):759-763. doi:10.1111/j.1464-5491.1993.tb00160.x

76. Bilgin M, Balci NC, Momtahen AJ, Bilgin Y, Klör HU, Rau WS. MRI and MRCP Findings of the Pancreas in Patients With Diabetes Mellitus: Compared Analysis With Pancreatic Exocrine Function Determined by Fecal Elastase 1. *J Clin Gastroenterol*. 2009;43(2):165-170. doi:10.1097/MCG.0b013e3181587912

77. Chiarelli F, Verrotti A, Altobelli E, Blasetti A, Morgese G. Size of the pancreas in type I diabetic children and adolescents. *Diabetes Care*. 1995;18(11):1505-1506.

78. Mossner J, Logsdon CD, Goldfine ID, Williams JA. Regulation of pancreatic acinar cell insulin receptors by insulin. *Am J Physiol-Gastrointest Liver Physiol*. 1984;247(2):G155-G160. doi:10.1152/ajpgi.1984.247.2.G155

79. Mössner J, Logsdon CD, Williams JA, Goldfine ID. Insulin, via Its Own Receptor, Regulates Growth and Amylase Synthesis in Pancreatic Acinar AR42J Cells. *Diabetes*. 1985;34(9):891-897. doi:10.2337/diab.34.9.891

80. FAT ABSORPTION AND PANCREATIC FUNCTION IN DIABETES MELLITUS. *Ann Intern Med*. 1958;49(4):820. doi:10.7326/0003-4819-49-4-820

81. Vacca JB. The Exocrine Pancreas in Diabetes Mellitus. *Ann Intern Med*. 1964;61(2):242. doi:10.7326/0003-4819-61-2-242

82. Okabayashi Y, Otsuki M, Ohki A, Nakamura T, Tani S, Baba S. Secretin-Induced Exocrine Secretion in Perfused Pancreas Isolated From Diabetic Rats. *Diabetes*. 1988;37(9):1173-1180. doi:10.2337/diab.37.9.1173

83. Okabayashi Y, Otsuki M, Ohki A, Suehiro I, Baba S. Effect of diabetes mellitus on pancreatic exocrine secretion from isolated perfused pancreas in rats. *Dig Dis Sci*. 1988;33(6):711-717. doi:10.1007/BF01540435

84. Patel R, Singh J, Yago MD, Vilchez JR, Martínez-Victoria E, Mañas M. Effect of insulin on exocrine pancreatic secretion in healthy and diabetic anaesthetised rats. *Mol Cell Biochem*. 2004;261(1):105-110. doi:10.1023/B:MCBI.0000028744.13307.73

85. Futakuchi S, Ishiguro H, Naruse S, et al. High glucose inhibits HCO 3 − and fluid secretion in rat pancreatic ducts. *Pflüg Arch - Eur J Physiol*. 2009;459(1):215-226. doi:10.1007/s00424-009-0731-6

86. Ignáth I, Hegyi P, Venglovecz V, et al. CFTR Expression But Not Cl− Transport Is Involved in the Stimulatory Effect of Bile Acids on Apical Cl−/HCO3 − Exchange Activity in Human Pancreatic Duct Cells. *Pancreas*. 2009;38(8):921-929. doi:10.1097/MPA.0b013e3181b65d34

87. Blinman TA, Gukovsky I, Mouria M, et al. Activation of pancreatic acinar cells on isolation from tissue: cytokine upregulation via p38 MAP kinase. *Am J Physiol Cell Physiol*. 2000;279(6):C1993-2003. doi:10.1152/ajpcell.2000.279.6.C1993

88. Park MK, Lee M, Petersen OH. Morphological and functional changes of dissociated single pancreatic acinar cells: testing the suitability of the single cell as a model for exocytosis and calcium signaling. *Cell Calcium*. 2004;35(4):367-379. doi:10.1016/j.ceca.2003.10.003

89. Ahn YB, Xu G, Marselli L, et al. Changes in gene expression in beta cells after islet isolation and transplantation using laser-capture microdissection. *Diabetologia*. 2007;50(2):334-342. doi:10.1007/s00125-006-0536-5

90. de Vos P, Smink AM, Paredes G, et al. Enzymes for Pancreatic Islet Isolation Impact Chemokine-Production and Polarization of Insulin-Producing β-Cells with Reduced Functional Survival of Immunoisolated Rat Islet-Allografts as a Consequence. *PloS One*. 2016;11(1):e0147992. doi:10.1371/journal.pone.0147992

91. Argent BE, Arkle S, Cullen MJ, Green R. MORPHOLOGICAL, BIOCHEMICAL AND SECRETORY STUDIES ON RAT PANCREATIC DUCTS MAINTAINED IN TISSUE CULTURE. *Q J Exp Physiol*. 1986;71(4):633-648. doi:10.1113/expphysiol.1986.sp003023

92. Katona M, Hegyi P, Kui B, et al. A novel, protective role of ursodeoxycholate in bile-induced pancreatic ductal injury. *Am J Physiol-Gastrointest Liver Physiol*. 2016;310(3):G193-G204. doi:10.1152/ajpgi.00317.2015

93. Venglovecz V, Hegyi P, Rakonczay Z, et al. Pathophysiological relevance of apical large-conductance Ca2+-activated potassium channels in pancreatic duct epithelial cells. *Gut*. 2011;60(3):361-369. doi:10.1136/gut.2010.214213

94. Gilon P, Jonas JC, Henquin JC. Culture duration and conditions affect the oscillations of cytoplasmic calcium concentration induced by glucose in mouse pancreatic islets. *Diabetologia*. 1994;37(10):1007-1014. doi:10.1007/BF00400464

95. Molnár R, Madácsy T, Varga Á, et al. Mouse pancreatic ductal organoid culture as a relevant model to study exocrine pancreatic ion secretion. *Lab Invest*. 2020;100(1):84-97. doi:10.1038/s41374-019-0300-3

96. Skrede KKr, Westgaard RH. The transverse hippocampal slice: a well-defined cortical structure maintainedin vitro. *Brain Res*. 1971;35(2):589-593. doi:10.1016/0006-8993(71)90508-7

97. Moser T, Neher E. Rapid Exocytosis in Single Chromaffin Cells Recorded from Mouse Adrenal Slices. *J Neurosci*. 1997;17(7):2314-2323. doi:10.1523/JNEUROSCI.17-07-02314.1997

98. Graaf IAD, Groothuis GM, Olinga P. Precision-cut tissue slices as a tool to predict metabolism of novel drugs. *Expert Opin Drug Metab Toxicol*. 2007;3(6):879-898. doi:10.1517/17425255.3.6.879

99. Enoki R, Jakobs TC, Koizumi A. Horizontal Slice Preparation of the Retina. *J Vis Exp*. 2006;(1):108. doi:10.3791/108

100. Speier S, Rupnik M. A novel approach to in situ characterization of pancreatic β-cells. *Pflüg Arch*. 2003;446(5):553-558. doi:10.1007/s00424-003-1097-9

101. Dolenšek J, Stožer A, Skelin Klemen M, Miller EW, Slak Rupnik M. The Relationship between Membrane Potential and Calcium Dynamics in Glucose-Stimulated Beta Cell Syncytium in Acute Mouse Pancreas Tissue Slices. Rakonczay Z, ed. *PLoS ONE*. 2013;8(12):e82374. doi:10.1371/journal.pone.0082374

102. Marciniak A, Cohrs CM, Tsata V, et al. Using pancreas tissue slices for in situ studies of islet of Langerhans and acinar cell biology. *Nat Protoc*. 2014;9(12):2809-2822. doi:10.1038/nprot.2014.195

103. Marciniak A, Selck C, Friedrich B, Speier S. Mouse Pancreas Tissue Slice Culture Facilitates Long-Term Studies of Exocrine and Endocrine Cell Physiology in situ. *PLoS ONE*. 2013;8(11):e78706. doi:10.1371/journal.pone.0078706

104. Stožer A, Gosak M, Dolenšek J, et al. Functional Connectivity in Islets of Langerhans from Mouse Pancreas Tissue Slices. Shvartsman S, ed. *PLoS Comput Biol*. 2013;9(2):e1002923. doi:10.1371/journal.pcbi.1002923

105. Serrill JD, Sander M, Shih HP. Pancreatic Exocrine Tissue Architecture and Integrity are Maintained by E-cadherin During Postnatal Development. *Sci Rep*. 2018;8(1):13451. doi:10.1038/s41598-018-31603-2

106. Ballian N, Brunicardi FC. Islet vasculature as a regulator of endocrine pancreas function. *World J Surg*. 2007;31(4):705-714. doi:10.1007/s00268-006-0719-8

107. Brosius F. Low-Dose Streptozotocin Induction Protocol (mouse) v2. Published online October 21, 2019. doi:10.17504/protocols.io.8izhuf6

108. Thomas JA, Buchsbaum RN, Zimniak A, Racker E. Intracellular pH measurements in Ehrlich ascites tumor cells utilizing spectroscopic probes generated in situ. *Biochemistry*. 1979;18(11):2210-2218. doi:10.1021/bi00578a012

109. Hegyi P, Rakonczay Z, Gray MA, Argent BE. Measurement of Intracellular pH in Pancreatic Duct Cells: A New Method for Calibrating the Fluorescence Data. *Pancreas*. 2004;28(4):427-434. doi:10.1097/00006676-200405000-00012

110. Hegyi P, Gray MA, Argent BE. Substance P inhibits bicarbonate secretion from guinea pig pancreatic ducts by modulating an anion exchanger. *Am J Physiol-Cell Physiol*. 2003;285(2):C268-C276. doi:10.1152/ajpcell.00574.2002

111. Hegyi P, Rakonczay Z, Tiszlavicz L, et al. Protein kinase C mediates the inhibitory effect of substance P on HCO_3^- secretion from guinea pig pancreatic ducts. *Am J Physiol-Cell Physiol*. 2005;288(5):C1030-C1041. doi:10.1152/ajpcell.00430.2003

112. Weintraub WH, Machen TE. pH regulation in hepatoma cells: roles for Na-H exchange, Cl-HCO3 exchange, and Na-HCO3 cotransport. *Am J Physiol-Gastrointest Liver Physiol*. 1989;257(3):G317-G327. doi:10.1152/ajpgi.1989.257.3.G317

113. Fernández-Salazar MP, Pascua P, Calvo JJ, et al. Basolateral anion transport mechanisms underlying fluid secretion by mouse, rat and guinea-pig pancreatic ducts. *J Physiol*. 2004;556(2):415-428. doi:10.1113/jphysiol.2004.061762

114. Pascua P, García M, Fernández-Salazar MP, et al. Ducts isolated from the pancreas of CFTR-null mice secrete fluid. *Pflüg Arch - Eur J Physiol*. 2009;459(1):203-214. doi:10.1007/s00424-009-0704-9

115. Perides G, Van Acker GJ, Laukkarinen JM, Steer ML. Experimental acute biliary pancreatitis induced by retrograde infusion of bile acids into the mouse pancreatic duct. *Nat Protoc*. 2010;5(2):335-341. doi:10.1038/nprot.2009.243

116. Laczkó D, Rosztóczy A, Birkás K, et al. Role of ion transporters in the bile acid-induced esophageal injury. *Am J Physiol-Gastrointest Liver Physiol*. 2016;311(1):G16-G31. doi:10.1152/ajpgi.00159.2015

117. De Boer P, Pirozzi NM, Wolters AHG, et al. Large-scale electron microscopy database for human type 1 diabetes. *Nat Commun*. 2020;11(1):2475. doi:10.1038/s41467-020-16287-5

118. Anello M, Lupi R, Spampinato D, et al. Functional and morphological alterations of mitochondria in pancreatic beta cells from type 2 diabetic patients. *Diabetologia*. 2005;48(2):282-289. doi:10.1007/s00125-004-1627-9

119. Shcheynikov N, Wang Y, Park M, et al. Coupling Modes and Stoichiometry of Cl−/HCO3− Exchange by slc26a3 and slc26a6. *J Gen Physiol*. 2006;127(5):511-524. doi:10.1085/jgp.200509392

120. Lee MG, Ohana E, Park HW, Yang D, Muallem S. Molecular Mechanism of Pancreatic and Salivary Gland Fluid and HCO_3^- Secretion. *Physiol Rev*. 2012;92(1):39-74. doi:10.1152/physrev.00011.2011

121. Dulin NO. Calcium-Activated Chloride Channel ANO1/TMEM16A: Regulation of Expression and Signaling. *Front Physiol*. 2020;11:590262. doi:10.3389/fphys.2020.590262

122. Huang F, Rock JR, Harfe BD, et al. Studies on expression and function of the TMEM16A calcium-activated chloride channel. *Proc Natl Acad Sci*. 2009;106(50):21413-21418. doi:10.1073/pnas.0911935106

123. Romanenko VG, Catalán MA, Brown DA, et al. Tmem16A Encodes the Ca2+-activated Cl− Channel in Mouse Submandibular Salivary Gland Acinar Cells. *J Biol Chem*. 2010;285(17):12990-13001. doi:10.1074/jbc.M109.068544

124. Gray MA, Winpenny JP, Porteous DJ, Dorin JR, Argent BE. CFTR and calcium-activated chloride currents in pancreatic duct cells of a transgenic CF mouse. *Am J Physiol-Cell Physiol*. 1994;266(1):C213-C221. doi:10.1152/ajpcell.1994.266.1.C213

125. Gray MA, Harris A, Coleman L, Greenwell JR, Argent BE. Two types of chloride channel on duct cells cultured from human fetal pancreas. *Am J Physiol-Cell Physiol*. 1989;257(2):C240-C251. doi:10.1152/ajpcell.1989.257.2.C240

126. Dauner K, Lißmann J, Jeridi S, Frings S, Möhrlen F. Expression patterns of anoctamin 1 and anoctamin 2 chloride channels in the mammalian nose. *Cell Tissue Res*. 2012;347(2):327-341. doi:10.1007/s00441-012-1324-9

127. Ni YL, Kuan AS, Chen TY. Activation and Inhibition of TMEM16A Calcium-Activated Chloride Channels. Reisert J, ed. *PLoS ONE*. 2014;9(1):e86734. doi:10.1371/journal.pone.0086734

128. Gray MA, Winpenny JP, Verdon B, O'Reilly CM, Argent BE. Properties and role of calcium-activated chloride channels in pancreatic duct cells. In: *Current Topics in Membranes*. Vol 53. Elsevier; 2002:231-256. doi:10.1016/S1063-5823(02)53036-2

129. Han Y, Shewan AM, Thorn P. HCO3− Transport through Anoctamin/Transmembrane Protein ANO1/TMEM16A in Pancreatic Acinar Cells Regulates Luminal pH. *J Biol Chem*. 2016;291(39):20345-20352. doi:10.1074/jbc.M116.750224

130. Spires D, Manis AD, Staruschenko A. Ion channels and transporters in diabetic kidney disease. In: *Current Topics in Membranes*. Vol 83. Elsevier; 2019:353-396. doi:10.1016/bs.ctm.2019.01.001

131. Da Costa-Pessoa JM, Damasceno RS, Machado UF, Beloto-Silva O, Oliveira-Souza M. High Glucose Concentration Stimulates NHE-1 Activity in Distal Nephron Cells: the Role of the Mek/Erk1/2/p90 ^{RSK} and p38MAPK Signaling Pathways. *Cell Physiol Biochem*. 2014;33(2):333-343. doi:10.1159/000356673

132. Davies JE, Siczkowski M, Sweeney FP, et al. Glucose-Induced Changes in Turnover of Na+/H+ Exchanger of Immortalized Lymphoblasts From Type I Diabetic Patients With Nephropathy. *Diabetes*. 1995;44(4):382-388. doi:10.2337/diab.44.4.382

133. Siczkowski M, Ng LL. Glucose-induced changes in activity and phosphorylation of the Na+/H+ exchanger, NHE-1, in vascular myocytes from Wistar-Kyoto and spontaneously hypertensive rats. *Metabolism*. 1996;45(1):114-119. doi:10.1016/S0026-0495(96)90208-5

134. Soya N, Xu H, Roldan A, et al. Folding correctors can restore CFTR posttranslational folding landscape by allosteric domain–domain coupling. *Nat Commun*. 2023;14(1):6868. doi:10.1038/s41467-023-42586-8

135. Marklew AJ, Patel W, Moore PJ, et al. Cigarette Smoke Exposure Induces Retrograde Trafficking of CFTR to the Endoplasmic Reticulum. *Sci Rep*. 2019;9(1):13655. doi:10.1038/s41598-019-49544-9

136. Ko SBH, Azuma S, Yoshikawa T, et al. Molecular Mechanisms of Pancreatic Stone Formation in Chronic Pancreatitis. *Front Physiol*. 2012;3. doi:10.3389/fphys.2012.00415

137. Gál E, Dolenšek J, Stožer A, Pohorec V, Ébert A, Venglovecz V. A Novel in situ Approach to Studying Pancreatic Ducts in Mice. *Front Physiol*. 2019;10:938. doi:10.3389/fphys.2019.00938

138. Schena FP, Gesualdo L. Pathogenetic Mechanisms of Diabetic Nephropathy. *J Am Soc Nephrol*. 2005;16(3_suppl_1):S30-S33. doi:10.1681/ASN.2004110970

139. Tuttle KR. Back to the Future: Glomerular Hyperfiltration and the Diabetic Kidney. *Diabetes*. 2017;66(1):14-16. doi:10.2337/dbi16-0056

140. Vallon V, Komers R. Pathophysiology of the Diabetic Kidney. In: Prakash YS, ed. *Comprehensive Physiology*. 1st ed. Wiley; 2011:1175-1232. doi:10.1002/cphy.c100049

I.

The Journal of Physiology

Role of CFTR in diabetes-induced pancreatic ductal fluid and HCO_3^- secretion

Attila Ébert[1,2], Eleonóra Gál[1], Emese Tóth[3,4], Titanilla Szögi[5], Péter Hegyi[3,6,7,8] and Viktória Venglovecz[1,6]

[1]*Department of Pharmacology and Pharmacotherapy, University of Szeged, Szeged, Hungary*
[2]*ELI ALPS, ELI-HU Non-Profit Ltd, Szeged, Hungary*
[3]*Translational Pancreatology Research Group, Interdisciplinary Center of Excellence for Research Development and Innovation, University of Szeged, Szeged, Hungary*
[4]*Department of Health Sciences, Department of Theoretical and Integrative Health Sciences, University of Debrecen, Debrecen, Hungary*
[5]*Department of Pathology, University of Szeged, Szeged, Hungary*
[6]*Institute for Translational Medicine, Szentágothai Research Centre, Medical School, University of Pécs, Pécs, Hungary*
[7]*Centre for Translational Medicine, Semmelweis University, Budapest, Hungary*
[8]*Division of Pancreatic Diseases, Heart and Vascular Center, Semmelweis University, Budapest, Hungary*

Handling Editors: Kim Barrett & Pawel Ferdek

The peer review history is available in the Supporting Information section of this article (https://doi.org/10.1113/JP285702#support-information-section).

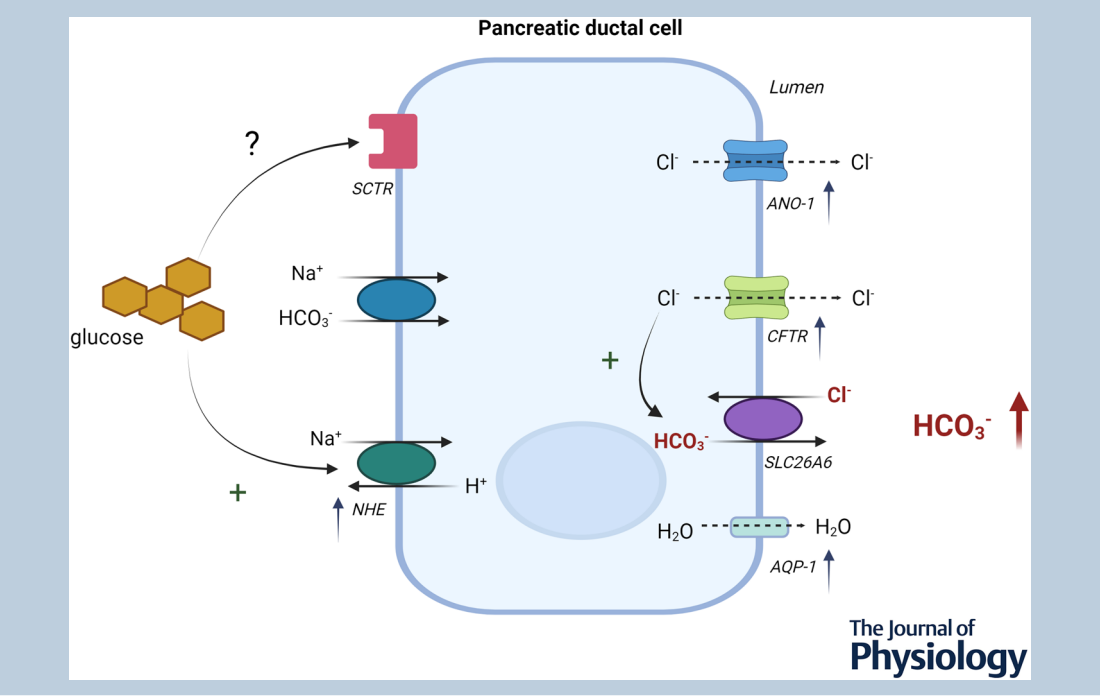

Attila Ébert is a PhD candidate at the Department of Pharmacology and Pharmacotherapy, University of Szeged, supervised by Dr Viktória Venglovecz. Attila obtained his MSc degree in molecular biology, microbiology and immunology at the Faculty of Science and Informatics, University of Szeged. His current research focuses on exocrine and endocrine pancreas interactions and pancreatogenic diabetes. His goal is to identify the physiological processes that lead to pancreatic disease and identify new targets for development of therapy. He is also currently working on the field of radiation biology and will continue to do pancreas research with a multidisciplinary approach.

DOI: 10.1113/JP285702

Abstract Type 1 diabetes is a disease of the endocrine pancreas; however, it also affects exocrine function. Although most studies have examined the effects of diabetes on acinar cells, much less is known regarding ductal cells, despite their important protective function in the pancreas. Therefore, we investigated the effect of diabetes on ductal function. Diabetes was induced in wild-type and cystic fibrosis transmembrane conductance regulator (CFTR) knockout mice following an I.P. administration of streptozotocin. Pancreatic ductal fluid and HCO_3^- secretion were determined using fluid secretion measurements and fluorescence microscopy, respectively. The expression of ion transporters was measured by real-time PCR and immunohistochemistry. Transmission electron microscopy was used for the morphological characterization of the pancreas. Serum secretin and cholecystokinin levels were measured by an enzyme-linked immunosorbent assay. Ductal fluid and HCO_3^- secretion, CFTR activity, and the expression of CFTR, Na^+/H^+ exchanger-1, anoctamine-1 and aquaporin-1 were significantly elevated in diabetic mice. Acute or chronic glucose treatment did not affect HCO_3^- secretion, but increased alkalizing transporter activity. Inhibition of CFTR significantly reduced HCO_3^- secretion in both normal and diabetic mice. Serum levels of secretin and cholecystokinin were unchanged, but the expression of secretin receptors significantly increased in diabetic mice. Diabetes increases fluid and HCO_3^- secretion in pancreatic ductal cells, which is associated with the increased function of ion and water transporters, particularly CFTR.

(Received 20 September 2023; accepted after revision 17 January 2024; first published online 22 February 2024)
Corresponding author V. Venglovecz: Department of Pharmacology and Pharmacotherapy, University of Szeged, H-6720 Szeged, Hungary. Email: venglovecz.viktoria@med.u-szeged.hu

Abstract figure legend Putative mechanism by which diabetes causes increased ductal secretion. The activity of the Cl^-/HCO_3^- exchanger is enhanced in diabetes through the overexpression of ductal acid–base transporters, namely, the cystic fibrosis transmembrane conductance regulator (CFTR), the Na^+/H^+ exchanger-1 (NHE-1), anoctamine-1 (ANO-1) and the aquaporin-1 (AQP-1) water channel. Furthermore, high extracellular glucose directly stimulates NHE-1, which may also contribute to increased secretion. Diabetes also causes the upregulation of secretin receptors (SCTRs) at the mRNA level, but the exact role of secretin in the stimulatory effect of diabetes requires further investigations.

Key points

- There is a lively interaction between the exocrine and endocrine pancreas not only under physiological conditions, but also under pathophysiological conditions
- The most common disease affecting the endocrine part is type-1 diabetes mellitus (T1DM), which is often associated with pancreatic exocrine insufficiency
- Compared with acinar cells, there is considerably less information regarding the effect of diabetes on pancreatic ductal epithelial cells, despite the fact that the large amount of fluid and HCO_3^- produced by ductal cells is essential for maintaining normal pancreatic functions
- Ductal fluid and HCO_3^- secretion increase in T1DM, in which increased cystic fibrosis transmembrane conductance regulator activation plays a central role.
- We have identified a novel interaction between T1DM and ductal cells. Presumably, the increased ductal secretion represents a defence mechanism in the prevention of diabetes, but further studies are needed to clarify this issue.

Introduction

The pancreas is a dual gland that performs exocrine and endocrine functions. Although the exocrine and endocrine pancreas are functionally and anatomically separate, there is a lively interaction between them; thus, a disease that affects either part can impact the other (Gal et al., 2021). The most common disease affecting the endocrine pancreas is diabetes mellitus (DM), which is the result of reduced insulin production or reduced insulin sensitivity. Depending on the underlying cause, DM is categorized as type 1 (T1DM) or type 2 (T2DM). T1DM is an autoimmune disease, in which the body destroys insulin-producing beta cells in the pancreas,

leading to reduced insulin production and ultimately hyperglycaemia. Several clinical and experimental studies have shown that exocrine function is also impaired in T1DM. The lack of insulin decreases the secretion of digestive enzymes, which results in exocrine pancreatic insufficiency (EPI) (Creutzfeldt et al., 2005; Hardt & Ewald, 2011; Hardt et al., 2003; Piciucchi et al., 2015; Radlinger et al., 2020; Zsori et al., 2018). Several factors may be involved in the development of EPI. One of the most accepted is the reduced trophic effect of insulin on acinar cells (Mossner et al., 1984, 1985); however, fibrosis, inflammation and microangiopathy, which develop during long-term diabetes, are probably also involved (Hayden et al., 2008; Rodriguez-Calvo et al., 2014; Zsori et al., 2018). Compared with acinar cells, there is considerably less information regarding the effect of diabetes on pancreatic ductal epithelial cells (PDECs). Although, PDECs comprise only a small proportion of the exocrine pancreas, they have an important physiological role. They secrete a HCO_3^--rich, isotonic fluid which neutralizes the acidic pH entering the duodenum from the stomach, thereby providing optimal pH conditions for digestion. In addition, HCO_3^- has an important protective role by neutralizing protons secreted by the acini, thereby preventing the premature activation of digestive enzymes (Behrendorff et al., 2010; Hegyi, Maleth et al., 2011; Hegyi, Pandol et al., 2011). Ductal fluid and HCO_3^- secretion are mediated by ion transporters, which are differentially expressed on the luminal and baso-lateral membranes, resulting in functional polarization of the ductal cells. Among the ion transporters, the apically localized Cl^-/HCO_3^- exchanger and the cystic fibrosis transmembrane conductance regulator (CFTR) Cl^- channel have an important role in HCO_3^- secretion (Park et al., 2010; Wang et al., 2006); however, little is known with respect to how diabetes affects the function of these transporters and many studies have yielded contradictory results. Futakuchi et al. (2009) showed that high extracellular glucose increases Na^+ uptake by the sodium-dependent glucose co-transporter-1, which increases intracellular Na^+ levels and ultimately induces membrane depolarization. Depolarization of the apical membrane reduces the electrochemical driving force for Cl^- and HCO_3^- efflux, and therefore, impairs fluid and HCO_3^- secretion (Futakuchi et al., 2009); however, other studies have found that diabetes increases basal fluid secretion with reduced protein output (Okabayashi, Otsuki, Ohki, Nakamura et al., 1988; Okabayashi, Otsuki, Ohki, Suehiro et al., 1988; Patel et al., 2004). By contrast to basal secretion, secretin-stimulated pancreatic juice flow is significantly reduced in diabetes (Okabayashi, Otsuki, Ohki, Nakamura et al., 1988). Most of these studies are outdated and, because of the conflicting results, it is not clear how diabetes affects ductal functions. Because ductal cells play an essential role in the maintenance of pancreas integrity, identification of the mechanism through which ductal fluid secretion is altered in diabetes may bring us closer to understanding the pathogenesis of exocrine insufficiency.

In the present study, we determined the effect of diabetes on the activity and expression of the main ductal ion transporters. We used isolated pancreatic ducts from streptozotocin-induced T1DM mice to measure changes in intracellular pH as well as protein and gene expression. We demonstrated that the activity and expression of the main acid–base transporters as well as ductal fluid and HCO_3^- secretion was increased in diabetes, in which the CFTR Cl^- channel plays a central role.

Methods

Ethical approval

Animal experiments were conducted in accordance with the Guide for the Care and Use of Laboratory Animals (Department of Health and Human Services, USA). In addition, the experimental protocol was approved by the local Ethical Board of the University of Szeged, Hungary, and by the Public Health and Food Chain committee, Csongrad County Government Office, Hungary (XI./128/2019).

Transgenic mice

CFTR knockout (KO) mice on an FVB/N background were kindly provided by Dr Ursula Seidler (Hannover Medical School, Hannover, Germany). The animals were housed in standard plastic cages under a 12:12 h light/dark photocycle at room temperature (23 ± 1°C) and had free access to standard or CFTR-specific laboratory chow and drinking solutions. Functional experiments were performed on litter-matched (age 8–12 weeks, male) wild-type (WT) and CFTR KO mice. The mice were genotyped prior to the experiments by isolating genomic DNA from the tail and amplifying by traditional PCR.

Chemicals and solutions

2,7-*Bis*-(2-carboxyethyl)−5(6)-carboxyfluorescein acetoxymethyl ester (BCECF-AM) and MQAE [*N*-(ethoxycarbonylmethyl)-6-methoxyquinolinium bromide] were purchased from Invitrogen (Eugene, OR, USA). BCECF-AM (2 mM) and MQAE (1 mM) were prepared in dimethyl sulfoxide and stored at −20°C. Chromatographically pure collagenase was purchased from Worthington (Lakewood, NJ, USA). Secretin (SCT) and forskolin were purchased from Tocris (Bristol, UK). The secretin enzyme-linked immunosorbent assay (ELISA) kit was purchased from Biotechne (Minneapolis,

Table 1. Composition of solutions

	Standard Hepes	Standard HCO_3^-	NH_4^+ in HCO_3^-	Cl^--free HCO_3^-
NaCl	140	115	95	
KCl	5	5	5	
$MgCl_2$	10	1	1	
$CaCl_2$	1	1	1	
HEPES	1			
D-glucose	10	10	10	10
$NaHCO_3$		25	25	25
NH_4Cl			20	
Na-gluconate				115
KNO_3				5
Ca-gluconate				6
Mg-gluconate				1

Values are concentrations (in mM).

MN, USA) and the cholecystokinin (CCK) ELISA kit was purchased from Raybiotech (Peachtree Corners, GA, USA). Cryomatrix, Hoechst33342, anti-β-actin antibody (Cat. MA5-15 739) and fluorescence-labelled secondary antibodies (Cat. A-32 723; A-21 244) were obtained from Thermo Scientific (Waltham, MA, USA). Anti-CFTR, anti-NHE1, anti-ANO1 and anti-AQP1 antibodies (Cat. ACL-006; ANX-010; ACL-011; and AQP-001, respectively) were purchased from Alomone Labs (Jerusalem, Israel). Tablets for the protease inhibitor cocktail were purchased from Roche (Budapest, Hungary). All other chemicals were obtained from Merck (Budapest, Hungary). The composition of the solutions used for microfluorimetry and video microscopy measurements are shown in Table 1. A standard Hepes-buffered solution was gassed with 100% O_2 and the pH was adjusted to 7.4 with NaOH. Standard HCO_3^-/CO_2-buffered solutions were gassed with a mixture of 95% O_2 and 5% C_{O_2} and adjusted to a pH of 7.4. All experiments were performed at 37°C.

Induction of diabetes

To establish a type 1 diabetes model, the protocol of the Diabetic Complications Consortium was used. Briefly, diabetes was induced in 8–12-week-old mice, by daily I.P. administration of 50 μg kg^{-1} body weight streptozotocin (STZ), dissolved in citrate buffer (pH 4.5), for 5 consecutive days. The mice were fasted for 6 h prior to STZ injection. Control animals received equal amounts of citrate buffer. The development of diabetes was confirmed by measuring fasting blood glucose levels 4 weeks after the first injection. Animals with blood glucose levels >12 mmol L^{-1} were considered diabetic. Blood glucose concentrations were determined using a blood glucose meter (77 Elektronika, Budapest, Hungary). The mice were killed after week 4 by pentobarbital overdose (200 mg kg^{-1} body weight I.P.) and exsanguinated through cardiac puncture. The pancreas was immediately removed, trimmed from fat and lymphatic tissue, and a portion was fixed in 6% neutral formaldehyde solution, embedded in paraffin blocks, cut into 3 μm thick sections, stained with haematoxylin and eosin, and observed by light microscopy. Small pieces of the pancreas were fixed in 3% glutaraldehyde for transmission electron microscopy. The other portion of the pancreas was used for the isolation of ducts. Blood samples were collected in Microvette CB300 fluoride/heparin-coated capillaries (Sarstedt, Nümbrecht, Germany), centrifuged at 2500 *g* for 15 min at 4°C, and the plasma was stored at −20°C until use.

Isolation of pancreatic ducts and measurement of intracellular pH

Intra/interlobular ducts were isolated from the pancreas of WT and CFTR KO mice by enzymatic digestion as previously described (Argent et al., 1986). Changes in intracellular pH (pH_i) were measured using the pH-sensitive fluorescent dye, BCECF and the microfluorimetric technique. Pancreatic ducts were incubated with 2 μM BCECF-AM for 1 h at 37°C then attached to a cover glass. This formed the base of a perfusion chamber, which was mounted on the stage of an IX71 live cell imaging fluorescence microscope (Olympus, Budapest, Hungary). The cells were excited at 440 and 490 nm and emission was monitored at 530 nm. Five to seven regions of interest (ROIs) were marked for each experiment and one measurement per second was obtained. The 490/440 fluorescence ratio was calibrated to pH_i using the high K^+-nigericin technique as previously described (Hegyi et al., 2004; Thomas et al., 1979).

Measurement of HCO_3^- secretion

To estimate HCO_3^- efflux, the activity of the Cl^-/HCO_3^- exchanger was measured by the NH_4Cl pre-pulse technique and the Cl^- withdrawal technique. For the NH_4Cl pre-pulse technique, ducts were exposed to 20 mM NH_4Cl in HCO_3^-/CO_2-buffered solution, which resulted in an immediate increase in pH_i resulting from the influx of NH_3 across the membrane. After maximal alkalinization, the pH_i began to recover. Under these conditions, the initial rate of pH_i ($\Delta pH/\Delta t$) recovery (over the first 30 s) reflects the rate of HCO_3^- secretion (base efflux) (Hegyi et al., 2003; Hegyi et al., 2005). After the removal of NH_4Cl, the pH_i suddenly decreased because of the dissociation of intracellular NH_4^+ to H^+ and NH_3. In HCO_3^-/CO_2-buffered solution, the initial rate of recovery from the acid load (over the

first 60 s) reflects the activity of Na^+/H^+ exchangers (NHEs) and the Na^+/HCO_3^- cotransporter (NBC). For the Cl^- withdrawal technique, Cl^- was removed from the external solution that caused a sudden alkalization of the pH_i resulting from the reverse operation of the Cl^-/HCO_3^- exchanger. The initial rate of alkalization (over the first 60 s) or the rate of recovery from alkalosis (over the first 60 s) reflects the activity of the exchanger. Transmembrane base flux [$(J(B^-)$] was calculated using: $J(B^-) = \Delta pH/\Delta t \times ß_{total}$, where $\Delta pH/\Delta t$ is the initial rate of recovery and β_{total} is the total buffering capacity (Hegyi et al., 2003; Weintraub & Machen, 1989).

Measurement of CFTR activity

CFTR activity was analysed by measuring the intracellular Cl^- concentration using MQAE fluorescent dye and forskolin. The fluorescence intensity of MQAE is inversely proportional to Cl^- because of its quenching effect on the dye. Pancreatic ducts were incubated with MQAE (5 μM) for 1 h at 37°C, then perfused with HCO_3^-/CO_2-buffered solution containing 20 μM forskolin. Excitation was set to 350 nm and emission was monitored at 510 nm. Five to seven ROIs were marked for each experiment and one measurement per second was obtained. The readings were displayed as fluorescence ratio (F/F_0) and a linear trend line was plotted on the curve for the first 2 min (120 s) of forskolin stimulation. The area under the plotted curve was calculated using the definite integral of the equation.

Measurement of pancreatic fluid secretion

To estimate the rate of ductal fluid secretion, we measured the swelling of the intra-interlobular ducts using the video microscopy technique described previously (Fernandez-Salazar et al., 2004). Briefly, intra-interlobular pancreatic ducts were attached to the cover glass of a perfusion chamber and mounted on the stage of an IX71 live cell imaging fluorescence microscope. To stimulate fluid secretion, the ducts were perfused with forskolin (5 μM) and low magnification, bright-field images were captured at intervals of 1 min using a CCD camera (Hamamatsu ORCA-ER; Olympus). The integrity of the ductal wall was confirmed at the end of each experiment using a hypotonic solution. Changes in relative luminal volume were analysed using Image J software (Fernandez-Salazar et al., 2004; Pascua et al., 2009).

Pancreatic fluid secretion was also assessed *in vivo* as previously described (Perides et al., 2010). Briefly, mice were anaesthetized with the combination of ketamine (100 mg kg^{-1} I.P.) and xylazine (12.5 mg kg^{-1} I.P.) and, for pain relief, a single buprenorphine (0.1 mg kg^{-1} I.P.) injection was administered. To maintain body temperature, animals were kept on a heating pad (37°C) during the entire experiment. After median laparotomy, the lumen of the common biliopancreatic duct was cannulated using a 30-gauge needle with filed ends. To prevent contamination with bile, the ductus hepaticus was occluded with a microvessel clip. Pancreatic fluid secretion was stimulated by I.P. administration of secretin (1 CU kg^{-1}) and the pancreatic juice was collected through a polyethylene tube over 60 min.

Immunohistochemistry

Isolated pancreatic ducts were embedded in cryomatrix, snap-frozen in liquid nitrogen, and cut into 10 μm thick sections. Immunofluorescence labelling was performed based on the protocol provided at www.novusbio.com. Briefly, tissue sections were fixed with 4% para-formaldehyde in phosphate-buffered saline (PBS) for 15 min and permeabilized by washing twice with PBS containing 1% goat serum (GS) and 0.4% Triton X-100 for 10 min. Blocking was carried out for 30 min in PBS-Tween 20 containing 5% GS, followed by incubation with primary antibodies overnight on 4°C. The sections were then incubated with Hoechst 33342 for 15 min followed by a washing step and incubation with secondary antibodies for 1 h. After a washing step, the sections were covered with Fluoromount mounting medium (Sigma, St Louis, MO, USA) and allowed to dry for 12 h under aluminium foil. Primary (2 μg mL^{-1} for CFTR, ANO1 and NHE-1 antibodies; 2.5 μg mL^{-1} for anti-AQP1; 4 μg mL^{-1} for anti-β-actin) and secondary (5 μg mL^{-1} for goat anti-rabbit Alexa Fluor 647; 8 μg mL^{-1} for goat anti-mouse Alexa Fluor 488) antibodies and Hoechst 33 342 (20 μg mL^{-1}) were diluted in PBS supplemented with 1% GS. All steps were carried out at room temperature unless specified otherwise. Images were captured using an LSM 880 confocal microscope (Carl Zeiss Technika Kft, Budaörs, Hungary). An optimal pinhole size and laser intensity was defined for every target antigen and the same settings were used to record all samples.

Quantitation of immunostainings

The images were evaluated using ImageJ (NIH, Bethesda, MD, USA). The measured area was restricted to the layer of epithelial cells and to a constant threshold value of intensity. The average intensity in the green and red channels was then determined. Red intensity values marking the antigens of interest were normalized to the green intensity values representing β-actin.

Real-time PCR (RT-PCR)

Intra-interlobular pancreatic ducts were isolated from six normal and six diabetic mice and pooled for total RNA

Table 2. Taqman assays used for the investigation of ion transporter expression

Gene symbol	Official full name	GenBank ref. no.	Taqman assay ID
CFTR	Cystic fibrosis transmembrane conductance regulator	NC_000072	Mm00445197_m1
ANO-1 or TMEM16A	Anoctamin-1	NC_000073.7	Mm00724407_m1
AQP-1	Aquaporin-1	NC_000072.7	Mm01326466_m1
AQP-5	Aquaporin-5	NC_000081.7	Mm00437578_m1
AQP-8	Aquaporin-8	NC_000073.7	Mm00431846_m1
Slc9a1	Solute carrier family 9 (Na^+/H^+ exchanger) member A1	NC_000001.11	Mm00444270_m1
Slc9a2	Solute carrier family 9 (Na^+/H^+ exchanger) member A2	NC_000067.7	Mm01237129_m1
Slc26a3 (DRA)	Solute carrier family 26 (Cl^-/HCO_3^- exchanger), member 3	NC_000078.7	Mm00445313_m1
Slc26a6 (PAT-1)	Solute carrier family 26 (Cl^-/HCO_3^- exchanger), member 6	NC_000075.7	Mm00506742_m1
Slc4a4	Solute carrier family 4 (Na^+/HCO_3^- co-transporter), member 4	NC_000071.7	Mm01347935_m1

extraction with a NucleoSpin RNA Kit (Macherey-Nagel, Düren, Germany) in accordance with the manufacturer's instructions. Total RNA (2 μg) was reverse-transcribed using the High-Capacity cDNA Reverse Transcription Kit (Applied Biosystems, Foster City, CA, USA). RT-PCR was performed on a Light Cycler 96 instrument (Roche Magyarország Kft, Budaörs, Hungary) using TaqMan probe sets for specific genes (Thermo Fisher Scientific, Darmstadt, Germany). Quantitative RT-PCR reactions were performed as previously described (Laczko et al., 2016). The results were expressed as fold-changes calculated by the $2^{-\Delta\Delta CT}$ method. Genes with expression values $\leq$0.5 were considered downregulated, whereas values $\geq$2 were considered upregulated. Values ranging from 0.51 to 1.99 were not considered to be significant. Table 2 provides information regarding the TaqMan assays.

Transmission electron microscopy

For post-embedding transmission electron microscopy, small pieces of the pancreas were fixed in 3% glutaraldehyde. The tissues were rinsed with PBS and further fixed for 1 h in 2% OsO_4. The samples were then dehydrated in increasing concentrations of ethanol, rinsed with uranyl acetate and acetone, and embedded in Embed 812 (Electron Microscopy Sciences, Hatfield, PA, USA). The embedded blocks were used to prepare ultrathin (70 nm) sections (Ultracut S ultra-microtome; Leica, Wetzlar, Germany), which were mounted on copper grids. The grids were counterstained with uranyl acetate and lead citrate (Merck Millipore, Darmstadt, Germany) and examined and imaged using a JEOL JEM 1400 transmission electron microscope (JEOL, Tokyo, Japan). Five digital photographs of the cells were captured at magnifications of 5000× and 8000× using TEM Centre software (JEOL).

ELISA

Plasma samples obtained by cardiac puncture were transferred to fluoride/heparin-coated capillaries and centrifuged at 2500 × *g* for 20 min at 4°C. The samples were stored at −20°C and thawed on ice before use. Pancreas homogenates were prepared by grinding 100 mg of tissue in liquid nitrogen using a mortar and pestle and dissolving it in 1 mL of ice-cold protease inhibitor cocktail. The SCT and CCK assays were performed following based on the manufacturer's instructions.

Statistical analysis

Prism, version 9.5.1 (GraphPad Software Inc., San Diego, CA, USA) was used to produce graphs and images. Data are presented as the mean ± SD and box and whisker plots showing the median, quartiles and extremes. Shapiro–Wilk and Kolmogorov–Smirnov tests were used to analyse data distribution. The equality of variances was analysed using an *F* test. One-way ANOVA (with Tukey's multiple comparisons test), Student's *t* test (with Welch's correction as needed), the Kruskal–Wallis test (with Dunn's multiple comparisons test) and the Mann–Whitney test were used to determine statistical significance.

Results

Morphology of the exocrine pancreas in diabetes

T1DM caused a decrease in the number and size of islets by the destruction of insulin-producing beta cells (Fig. 1*A*). In addition, characteristics of chronic pancreatitis, such as fibrosis, acinar atrophy and leukocyte infiltration, were also observed at low levels. By contrast, the structure of the ducts was preserved. Electron microscopic examination of the pancreas showed enlarged mitochondria and a fragmented mitochondrial internal membrane structure in the acini (Fig. 1*B*). Enlargement of the mitochondria was also observed in ducts and islets, but to a much lesser extent compared with the acini.

Pancreatic ductal fluid secretion increases in diabetes

The volume of fluid secreted by ductal cells is an important indicator of ductal function. Therefore, the rate of fluid secretion was determined under *in vitro* and *in vivo* conditions. For the *in vitro* measurements, the rate of fluid secretion was estimated from the volume change of the isolated ductal fragments (Fig. 2*A* and *B*). Following forskolin stimulation, the amount of fluid secreted by the diabetic ducts was significantly higher compared to that of non-diabetic ducts (13.2 ± 2.14 *vs.* 9.29 ± 0.51%). *In vivo* fluid secretion studies revealed similar results to that observed *in vitro*. Both basal and secretin-stimulated (1 CU kg^{-1}) fluid secretion were significantly increased in diabetic mice compared with normal mice (0.73 ± 0.12 *vs.* 1.15 ± 0.08 μL h^{-1} g^{-1} body weight basal secretion and 1.48 ± 0.24 *vs.* 2.48 ± 0.25 μL h^{-1} g^{-1} body weight stimulated secretion) (Fig. 2*C*).

Diabetes increases the activity and expression of ductal acid–base transporters

Intra-interlobular ducts were isolated from normal and diabetic mice and the alkaline load method was used to measure the activity of acid–base transporters in the ductal cells. In previous studies, we found that the degree of regeneration from alkalosis in HCO_3^-/CO_2-containing extracellular solution reflects the activity of the Cl^-/HCO_3^- exchanger, whereas the regeneration from acidosis indicates the activity of the NHE and the NBC (Hegyi et al., 2003). Both alkali and acid regeneration were increased in diabetic mice compared with control mice [rate of alkali regeneration: 3.2 ± 0.09 *vs.* 4.86 ± 0.14 $-J(B^-$ $min^{-1})$; rate of acid regeneration 7.25 ± 0.3 *vs.* 11.45 ± 0.34 $-J(B^-$ $min^{-1})$], indicating that diabetes increases the activity of these transporters (Fig. 3*Aa–Ac*). To confirm this result, the Cl^- withdrawal method was used (Fig. 3*Ba–Bc*). The removal of extracellular Cl^- in the presence of HCO_3^- induces a robust alkalosis, because of the reverse mode of the exchanger. During the re-administration of extracellular Cl^-, the pH_i is regenerated and the rate of regeneration reflects the activity of the Cl^-/HCO_3^- exchanger. Similar to the alkali-load method, the activity of the exchanger was also enhanced during diabetes (Fig. 3*Bb*), although no differences in pH_i were observed (Fig. 3*Bc*).

Next, we examined mRNA and protein expression of the major acid–base transporters using RT-PCR and immunohistochemistry. Intra-interlobular pancreatic ducts were isolated from normal and diabetic mice and the expression of CFTR, anoctamine-1 (ANO-1), NHEs (NHE-1 and NHE2), Cl^-/HCO_3^- exchangers (Slc26a3 and Slc26a6), NBC and aquaporins (AQP1, AQP5 and AQP8) was measured (Fig. 4*A*). Among the transporters, the expression of CFTR, ANO-1, NHE-1 and AQP-1 mRNA was significantly increased in diabetes; however, no differences were observed in the expression of the other transporters. The results obtained by PCR were also confirmed at the protein level (Fig. 4*B* and *C*). Using immunostaining, we confirmed the increased protein expression of CFTR, ANO-1, NHE-1 and AQP-1 in diabetic mice.

The central role of CFTR in diabetes-induced HCO_3^- secretion

The CFTR Cl^- channel plays an essential role in ductal HCO_3^- secretion. Its expression also increases in diabetes; thus, we considered how the activity of the channel changes under diabetic conditions. To estimate the activity of the channel, the Cl^--sensitive fluorescent dye, MQAE, and the specific CFTR activator, forskolin, were used (Fig. 5*A* and *B*). Administration of 20 μM forskolin increased Cl^- efflux in the normal and diabetic mice; however, the increase was significantly higher in diabetes.

To confirm the role of CFTR in diabetes-induced HCO_3^- secretion, we examined the activity of the Cl^-/HCO_3^- exchanger in the absence of CFTR, using CFTR knockout mice. Diabetes was induced in both wild-type (WT) and CFTR KO mice, and the activity of the exchanger was assessed by the alkali-load technique (Fig. 6*A*). In the absence of CFTR, the rate of HCO_3^- secretion was significantly reduced compared to the WT mice [3.2 ± 0.09 *vs.* 2.27 ± 0.1 $-J(B^-$ $min^{-1})$]. KO mice with induced diabetes also exhibited increased HCO_3^- secretion rates compared with their non-diabetic counterparts [3.01 ± 0.08 *vs.* 2.27 ± 0.1 $-J(B^-$ $min^{-1})$]; however, this increment fell short compared to that observed between diabetic and non-diabetic WT mice [3.01 ± 0.08 *vs.* 4.86 ± 0.14 $-J(B^-$ $min^{-1})$] and did not reach statistical significance. Interestingly, no difference was observed in the rate of regeneration from acidosis between WT and KO mice; however, in the absence of

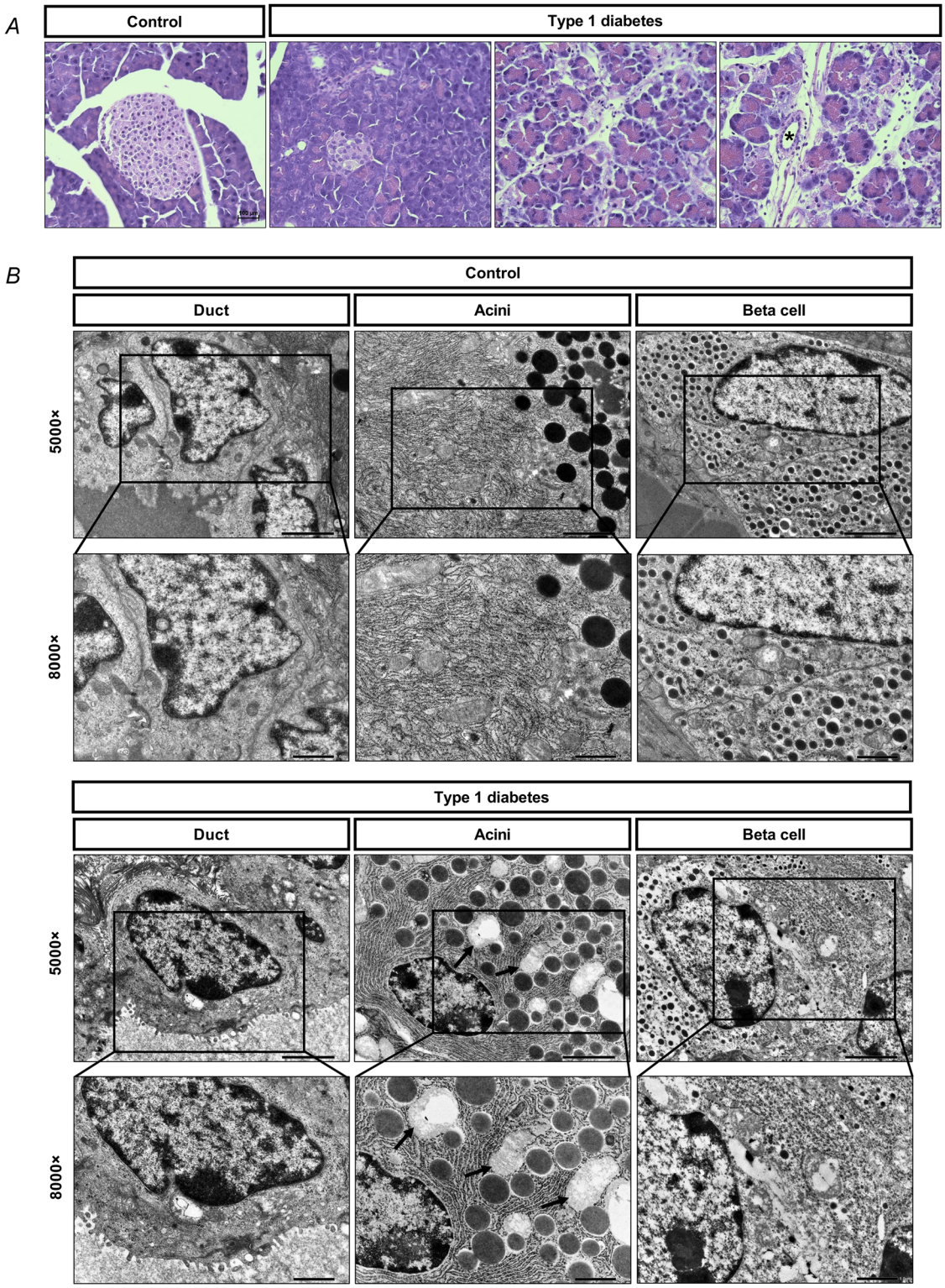

Figure 1. Effect of diabetes on pancreas morphology
A, haematoxylin and eosin staining of the pancreas from normal and type-1 diabetic mice. An asterisk shows the pancreatic duct. Scale bar = 100 μm. *B*, representative electron micrograph images of pancreatic duct, acini, and β cells from control and type-1 diabetic mice. Black arrows on the upper (magnification, 5000×) and lower (magnification, 8000×) panels indicate mitochondria.

CFTR, the diabetes-induced activity of NHE and/or NBC was significantly decreased [11.4 ± 0.34 *vs.* 9.4 ± 0.32 $J(B^-\ min^{-1})$] (Fig. 6*B*).

In the absence of CFTR, the rate of fluid secretion was far below that of WT mice (0.53 ± 0.08 *vs.* 1.19 ± 0.06 $\mu L\ h^{-1}\ g^{-1}$) (Fig. 6*C*). The presence of diabetes slightly increased the amount of fluid secretion in CFTR KO mice (0.84 ± 0.05 *vs.* 0.53 ± 0.17 $\mu L\ h^{-1}\ g^{-1}$), but did not result in a significant difference. Taken together, these results indicate that CFTR plays an important role in diabetes-induced, increased fluid and HCO_3^- secretion.

Effects of high glucose on the activity of acid–base transporters

The mechanism through which the functioning of transporters is increased in diabetes was examined. T1DM is often associated with hyperglycaemia; therefore, we determined the effect of acute and chronic glucose treatment on the activity of the transporters using the previously described alkali-load technique. During acute treatment, the isolated ducts were perfused with standard HCO_3^-/CO_2 solution containing 44.4 mM glucose, 8 min before the ammonia pulse, during the ammonia pulse, and 8 min after the ammonia pulse. During chronic treatment, the ducts were incubated in culture media supplemented with 44.4 mM glucose overnight. Upon acute glucose administration, no difference was observed in the rate of regeneration from alkalosis or acidosis between normal and diabetic mice (Fig. 7*Aa* and *Ab*). Similarly, chronic treatment did not affect the rate of regeneration from alkalosis, but increased the recovery from acidosis, indicating that the activity of NHE and/or NBC increases in response to chronic high glucose (Fig. 7*Ab*). The activity of the Cl^-/HCO_3^- exchanger was also examined using the Cl^- withdrawal technique; however, neither the acute, nor the chronic high glucose treatment caused any change in activity (Fig. 7*Ba*) or change in the maximal pH_i (Fig. 7*Bb*).

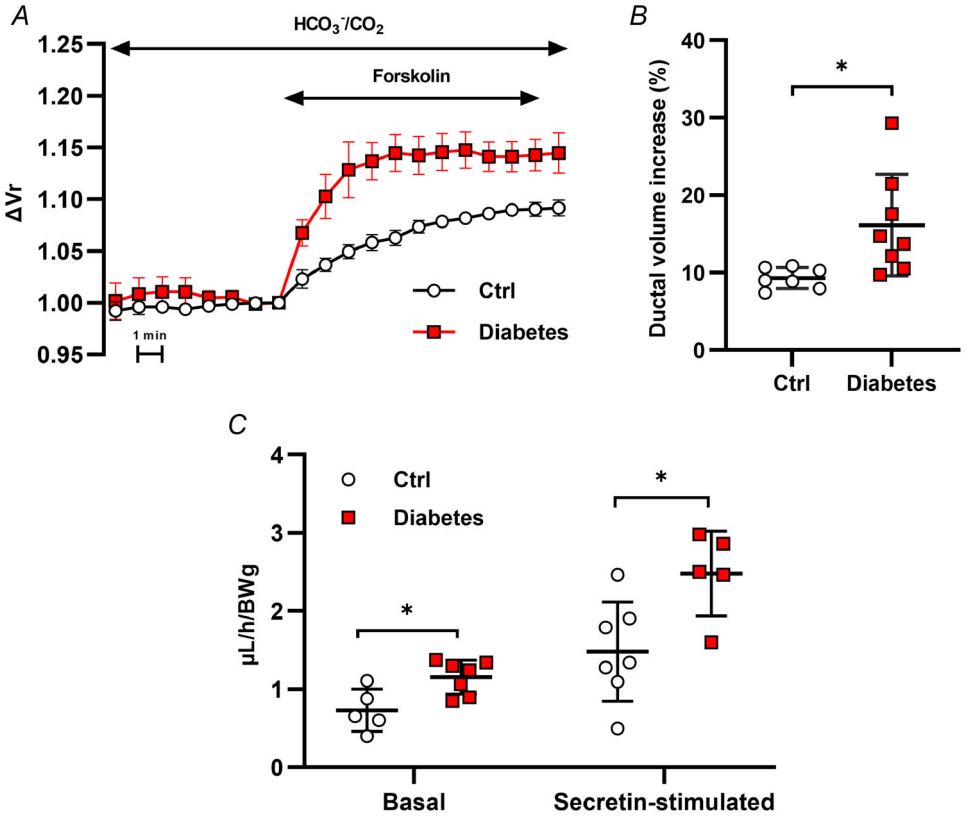

Figure 2. Effect of diabetes on ductal fluid secretion
A, pancreatic ductal fluid secretion was measured on intact pancreatic ducts isolated from control and diabetic mice. Swelling of pancreatic ducts was measured using video microscopy and analysed using Image J. *B*, ductal volume increase was measured during forskolin (5 μM) stimulation (between 8 and 18 time points) and expressed as a percentage. Data are shown as the mean ± SD (n = 7–8 ducts/three mice/groups). *P = 0.021 *vs.* Control using Welch's t test. *C*, bar chart showing the rate of *in vivo* pancreatic fluid secretion under basal and secretin-stimulated (1 CU kg^{-1}) conditions in control and diabetic mice. Data are shown as the mean ± SD (n = 5–7 mice/groups). *P = 0.013 (basal secretion) and 0.0174 (secretin-stimulated secretion) *vs.* Control, using an unpaired t test.

Serum levels of secretin and cholecystokinin in diabetic mice

To determine whether hormonal effects are involved in the increased secretion, we measured serum secretin and CCK levels in the diabetic mice. The primary physiological function of secretin is to stimulate the secretion of HCO_3^--rich pancreatic fluid, whereas CCK promotes the release of digestive enzymes. Neither serum secretin, nor serum CCK levels were different between the control and diabetic mice (Fig. 8*A* and *B*). Secretin was also examined in pancreatic homogenate (Fig. 8*C*) and we observed a slight increase in diabetic animals, although this was not significant. Finally, we examined whether there was a difference in the amount of ductal secretin receptors (SCTR) (Fig. 8*D*). RT-PCR revealed that the expression of SCTRs was significantly increased in the intra-interlobular ducts isolated from diabetic mice compared to the ducts isolated from control mice. Protein expression of SCTR also increased in the diabetic ducts, although this was not significant (Fig. 8*E* and *F*).

Discussion

Diabetes has long-term effects on exocrine function; however, less is known about the underlying mechanisms, particularly with respect to ductal cells. In the present study, we showed that the fluid and HCO_3^- secretion of ductal cells increased as a result of diabetes, in which

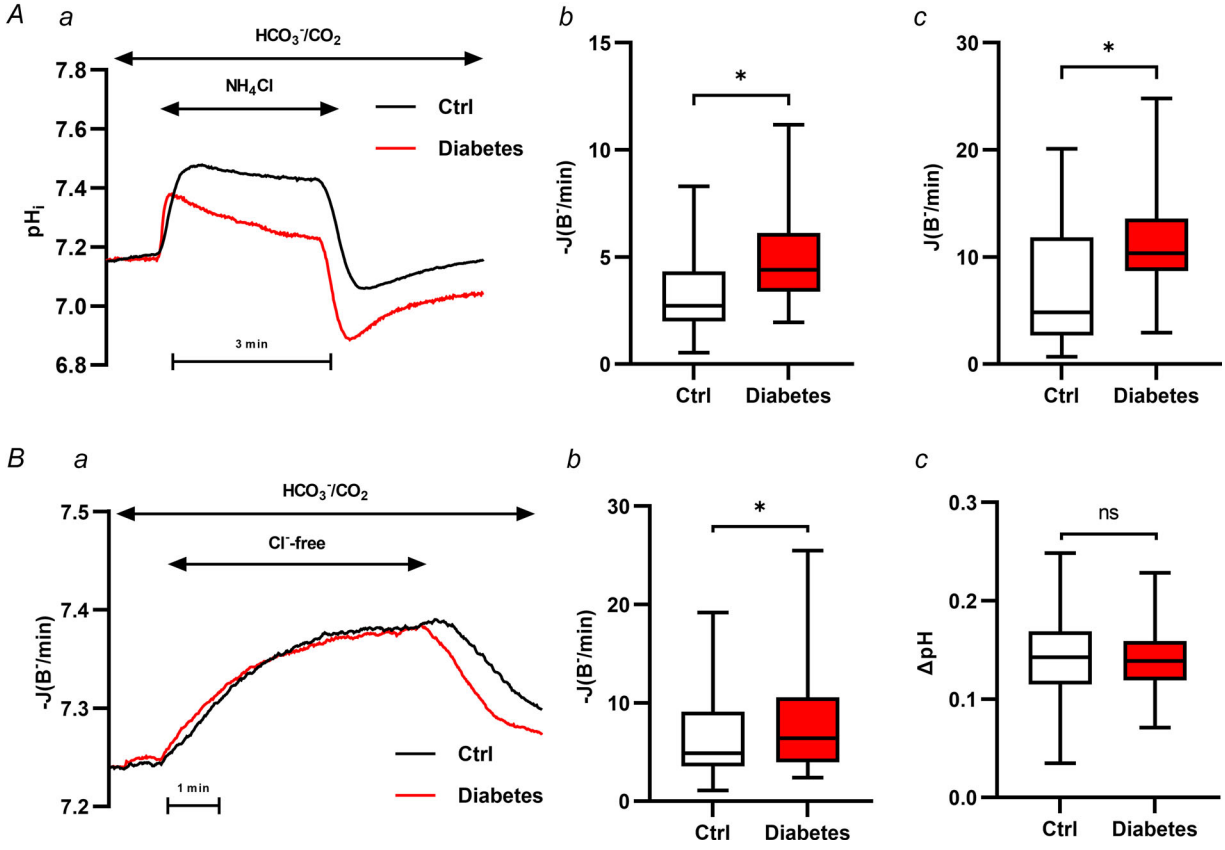

Figure 3. Effect of diabetes on the activity of ion transporters from isolated mice pancreatic ducts
A, ion transporter activity was examined using the NH_4Cl pre-pulse technique. *Aa*, representative pH_i traces showing the effect of diabetes (red line) on the activity of acid–base transporters in HCO_3^-/CO_2-buffered solution. The rate of regeneration from alkalosis (*Ab*) reflects the activity of the Cl^-/HCO_3^- exchanger, whereas regeneration from acidosis (*Ac*) reflects the activity of the Na^+/H^+ exchanger and the Na^+/HCO_3^- cotransporter. $-J(B^-\ min^{-1})$ and $J(B^-\ min^{-1})$ were calculated from the $\Delta pH/\Delta t$ obtained by a linear regression analysis of pH_i measurements made over the first 30 or 60 s, respectively (n = 172–274 ROIs/14–24 ducts/4–5 mice/groups). *$P < 0.0001$ *vs.* Control using the Mann–Whitney test. *B*, activity of the Cl^-/HCO_3^- exchanger was measured using the Cl^- withdrawal technique. *Ba*, representative pH_i traces show the effect of extracellular Cl^- removal on control (black line) and diabetic (red line) pancreatic ducts in HCO_3^-/CO_2-buffered solution. Box and whisker plots show the rate of regeneration from alkalosis after re-administration of extracellular Cl^- (*Bb*) and the maximal pH_i change (*Bc*). $-J(B^-\ min^{-1})$ was calculated from the $\Delta pH/\Delta t$ obtained by linear regression analysis of pH_i measurements made over the first 60 s (n = 219–230 ROIs/21 ducts/4 mice/groups). *$P = 0.0002$ *vs.* Control using the Mann–Whitney test. ns: $P = 0.2687$ *vs.* Control using Welch's *t* test.

increased activation and expression of CFTR and NHE-1 plays a key role.

First, we examined how T1DM affects the morphology of the exocrine and endocrine pancreas using electron microscopy. Acinar cells were identified by the presence of large, dark secretory granules and abundant endoplasmic reticulum and mitochondria. Islets were distinguished by the presence of cell clustering, smaller secretory granules and less endoplasmic reticulum. Although ductal cells typically have large nuclei, the cells enclose a lumen and cilia are present on the apical membrane of the cells. The most characteristic difference between the normal and diabetic pancreas is the morphological change of mitochondria in acinar cells. In diabetes, the mitochondria were less elongated and more round in shape. In addition, enlargement of the mitochondria and disruption of the inner membrane structure were also observed. Similar results were observed in the

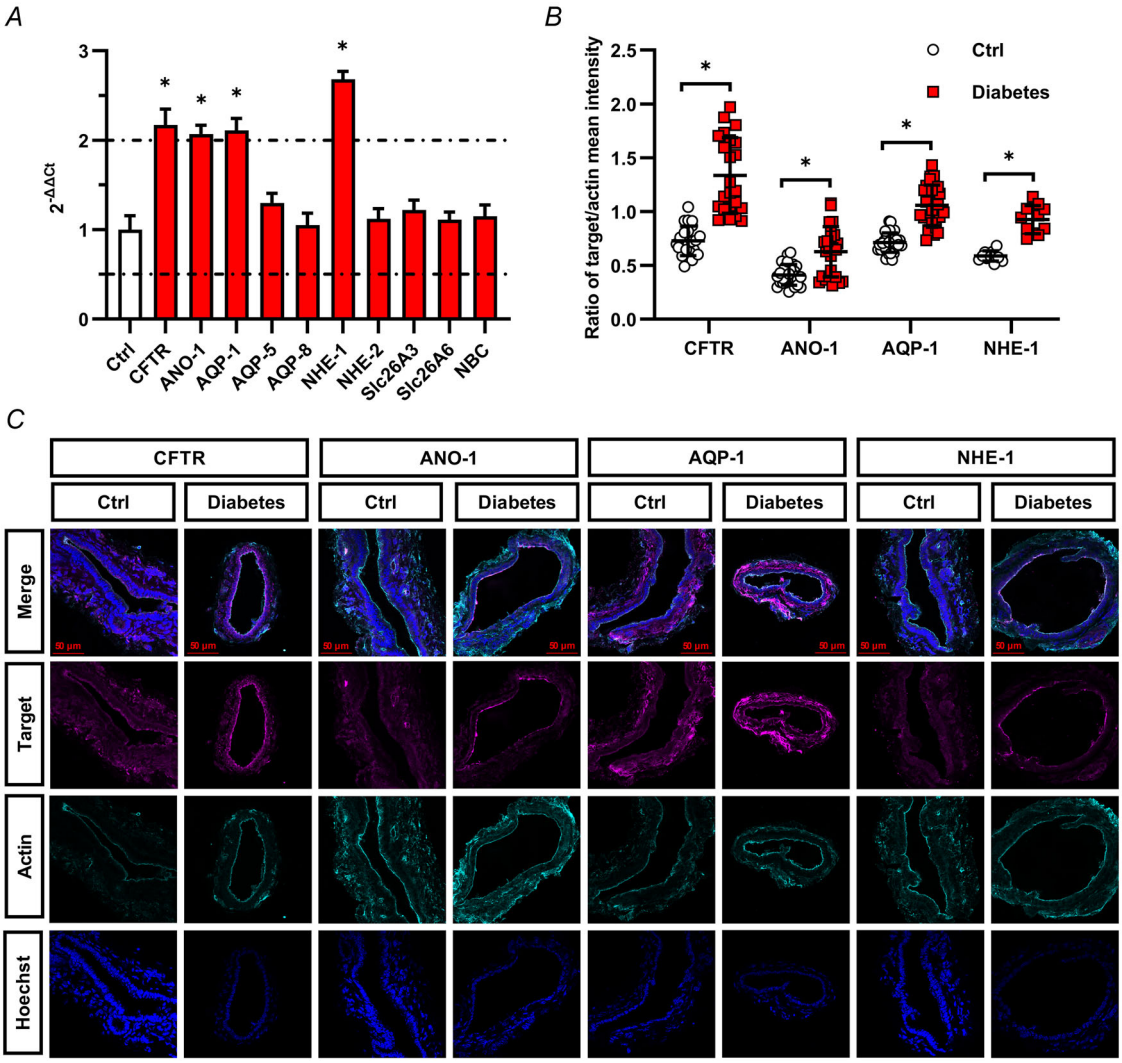

Figure 4. Effect of diabetes on the mRNA and protein expression of pancreatic ductal ion transporters
Intra-interlobular pancreatic ducts were isolated from control and diabetic mice and the mRNA (*A*) and protein (*B* and *C*) expression of the acid–base transporters was measured by RT-PCR and immunostaining, respectively. *A*, genes with expression values $\leq$0.5 were considered to be downregulated, whereas values $\geq$2 were considered to be upregulated. *B*, quantification of the fluorescence signals was carried out using ImageJ as described in the Methods. Data are shown as the mean $\pm$ SD. CFTR, cystic fibrosis transmembrane conductance regulator (n = 23 ROIs/8 ducts/4 mice/groups). *P < 0.0001 *vs*. Control using Welch's t test. ANO-1, anoctamine-1 (n = 24–26 ROIs/6–7 ducts/3 mice/groups). *P < 0.0001 *vs*. Control using Welch's t test. AQP-1, aquaporin-1 (n = 30–31 ROIs/8–9 ducts/3 mice/groups). *P = 0.0001 *vs*. Control using Welch's t test. NHE-1, Na^+/H^+ exchanger-1 (n = 11 ROIs/3 ducts/2 mice/groups). *P < 0.0001 *vs*. Control using Welch's t test. *C*, representative immunofluorescence staining of pancreatic ducts showing the expression of CFTR, ANO-1, AQP-1, and NHE-1 in control and diabetic ducts.

intermediate cells of T1DM patients (de Boer et al., 2020) and in the beta cells of T2DM patients (Anello et al., 2005). By contrast to acini, ductal mitochondria remained mostly intact. Because mitochondria play an important role in maintaining the normal energy production and balance of the cells, it is possible that mitochondrial damage occurring in acini contributes to the development of EPI. Meanwhile, the morphology of ductal cells remained largely unaltered, which suggests that ductal functions are preserved in T1DM.

The pancreatic ductal epithelium has a secretory function and produces a HCO_3^--rich luminal fluid. This

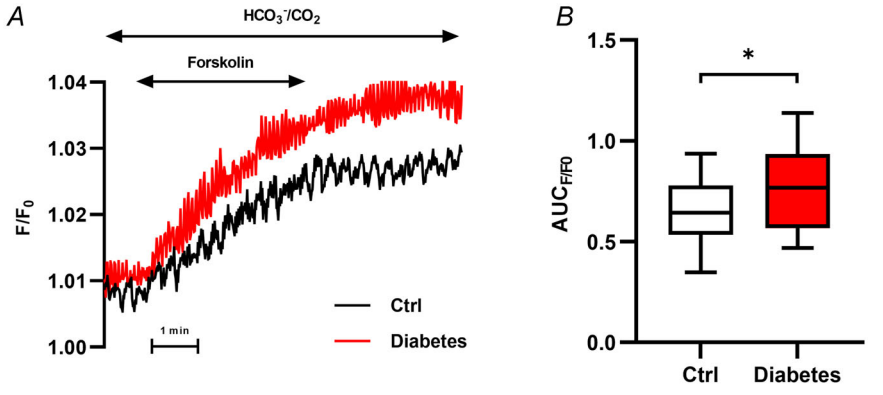

Figure 5. Effect of diabetes on the activity of the CFTR
A, intra-interlobular pancreatic ducts were isolated from control and diabetic mice and the rate of Cl^- efflux was estimated using a Cl^--sensitive fluorescent dye and the specific CFTR activator, forskolin (20 μM). *B*, the area under the curve was calculated for the first 2 min of forskolin stimulation (n = 42–77 ROIs/3–5 ducts/3 mice/groups). $^*P$ = 0.0053 *vs.* Control using the Mann–Whitney test.

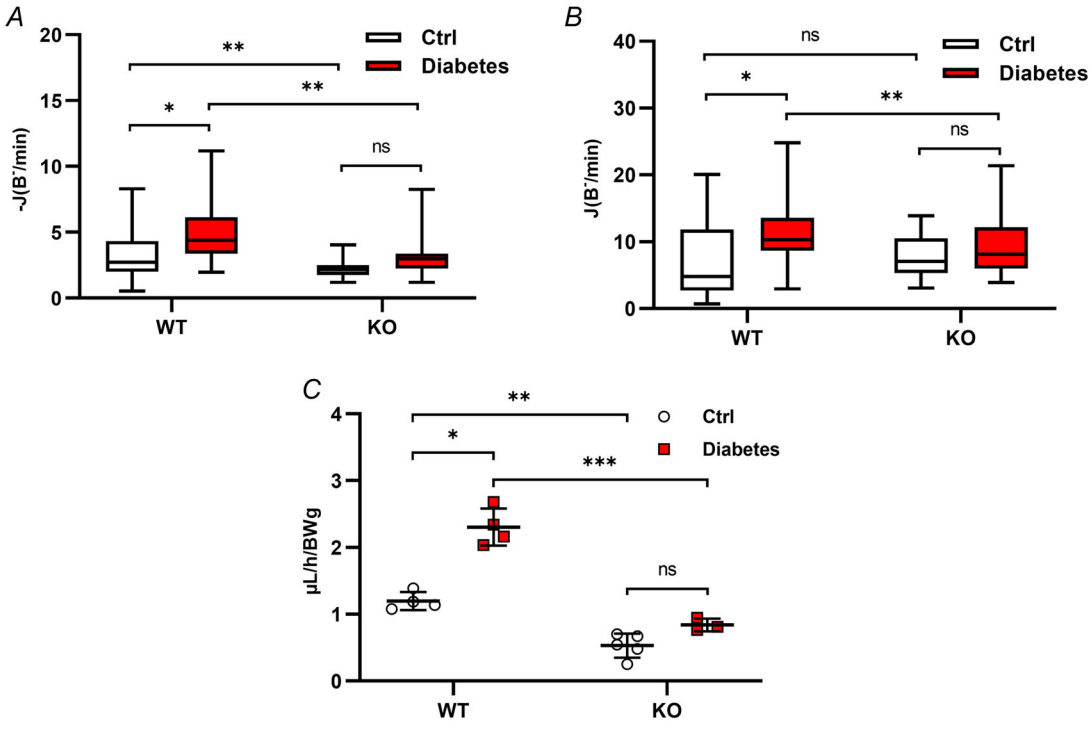

Figure 6. Role of the CFTR in diabetes
Intra-interlobular pancreatic ducts were isolated from wild-type (WT) and CFTR knockout (KO) mice with or without diabetes and the activity of the acid–base transporters was measured by the NH_4Cl pre-pulse technique in HCO_3^-/CO_2-buffered solution. The rate of regeneration from alkalosis (*A*) reflects the activity of the Cl^-/HCO_3^- exchanger, whereas regeneration from acidosis (*B*) reflects the activity of the Na^+/H^+ exchanger and the Na^+/HCO_3^- cotransporter. $-J(B^-$ min$^{-1})$ and $J(B^-$ min$^{-1})$ were calculated from the $\Delta pH/\Delta t$ obtained by linear regression analysis of the pH_i measurements made over the first 30 or 60 s, respectively. Data are shown as the mean ± SD (n = 60–160 ROIs/5–13 ducts/3 mice/groups). $^*P < 0.0001$ *vs.* Control, $^{**}P \leq 0.0001$ *vs.* WT using the Kruskal–Wallis test. In the case of regeneration from alkalosis, ns: $P = 0.118$ *vs.* KO/Control. In the case of regeneration from acidosis, ns: $P = 0.9799$ *vs.* WT/Control and ns: $P = 0.2723$ *vs.* KO/Control. *C*, scatter plot showing the rate of *in vivo* pancreatic fluid secretion under secretin-stimulated (1 CU kg^{-1}) conditions in WT and CFTR KO mice with or without diabetes. Data are shown as the mean ± SD (n = 3–5 mice/groups). $^*P < 0.0001$ *vs.* Control, $^{**}P = 0.011$ *vs.* WT, $^{***}P < 0.0001$ *vs.* WT, using one-way ANOVA. ns: $P = 0.1692$ *vs.* KO/Control.

fluid provides a carrier for the transport of digestive enzymes and counteracts the acid produced by the stomach and acini. Using *in vivo* and *in vitro* approaches, we demonstrated that the amount of pancreatic fluid was significantly increased in streptozotocin-induced T1DM mice. The elevated fluid secretion was observed under basal and secretin-stimulated conditions. The rate of fluid secretion primarily depends on the rate of HCO_3^- secretion, and therefore on the activity of ductal ion transporters. The major route for HCO_3^- secretion in the ductal cells is the apically localized Cl^-/HCO_3^- exchanger Slc26a6, which mediates the electrogenic exchange of 1 Cl^- and 2 HCO_3^- (Shcheynikov et al., 2006). Using the alkali-load method, we found that the activity of the Cl^-/HCO_3^- exchanger increased in diabetes, which was also confirmed by the Cl^- withdrawal technique. In the Cl^- withdrawal technique, removal of extracellular Cl^- causes a sudden alkalization because of the altered function of the exchanger. In the absence of Cl^-, the exchanger operates in reverse mode and absorbs HCO_3^- in exchange for Cl^-. The absorbed HCO_3^- binds free protons and induces alkalosis in the cell. Therefore, this technique allows for the direct measurement of exchanger activity. Interestingly, there was no difference in the degree of alkalosis, nor in the maximum pH change between the control and the diabetic ducts, which suggests that diabetes does not affect the function of the exchanger in reverse mode. Because the CFTR Cl^- channel and the Cl^-/HCO_3^- exchanger work closely with one another, we measured

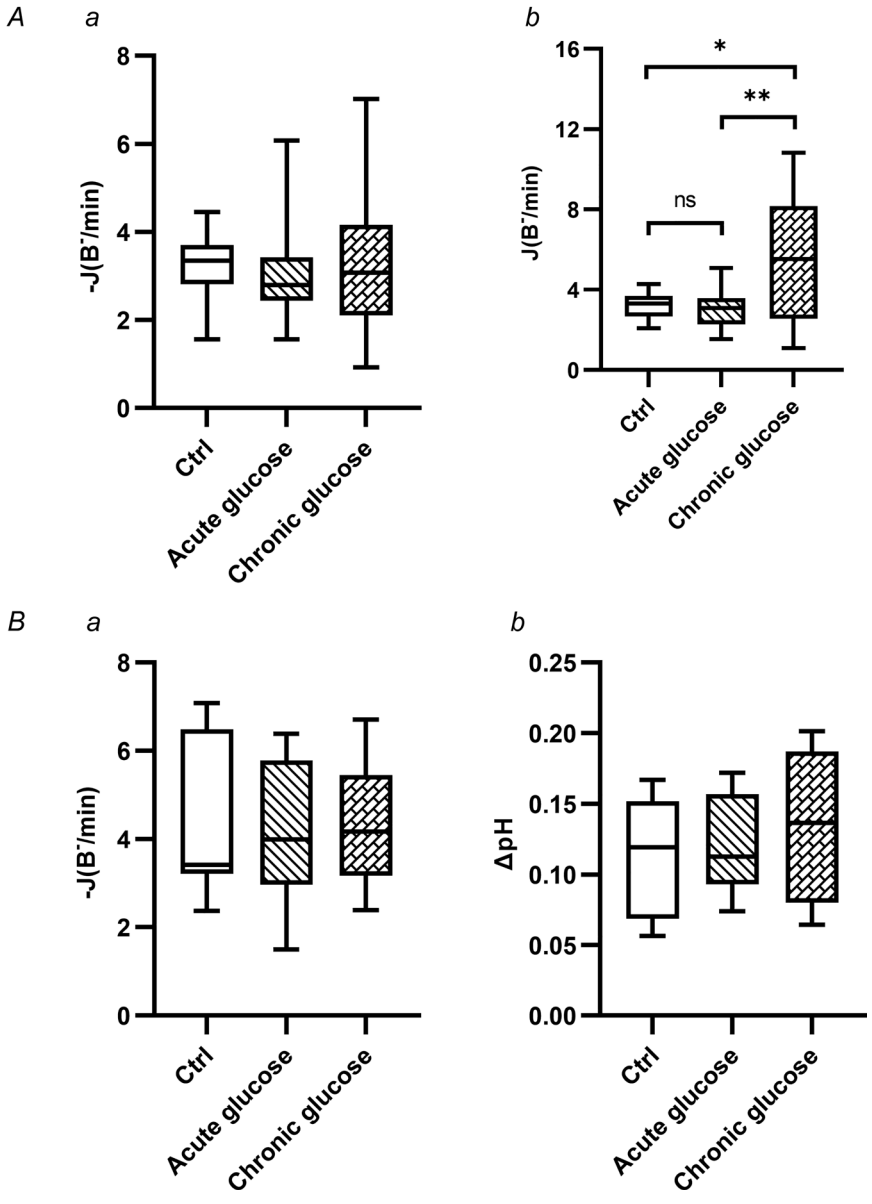

Figure 7. Effect of extracellular glucose on the activity of ion transporters from isolated mouse pancreatic ducts
Intra-interlobular pancreatic ducts isolated from control mice were incubated with 44.4 mM glucose during the ammonia pulse (acute treatment) or overnight (chronic treatment). *A*, activity of the ion transporters was measured using the NH_4Cl pre-pulse technique. The rate of regeneration from alkalosis (*Aa*) reflects the activity of the Cl^-/HCO_3^- exchanger, whereas regeneration from acidosis (*Ab*) reflects the activity of the Na^+/H^+ exchanger and the Na^+/HCO_3^- cotransporter. $-J(B^-\ min^{-1})$ and $J(B^-\ min^{-1})$ were calculated from the $\Delta pH/\Delta t$ obtained by linear regression analysis of the pH_i measurements made over the first 30 or 60 s, respectively (n = 44–76 ROIs/3–5 ducts/3 mice/groups). For the regeneration from the alkaline load P = 0.2144 (acute glucose) and 0.5524 (chronic glucose) *vs*. Control, using the Kruskal–Wallis test. For regeneration from the acidic load, ns: P = 0.9702 *vs*. Control, $^*P$ = 0.0175 *vs*. Control and $^{**}P < 0.0001$ *vs*. Acute glucose, using the Kruskal–Wallis test. *B*, activity of the Cl^-/HCO_3^- exchanger was measured using the Cl^- withdrawal technique. Bar charts showing the rate of regeneration from alkalosis after re-administration of extracellular Cl^- (*Ba*) and the maximal pH_i change (*Bb*). $-J(B^-\ min^{-1})$ was calculated from the $\Delta pH/\Delta t$ obtained by linear regression analysis of the pH_i measurements made over the first 60 s (n = 44–60 ROIs/3–4 ducts/3 mice/groups). For the regeneration from the alkaline load, $P < 0.9999$. For pH_i change, P = 0.7677 (acute glucose) and 0.2583 (chronic glucose) *vs*. Control, using the Kruskal–Wallis test.

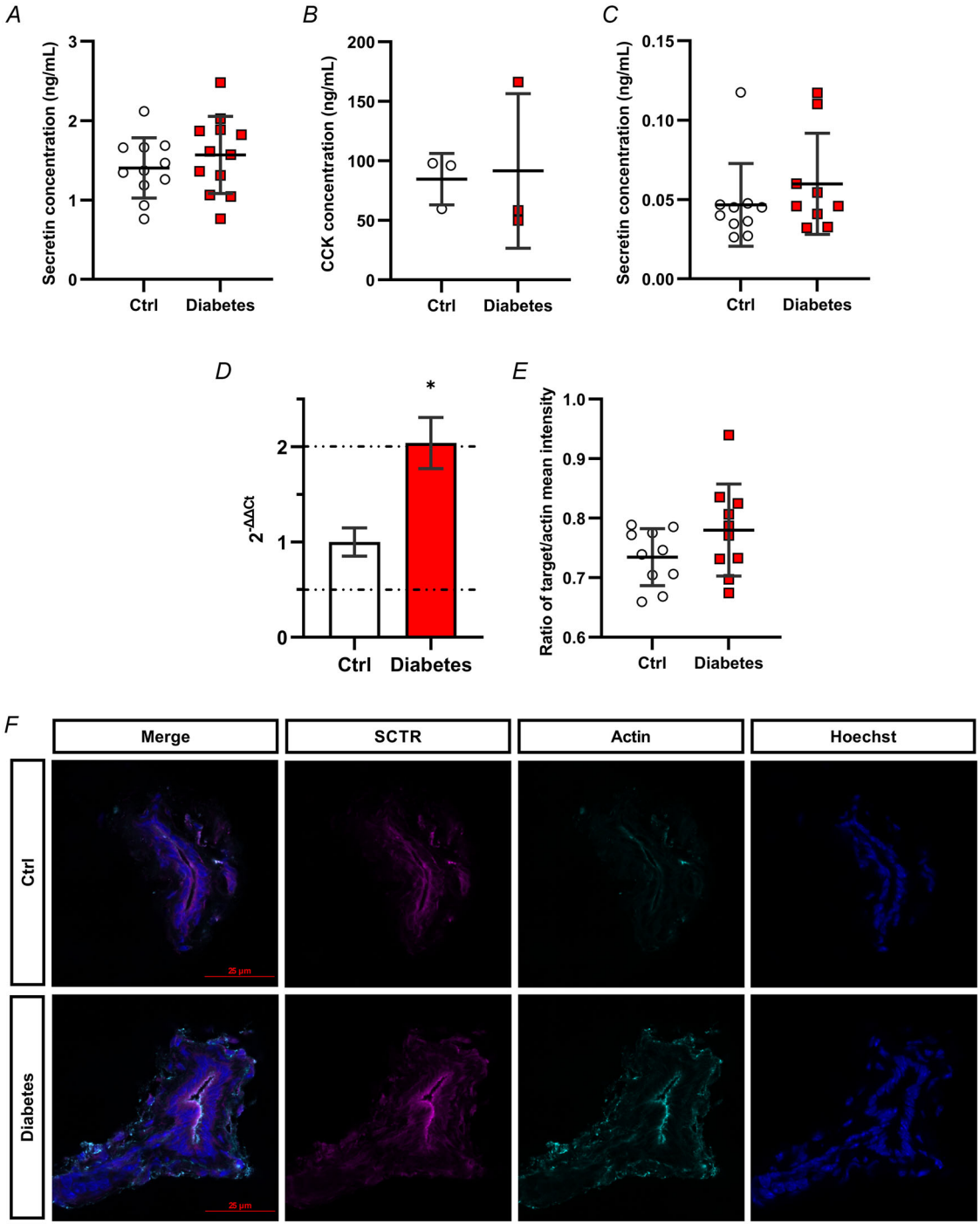

Figure 8. Effect of diabetes on secretin and cholecystokinin levels and the expression of SCTR
Plasma and pancreas samples were obtained from control and diabetic mice and the serum levels of secretin (*A*) and cholecystokinin (*B*) and the levels of secretin in the pancreas homogenate (*C*) were measured by ELISA. Data are shown as the mean ± SD (n = 3–12 mice/groups). P = 0.3803 for serum secretin, P = 0.8689 for serum cholecystokinin and P = 0.3337 for tissue homogenate secretin, using a two-sample t test. Intra-interlobular pancreatic ducts were isolated from control and diabetic mice and the mRNA (*D*) and protein (*E* and *F*) expression of SCTR were measured by RT-PCR and immunostaining, respectively. SCTR mRNA expression values ≤0.5 were considered to be downregulated, whereas values ≥2 were considered to be upregulated. Data are shown as the mean ± SD. For secretin protein expression, n = 10 ROIs/4 ducts/3 mice/groups. P = 0.1311 using a two-sample t test.

the activity of CFTR using a Cl^- sensitive fluorescent dye along with the specific CFTR activator, forskolin. We detected increased CFTR activity in diabetic ducts, which presumably contributes to an increased rate of HCO_3^- secretion. The NH_4Cl pre-pulse technique also enables the investigation of alkalizing transporters by measuring the rate of regeneration from acidosis. Similar to alkali recovery, we observed a significant increase in acid recovery, indicating that the activity of alkalizing transporters was also increased as a result of diabetes. In ductal cells, the major alkalizing transporters are NHE and NBC. NHE is an electroneutral transporter that mediates the exchange of intracellular H^+ to extracellular Na^+, whereas NBC is an electrogenic co-transporter, through which Na^+ and HCO_3^- enter the cell with isotype-dependent stoichiometry. Both transporters have an important role in ductal HCO_3^- secretion because NBC promotes HCO_3^- accumulation, whereas NHE removes H^+, a by-product of HCO_3^- from the cell (Lee et al., 2012). Consequently, if the activity of the anion exchanger increases, NHE and NBC activity also increases, as confirmed by our experiments.

Next, we identified the mechanism which is responsible for increased transporter activity. As a first step, we measured the expression of the major acid–base transporters. We found that both the mRNA and protein expression of CFTR was significantly increased in diabetic ducts, which may explain the increased activity of CFTR in diabetes. In addition, overexpression of other acid–base transporters, which are involved in the HCO_3^- secretion, was also observed as a result of diabetes. ANO-1 or TMEM16A is a Ca^{2+}-activated Cl^- channel that exhibits multiple cellular functions in the body, including the regulation of epithelial secretion (Dulin, 2020). The presence of ANO-1 has been confirmed in salivary and pancreatic acini (Huang et al., 2009; Romanenko et al., 2010), but not in ductal cells. Although, the presence of a Ca^{2+}-activated Cl^- channel was observed in pancreatic ductal cells (Grey et al., 1989; Grey et al., 1994), the molecular identity of this channel has not yet been determined. The present study is the first to demonstrate the presence of ANO-1 on the luminal membrane of ductal cells and we found that diabetes increases the expression of this Cl^- channel. The antibody we used is directed against the third extracellular loop of mouse ANO-1 and has been shown to be highly specific against the protein (Dauner et al., 2012). ANO-1 has been intensively studied subsequent to its discovery. It has been shown that the channel can be activated by divalent cations, especially by Ca^{2+} (Ni et al., 2014). It is conceivable that the increase in intracellular Ca^{2+} level leads to the activation of the channel also in pancreatic ductal cells, as shown in acinar cells and salivary ducts (Lee et al., 2012). However, other pathways may also be involved because, in addition to Ca^{2+}, several other mechanisms have been described to activate the channel, such as release of extracellular ATP, decrease in intracellular pH or heat stress (Dulin, 2020).

We hypothesize that, in addition to CFTR, ANO-1 also functions in close co-ordination with the anion exchanger or acts as an alternative HCO_3^- pathway, as shown in acinar cells (Han et al., 2016). Increased expression of this channel may also contribute to increased HCO_3^- secretion in diabetes. Nevertheless, further functional studies are needed to clarify the role of ductal ANO-1 in pancreatic fluid secretion. In addition to ANO-1, the expression of AQP-1 was also increased in diabetes. AQP-1 is a constitutively expressed water channel and its presence on the plasma membrane of centroacinar cells and interlobular ducts has been demonstrated (Burghardt et al., 2003; Venglovecz et al., 2018). AQP-1 regulates transcellular water movement and, as the major water channel on ductal cells, it is responsible for the secretion of most of the fluid into the pancreatic juice (Lee et al., 2012). Overexpression of AQP-1 in diabetes is probably a compensatory mechanism for increased anion secretion because transcellular ion movements are accompanied by water transport to compensate for altered osmotic conditions. Therefore, increased AQP-1 expression may explain increased fluid secretion in diabetes. We also examined other AQP isoforms present in the pancreas (AQP-5 and -8) (Burghardt et al., 2003); however, we found no changes in their expression compared with the control. Among the NHEs, increased NHE-1 expression was also observed in diabetic ducts. Nine members of the NHE family are known, of which NHE-1 is expressed in almost every cell and it is also present on the basolateral membrane of pancreatic ducts (Lee et al., 2012). By contrast to NHE-1, we did not find alterations in the expression of NBC, indicating that NHE, rather than NBC, is responsible for the increased rate of acid regeneration in diabetes. Among the Slc26 anion exchangers, Slc26a3 and Slc26a6 isoforms occur in pancreatic ducts and play an important role in ductal HCO_3^- secretion (Lee et al., 2012). Although our functional studies revealed that Cl^-/HCO_3^- exchange activity is increased in diabetes, we found no difference in expression compared to the control. These results indicate that the increased activity of CFTR and/or ANO-1 and NHE-1 stimulates Cl^-/HCO_3^- exchange. The primary role of CFTR on stimulating the effects of diabetes is also supported by the results obtained from CFTR KO ducts and mice. In the absence of CFTR, both fluid and HCO_3^- secretion was significantly decreased compared to the control. In CFTR KO mice in which diabetes was induced, although there was a small increase in both parameters compared to the control, non-diabetic KO mice, it was not significant. This indicates that the presence of functionally active CFTR is essential for the stimulatory effect on diabetes.

We next examined the mechanism that causes the increased activity/expression of transporters during diabetes. T1DM is associated with hyperglycaemia; therefore, we tested the effect of acute and chronic glucose treatment on transporter activity. The concentration of glucose was selected based on a previous report (Futakuchi et al., 2009). Using the alkali load and Cl^- withdrawal techniques, we found that neither acute, nor chronic glucose treatment affected anion exchange activity. By contrast, chronic glucose treatment increased the rate of regeneration from acidosis, which suggests that hyperglycaemia, which occurs during diabetes, directly increases the activity of NHE and/or NBC. Previous studies showed that high extracellular glucose increases NHE-1 activity in distal nephron cells, vascular myocytes and lymphoblasts of diabetic nephropathy patients (da Costa-Pessoa et al., 2014; Davies et al., 1995; Siczkowski & Ng, 1996). These studies suggest that glucose-induced NHE-1 activity depends on protein kinase C or the Mek/Erk1/2/p90(RSK) and p38MAPK pathways, depending on the cell type. In the present study, we did not identify the mechanism by which high extracellular glucose stimulates NHE-1, although the results suggest that the stimulatory effect of diabetes on HCO_3^- secretion may include increased NHE-1 activity. In addition to hyperglycaemia, we also examined hormonal effects on secretion. The rate of HCO_3^- secretion is primarily influenced by the gastrointestinal hormone secretin, which is secreted by S cells in the duodenum (DiGregorio & Sharma, 2023). The secretion of secretin is induced at low duodenal pH, which is formed under the influence of gastric acid during a meal. The primary function of secretin is to neutralize pH in the duodenum, thus creating optimal conditions for the function of digestive enzymes (DiGregorio & Sharma, 2023). To increase duodenal pH, secretin stimulates ductal HCO_3^- through the activation of basolaterally localized secretin receptors (Ishihara et al., 1991). Activation of the secretin receptors increases intracellular cAMP levels, which increases the opening time of the CFTR channel, through phosphorylation by protein kinase A (Afroze et al., 2013). Following CTFR activation, outflow of Cl^- increases into the extracellular space. To compensate for the increased Cl^- outflow, the activity of the Cl^-/HCO_3^- exchanger increases by several fold, which results in HCO_3^- secretion. In the present study, we have demonstrated for the first time that mRNA expression of secretin receptors is significantly increased in response to diabetes. An increase was also observed at the protein level, although this was not significant. We speculate that the effect of secretin increases on ductal cells to some extent in diabetes, although further studies are needed to confirm this hypothesis.

In conclusion, our results demonstrate that the stimulatory effect of diabetes on ductal HCO_3^- secretion is a complex process, with several factors being involved. The Cl^-/HCO_3^- exchanger activity is enhanced by the overexpression of ductal acid–base transporters, particularly CFTR and NHE-1. In addition, high extracellular glucose stimulates alkalizing transporters, such as NHE-1, which may also contribute to increased secretion. The role of the increased secretion, and also whether it is a temporary or permanent condition, is not known. It has long been known that exocrine secretion is partly under endocrine control (Camello et al., 1994; Chayvialle & Vagne, 1981). Among the endocrine hormones, insulin increases ductal fluid secretion, whereas glucagon, somatostatin and pancreatic polypeptide inhibit it (Bertelli & Bendayan, 2005). By contrast, opinions differ as to how diabetes affects ductal function. The most accepted view is that exocrine functions are mostly impaired by long-standing diabetes. One explanation for the reduced ductal secretion could be that the stimulatory effect of insulin decreases on the ductal cells. On the other hand, the present study showed that ductal secretion increases as a result of diabetes, at least in the initial stage. A recent study reported that high concentration of HCO_3^- promotes glucose-induced insulin secretion by enhancing Ca^{2+} influx (Zhang et al., 2022). Our study indicates that ductal HCO_3^- secretion serves as a protective mechanism and therefore represents a potential therapeutic target for the prevention or treatment of diabetes. Although this hypothesis is promising, further studies are needed in this area.

References

Afroze, S., Meng, F., Jensen, K., McDaniel, K., Rahal, K., Onori, P., Gaudio, E., Alpini, G., & Glaser, S. S. (2013). The physiological roles of secretin and its receptor. *Annals of Translational Medicine*, **1**, 29.

Anello, M., Lupi, R., Spampinato, D., Piro, S., Masini, M., Boggi, U., Del Prato, S., Rabuazzo, A. M., Purrello, F., & Marchetti, P. (2005). Functional and morphological alterations of mitochondria in pancreatic beta cells from type 2 diabetic patients. *Diabetologia*, **48**(2), 282–289.

Argent, B. E., Arkle, S., Cullen, M. J., & Green, R. (1986). Morphological, biochemical and secretory studies on rat pancreatic ducts maintained in tissue culture. *Quarterly Journal of Experimental Physiology*, **71**(4), 633–648.

Behrendorff, N., Floetenmeyer, M., Schwiening, C., & Thorn, P. (2010). Protons released during pancreatic acinar cell secretion acidify the lumen and contribute to pancreatitis in mice. *Gastroenterology*, **139**(5), 1711–1720. e5, 1720 e1711-1715.

Bertelli, E., & Bendayan, M. (2005). Association between endocrine pancreas and ductal system. More than an epiphenomenon of endocrine differentiation and development? *Journal of Histochemistry and Cytochemistry*, **53**(9), 1071–1086.

Burghardt, B. (2003). Distribution of aquaporin water channels AQP1 and AQP5 in the ductal system of the human pancreas. *Gut*, **52**(7), 1008–1016.

Camello, P. J., Wisdom, D. M., Singh, J., & Salido, G. M. (1994). Hormonal control of exocrine pancreatic secretion in the isolated intact rat pancreas. *Revista Espanola De Fisiologia*, **50**, 35–40.

Chayvialle, J. A., & Vagne, M. (1981). [Hormonal control of pancreatic exocrine secretion (author's transl)]. *Gastroenterologie Clinique Et Biologique*, **5**, 212–221.

Creutzfeldt, W., Gleichmann, D., Otto, J., Stockmann, F., Maisonneuve, P., & Lankisch, P. G. (2005). Follow-up of exocrine pancreatic function in type-1 diabetes mellitus. *Digestion*, **72**, 71–75.

Da Costa-Pessoa, J. M., Damasceno, R. S., Machado, U. F., Beloto-Silva, O., & Oliveira-Souza, M. (2014). High glucose concentration stimulates NHE-1 activity in distal nephron cells: The role of the Mek/Erk1/2/p90RSK and p38MAPK signaling pathways. *Cellular Physiology and Biochemistry*, **33**(2), 333–343.

Dauner, K., Lißmann, J., Jeridi, S., Frings, S., & Möhrlen, F. (2012). Expression patterns of anoctamin 1 and anoctamin 2 chloride channels in the mammalian nose. *Cell and Tissue Research*, **347**(2), 327–341.

Davies, J. E., Siczkowski, M., Sweeney, F. P., Quinn, P. A., Krolewski, B., Krolewski, A. S., & Ng, L. L. (1995). Glucose-induced changes in turnover of Na^+/H^+ exchanger of immortalized lymphoblasts from type I diabetic patients with nephropathy. *Diabetes*, **44**(4), 382–388.

De Boer, P., Pirozzi, N. M., Wolters, A. H. G., Kuipers, J., Kusmartseva, I., Atkinson, M. A., Campbell-Thompson, M., & Giepmans, B. N. G. (2020). Large-scale electron microscopy database for human type 1 diabetes. *Nature Communications*, **11**(1), 2475.

DiGregorio, N., & Sharma, S. (2023). Physiology, Secretin. In *StatPearls*. Treasure Island (FL) ineligible companies. Disclosure: Sandeep Sharma declares no relevant financial relationships with ineligible companies.

Dulin, N. O. (2020). Calcium-activated chloride channel ANO1/TMEM16A: Regulation of expression and signaling. *Frontiers in Physiology*, **11**, 590262.

Fernández-Salazar, M. P., Pascua, P., Calvo, J. J., López, M. A., Case, R. M., Steward, M. C., & San Román, J. I. (2004). Basolateral anion transport mechanisms underlying fluid secretion by mouse, rat and guinea-pig pancreatic ducts. *The Journal of Physiology*, **556**(2), 415–428.

Futakuchi, S., Ishiguro, H., Naruse, S., Ko, S. B. H., Fujiki, K., Yamamoto, A., Nakakuki, M., Song, Y., Steward, M. C., Kondo, T., & Goto, H. (2009). High glucose inhibits HCO3(-) and fluid secretion in rat pancreatic ducts. *Pflugers Archiv: European Journal of Physiology*, **459**(1), 215–226.

Gál, E., Dolenšek, J., Stožer, A.ž, Czakó, L., Ébert, A., & Venglovecz, V. (2021). Mechanisms of post-pancreatitis diabetes mellitus and cystic fibrosis-related diabetes: A review of preclinical studies. *Frontiers in Endocrinology (Lausanne)*, **12**, 715043.

Gray, M. A., Harris, A., Coleman, L., Greenwell, J. R., & Argent, B. E. (1989). Two types of chloride channel on duct cells cultured from human fetal pancreas. *American Journal of Physiology*, **257**(2), C240–C251.

Gray, M. A., Winpenny, J. P., Porteous, D. J., Dorin, J. R., & Argent, B. E. (1994). CFTR and calcium-activated chloride currents in pancreatic duct cells of a transgenic CF mouse. *American Journal of Physiology*, **266**(1), C213–C221.

Han, Y., Shewan, A. M., & Thorn, P. (2016). HCO3-transport through anoctamin/transmembrane protein ANO1/TMEM16A in pancreatic acinar cells regulates luminal pH. *Journal of Biological Chemistry*, **291**(39), 20345–20352.

Hardt, P. D., & Ewald, N. (2011). Exocrine pancreatic insufficiency in diabetes mellitus: A complication of diabetic neuropathy or a different type of diabetes? *Experimental Diabetes Research*, **2011**, 1.

Hardt, P. D., Hauenschild, A., Nalop, J., Marzeion, A. M., Jaeger, C., Teichmann, J., Bretzel, R. G., Hollenhorst, M., & Kloer, H. U. (2003). High prevalence of exocrine pancreatic insufficiency in diabetes mellitus. A multicenter study screening fecal elastase 1 concentrations in 1,021 diabetic patients. *Pancreatology*, **3**(5), 395–402.

Hayden, M. R., Karuparthi, P. R., Habibi, J., Lastra, G., Patel, K., Wasekar, C., Manrique, C. M., Ozerdem, U., Stas, S., & Sowers, J. R. (2008). Ultrastructure of islet microcirculation, pericytes and the islet exocrine interface in the HIP rat model of diabetes. *Experimental Biology and Medicine (Maywood, N.J.)*, **233**(9), 1109–1123.

Hegyi, P., Gray, M. A., & Argent, B. E. (2003). Substance P inhibits bicarbonate secretion from guinea pig pancreatic ducts by modulating an anion exchanger. *American Journal of Physiology-Cell Physiology*, **285**(2), C268–C276.

Hegyi, P., Maléth, J., Venglovecz, V., & Rakonczay, Z. (2011). Pancreatic ductal bicarbonate secretion: Challenge of the acinar Acid load. *Frontiers in Physiology*, **2**, 36.

Hegyi, P., Pandol, S., Venglovecz, V., & Rakonczay, Z. (2011). The acinar-ductal tango in the pathogenesis of acute pancreatitis. *Gut*, **60**(4), 544–552.

Hegyi, P. T., Rakonczay, Z. N., Gray, M. A., & Argent, B. E. (2004). Measurement of intracellular pH in pancreatic duct cells: A new method for calibrating the fluorescence data. *Pancreas*, **28**(4), 427–434.

Hegyi, P., Rakonczay, Z., Tiszlavicz, L., Varró, A., Tóth, A., Rácz, G., Varga, G., Gray, M. A., & Argent, B. E. (2005). Protein kinase C mediates the inhibitory effect of substance P on HCO3- secretion from guinea pig pancreatic ducts. *American Journal of Physiology-Cell Physiology*, **288**(5), C1030–C1041.

Huang, F., Rock, J. R., Harfe, B. D., Cheng, T., Huang, X., Jan, Y. N., & Jan, L. Y. (2009). Studies on expression and function of the TMEM16A calcium-activated chloride channel. *The Proceedings of the National Academy of Sciences*, **106**(50), 21413–21418.

Ishihara, T., Nakamura, S., Kaziro, Y., Takahashi, T., Takahashi, K., & Nagata, S. (1991). Molecular cloning and expression of a cDNA encoding the secretin receptor. *Embo Journal*, **10**(7), 1635–1641.

Laczkó, D., Rosztóczy, A., Birkás, K., Katona, M., Rakonczay, Z., Tiszlavicz, L., Róka, R., Wittmann, T., Hegyi, P., & Venglovecz, V. (2016). Role of ion transporters in the bile acid-induced esophageal injury. *American Journal of Physiology-Gastrointestinal and Liver Physiology*, **311**(1), G16–G31.

Lee, M. G., Ohana, E., Park, H. W., Yang, D., & Muallem, S. (2012). Molecular mechanism of pancreatic and salivary gland fluid and HCO3 secretion. *Physiological Reviews*, **92**(1), 39–74.

Mossner, J., Logsdon, C. D., Goldfine, I. D., & Williams, J. A. (1984). Regulation of pancreatic acinar cell insulin receptors by insulin. *American Journal of Physiology*, **247**, G155–G160.

Mössner, J., Logsdon, C. D., Williams, J. A., & Goldfine, I. D. (1985). Insulin, via its own receptor, regulates growth and amylase synthesis in pancreatic acinar AR42J cells. *Diabetes*, **34**(9), 891–897.

Ni, Y.u-L.i, Kuan, A.i-S., & Chen, T.-Y. U. (2014). Activation and inhibition of TMEM16A calcium-activated chloride channels. *PLoS ONE*, **9**(1), e86734.

Okabayashi, Y., Otsuki, M., Ohki, A., Nakamura, T., Tani, S., & Baba, S. (1988). Secretin-induced exocrine secretion in perfused pancreas isolated from diabetic rats. *Diabetes*, **37**(9), 1173–1180.

Okabayashi, Y., Otsuki, M., Ohki, A., Suehiro, I., & Baba, S. (1988). Effect of diabetes mellitus on pancreatic exocrine secretion from isolated perfused pancreas in rats. *Digestive Diseases and Sciences*, **33**(6), 711–717.

Park, H. W., Nam, J. H., Kim, J. Y., Namkung, W., Yoon, J. S., Lee, J.-S., Kim, K. S., Venglovecz, V., Gray, M. A., Kim, K. H., & Lee, M. G. (2010). Dynamic regulation of CFTR bicarbonate permeability by [Cl-]i and its role in pancreatic bicarbonate secretion. *Gastroenterology*, **139**(2), 620–631.

Pascua, P., García, M., Fernández-Salazar, M. P., Hernández-Lorenzo, M. P., Calvo, J. J., Colledge, W. H., Case, R. M., Steward, M. C., & San Román, J. I. (2009). Ducts isolated from the pancreas of CFTR-null mice secrete fluid. *Pflugers Archiv: European Journal of Physiology*, **459**(1), 203–214.

Patel, R., Singh, J., Yago, M. D., Vilchez, J. R., Martínez-Victoria, E., & Mañas, M. (2004). Effect of insulin on exocrine pancreatic secretion in healthy and diabetic anaesthetised rats. *Molecular and Cellular Biochemistry*, **261**(1), 105–110.

Perides, G., Van Acker, G. J.d, Laukkarinen, J. M., & Steer, M. L. (2010). Experimental acute biliary pancreatitis induced by retrograde infusion of bile acids into the mouse pancreatic duct. *Nature Protocols*, **5**(2), 335–341.

Piciucchi, M., Capurso, G., Archibugi, L., Delle Fave, M. M., Capasso, M., & Delle Fave, G. (2015). Exocrine pancreatic insufficiency in diabetic patients: Prevalence, mechanisms, and treatment. *International Journal of Endocrinology*, **2015**, 1.

Radlinger, B., Ramoser, G., & Kaser, S. (2020). Exocrine Pancreatic Insufficiency in Type 1 and Type 2 Diabetes. *Current Diabetes Reports*, **20**(6), 18.

Rodriguez-Calvo, T., Ekwall, O., Amirian, N., Zapardiel-Gonzalo, J., & Von Herrath, M. G. (2014). Increased immune cell infiltration of the exocrine pancreas: A possible contribution to the pathogenesis of type 1 diabetes. *Diabetes*, **63**(11), 3880–3890.

Romanenko, V. G., Catalán, M. A., Brown, D. A., Putzier, I., Hartzell, H. C., Marmorstein, A. D., Gonzalez-Begne, M., Rock, J. R., Harfe, B. D., & Melvin, J. E. (2010). Tmem16A encodes the Ca^{2+}-activated Cl- channel in mouse submandibular salivary gland acinar cells. *Journal of Biological Chemistry*, **285**(17), 12990–13001.

Shcheynikov, N., Wang, Y., Park, M., Ko, S. B. H., Dorwart, M., Naruse, S., Thomas, P. J., & Muallem, S. (2006). Coupling modes and stoichiometry of Cl-/HCO3- exchange by slc26a3 and slc26a6. *Journal of General Physiology*, **127**(5), 511–524.

Siczkowski, M., & Ng, L. L. (1996). Glucose-induced changes in activity and phosphorylation of the Na^+/H^+ exchanger, NHE-1, in vascular myocytes from Wistar-Kyoto and spontaneously hypertensive rats. *Metabolism*, **45**(1), 114–119.

Thomas, J. A., Buchsbaum, R. N., Zimniak, A., & Racker, E. (1979). Intracellular pH measurements in Ehrlich ascites tumor cells utilizing spectroscopic probes generated in situ. *Biochemistry*, **18**(11), 2210–2218.

Venglovecz, V., Pallagi, P., Kemeny, L. V., Balazs, A., Balla, Z., Becskehazi, E., Gal, E., Toth, E., Zvara, A., Puskas, L. G., Borka, K., Sendler, M., Lerch, M. M., Mayerle, J., Kuhn, J. P., Rakonczay, Z., Jr., & Hegyi, P. (2018). The importance of aquaporin 1 in pancreatitis and its relation to the CFTR Cl(-) channel. *Frontiers in Physiology*, **9**, 854.

Wang, Y., Soyombo, A. A., Shcheynikov, N., Zeng, W., Dorwart, M., Marino, C. R., Thomas, P. J., & Muallem, S. (2006). Slc26a6 regulates CFTR activity in vivo to determine pancreatic duct HCO3- secretion: Relevance to cystic fibrosis. *Embo Journal*, **25**(21), 5049–5057.

Weintraub, W. H., & Machen, T. E. (1989). pH regulation in hepatoma cells: Roles for Na-H exchange, Cl-HCO3 exchange, and Na-HCO3 cotransport. *American Journal of Physiology*, **257**, G317–G327.

Zhang, Y.-C., Xiong, F.-R., Wang, Y.-Y., Shen, H., Zhao, R.u-X., Li, S., Lu, J., & Yang, J.-K. (2022). High bicarbonate concentration increases glucose-induced insulin secretion in pancreatic beta-cells. *Biochemical and Biophysical Research Communications*, **589**, 165–172.

Zsóri, G., Illés, D., Terzin, V., Iványi, E., & Czakó, L. (2018). Exocrine pancreatic insufficiency in type 1 and type 2 diabetes mellitus: Do we need to treat it? A systematic review. *Pancreatology*, **18**(5), 559–565.

Additional information

Data availability statement

All data ($n \leq 30$) supporting the findings of this study the present available within the paper. All other data (>30) are available at online (https://figshare.com/account/items/24899709) or will be made available from the corresponding author upon reasonable request.

Competing interests

The authors declare that they have no competing interests.

Author contributions

A.É. performed all of the experiments and analysed the data. E.G. performed the RT-PCR. E.T. was involved in the pancreatic fluid and HCO_3^- measurements. T.S. performed electron microscopy. P.H. was involved in data interpretation and edited the manuscript. V.V. supervised the project and drafted the manuscript. All authors approved the final version of the manuscript submitted for publication.

Funding

CF-Trust CFRD-SRC: Attila Ébert, Emese Tóth, Péter Hegyi, Viktoria Venglovecz, SRC 007; National Research, Development and Innovation Office: Attila Ébert, Eleonóra Gál, Viktoria Venglovecz, SNN134497

Acknowledgements

We are grateful for support for this study provided by the CF-Trust CFRD-SRC Grant (No.: SRC 007) and the National Research, Development and Innovation Office (SNN134497) and New National Excellence Program Of The Ministry Of Human Capacities (UNKP-18-4 to VV).

Keywords

CFTR, diabetes, endocrine-exocrine interaction, fluid and HCO_3^- secretion, pancreatic ductal cells, secretin

Supporting information

Additional supporting information can be found online in the Supporting Information section at the end of the HTML view of the article. Supporting information files available:

Peer Review History

II.

frontiers in Physiology

METHODS
published: 24 July 2019
doi: 10.3389/fphys.2019.00938

A Novel *in situ* Approach to Studying Pancreatic Ducts in Mice

Eleonóra Gál[1†], *Jurij Dolenšek*[2,3†], *Andraž Stožer*[2†], *Viljem Pohorec*[2], *Attila Ébert*[1] and *Viktória Venglovecz*[1*]

[1] Department of Pharmacology and Pharmacotherapy, University of Szeged, Szeged, Hungary, [2] Faculty of Medicine, University of Maribor, Maribor, Slovenia, [3] Faculty of Natural Sciences and Mathematics, University of Maribor, Maribor, Slovenia

Introduction: The tissue slice technique offers several benefits compared to isolated cells and cell clusters that help us understand the (patho)physiology of several organs *in situ*. The most prominent features are preserved architecture and function, with intact homotypic and heterotypic interactions between cells in slices. In the pancreas, this technique has been utilized successfully to study acinar and endocrine islet cells. However, it has never been used to investigate ductal function. Since pancreatic ductal epithelial cells (PDECs) play an essential role in the physiology of the pancreas, our aim was to use this technique to study PDEC structure and function *in situ*.

Materials and methods: Eight- to sixteen weeks old C57BL/6 mice were used for preparation of pancreas tissue slices. Low melting point agarose was injected into the common bile duct and the whole organ was extracted. For morphological studies, pieces of tissue were embedded in agarose and cryosectioned to obtain 15 μm thick slices. In order to visualize pancreatic ducts, (i) the Giemsa dye was added to the agarose and visualized using light microscopy or (ii) immunostaining for the cystic fibrosis transmembrane conductance regulator (CFTR) was performed. For functional characterization, agarose-embedded tissue was immediately cut to 140 μm thick tissue slices that were loaded with the cell permeant form of the Oregon Green 488 BAPTA-1 dye and used for confocal calcium imaging.

Results: Giemsa staining has shown that the injected agarose reaches the head and body of the pancreas to a greater extent than the tail, without disrupting the tissue architecture. Strong CFTR expression was detected at the apical membranes of PDECs and acinar cells, whereas islet cells were completely negative for CFTR. Stimulation with chenodeoxycholic acid (CDCA, 1 mM) resulted in a robust transient increase in intracellular calcium concentration that was readily visible in >40 ductal cells per slice.

Conclusion: Our results confirm that the acutely-isolated pancreas tissue slice technique is suitable for structural and functional investigation of PDECs and their relationship with other cell types, such as acini and endocrine cells *in situ*. In combination with different genetic, pharmacological or dietary approaches it could become a method of choice in the foreseeable future.

Keywords: pancreas, slice, duct, calcium, CFTR, Giemsa, chenodeoxycholic acid

OPEN ACCESS

Edited by:
Pawel Ferdek, Jagiellonian University, Poland

Reviewed by:
Alexei Tepikin, University of Liverpool, United Kingdom
Shuang Peng, Jinan University, China

***Correspondence:**
Viktória Venglovecz
venglovecz.viktoria@med.u-szeged.hu

† These authors have contributed equally to this work

Specialty section:
This article was submitted to Gastrointestinal Sciences, a section of the journal Frontiers in Physiology

Received: *30 April 2019*
Accepted: *09 July 2019*
Published: *24 July 2019*

Citation:
Gál E, Dolenšek J, Stožer A, Pohorec V, Ébert A and Venglovecz V (2019) A Novel in situ Approach to Studying Pancreatic Ducts in Mice. Front. Physiol. 10:938. doi: 10.3389/fphys.2019.00938

INTRODUCTION

The tissue slice technique is a suitable *in situ* experimental system for investigating structure and function of different tissues, such as the brain, liver, adrenal gland, and retina (Skrede and Westgaard, 1971; Moser and Neher, 1997; Enoki et al., 2006; Graaf et al., 2007). Speier et al. applied and optimized this technique to study pancreatic beta cell function (Speier and Rupnik, 2003). Since then, it was successfully used to study the functional organization and calcium dynamics of beta cells within islets (Dolenšek et al., 2013; Stožer et al., 2013a,b). The technique has also been applied to characterize acinar cell morphology and secretory function (Marciniak et al., 2013, 2014; Liang et al., 2017). Although there are several *in vitro* approaches for the isolation of both islets and acini from the pancreas, importantly, the greatest advantages of tissue slice preparation technique is that it does not require enzymatic digestion and the architecture and viability of the cells are retained in an intact, nearly physiological environment. It is also important to emphasize that this technique is suitable for both morphological and functional imaging, as well as for electrophysiological studies and investigating interactions between neighboring cells or between the exocrine and endocrine part of the pancreas (Marciniak et al., 2013; Klemen et al., 2014).

Basically, there are two major cell types in the exocrine pancreas, the acinar cells and the pancreatic ductal epithelial cells (PDECs). Although PDECs comprise only a very small fraction of the entire organ, they play an essential role in maintaining the integrity of the pancreas. PDECs secrete an HCO_3^--rich, alkaline solution that neutralizes the acidic pH of gastric juice, curtails premature trypsinogen activation, and delivers digestive enzymes from the pancreas to the small intestine (Argent Be, 1994; Argent, 2006; Dolensek et al., 2017). Insufficient or decreased HCO_3^--secretion can lead to cystic fibrosis or trigger acute or chronic pancreatitis (Scheele et al., 1996; Venglovecz et al., 2008, 2011; Hegyi and Rakonczay, 2010). Therefore, intensive research has been conducted to characterize the ductal function both under physiological and pathophysiological conditions (Hegyi et al., 2011; Judák et al., 2014; Katona et al., 2016; Venglovecz et al., 2018). In the 80's, Barry Argent and his colleagues worked out a novel technique that allows the isolation of intact intra-interlobular pancreatic ducts from the pancreas of rodents (Argent et al., 1986). This methodological development was a very important milestone in the physiology of the pancreas, since it pointed out that ductal cells not only provide a framework for acini, but also secrete HCO_3^-. However, this technique has many limitations. Ducts are isolated from the pancreas after an enzymatic digestion that may result in functional changes. The isolation procedure is long and the ducts should be incubated overnight in order to facilitate their regeneration, similarly to isolation and cultivation of islets of Langerhans, which can importantly affect their function (Gilon et al., 1994). In addition, the biggest disadvantage of this technique is that the ductal cells are isolated from their normal environment and, therefore not influenced by other cell types, which can fundamentally support and influence their function. We strongly believe that the pancreas slice preparation is much closer to the physiological conditions than the duct isolation technique and therefore provides a better experimental model to study the function of PDECs both under physiological and pathophysiological conditions.

Our aim in this study was to use the acutely-isolated pancreas tissue slice technique for the morphological and functional investigation of PDECs. We have shown that the ductal cells preserve their viability after the preparation and that the technique is suitable for functional multicellular calcium imaging.

Abbreviations: CDCA, chenodeoxycholic acid; CFTR, cystic fibrosis transmembrane conductance regulator; ECS, extracellular solution; OGB-1, Oregon Green 488 BAPTA-1; PDECs, pancreatic ductal epithelial cells.

MATERIALS AND METHODS

Ethical Approval

Animal experiments were conducted in compliance with the *Guide for the Care and Use of Laboratory Animals* (United States, Department of Health and Human Services, NIH publication No 85-23, revised 1985) and the experimental protocol was approved by the local Ethical Board of the University of Szeged, the National Scientific Ethical Committee on Animal Experimentation (Budapest, Hungary), and the Veterinary administration of the Republic of Slovenia (permit number: U34401-12/2015/3).

Chemicals and Solutions

Cystic fibrosis transmembrane conductance regulator (CFTR) human, polyclonal antibody was ordered from Alomone Labs (Jerusalem, Israel). Alexa Fluor Goat Anti-Rabbit IgG secondary antibody was obtained from Abcam (Cambridge, UK). Cell permeant acetoxymethyl ester of Oregon Green 488 BAPTA-1 (OGB-1) was from Invitrogen (Eugene, OR, USA). All other laboratory chemicals were ordered from Sigma-Aldrich Kft. (Budapest, Hungary). Extracellular solution (ECS) contained (in mM): 125 NaCl, 2.5 KCl, 26 $NaHCO_3$, 1.25 NaH_2PO_4, 6 glucose, 6 lactic acid, 3 myo-inositol, 0.5 ascorbic acid, 2 Na-pyruvate, 1 $MgCl_2$, and 2 $CaCl_2$. ECS was gassed with 95% O_2/5% CO_2 to set pH to 7.4. For calcium dye loading, we used a HEPES-buffered solution containing (in mM): 150 NaCl, 10 HEPES, 6 glucose, 5 KCl, 2 $CaCl_2$, 1 $MgCl_2$; titrated to pH = 7.4 using 1 M NaOH. For stimulation of PDECs during confocal imaging, we used 1 mM chenodeoxycholic acid (CDCA) dissolved in ECS.

Preparation of Pancreas Tissue Slices

Eight- to Sixteen weeks old C57BL/6 mice of either sex were used. Preparation of acutely-isolated pancreas tissue slices has been described in detail previously (Speier and Rupnik, 2003; Stožer et al., 2013a; Marciniak et al., 2014). Briefly, after sacrificing the animal, the abdomen was accessed via median laparatomy, the papilla of Vater clamped distally and 1.5–2.5 ml of low-melting-point agarose (1.5–1.8%, with or without Giemsa dye, according to protocol) was injected into the common bile duct using 30 G needles. The injected pancreas was then cooled with

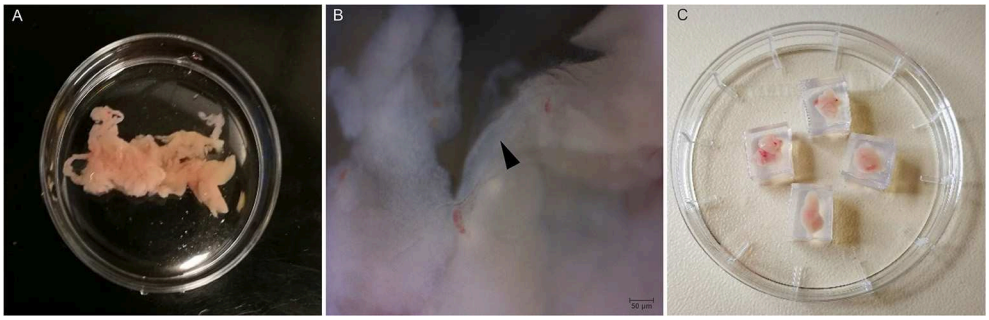

FIGURE 1 | Preparation of pancreas slices. **(A)** Mouse pancreas after injection with agarose. **(B)** Higher magnification (40X) of the isolated pancreas with an intralobular duct (black arrow head). **(C)** Pancreas tissue pieces embedded in agarose cubes.

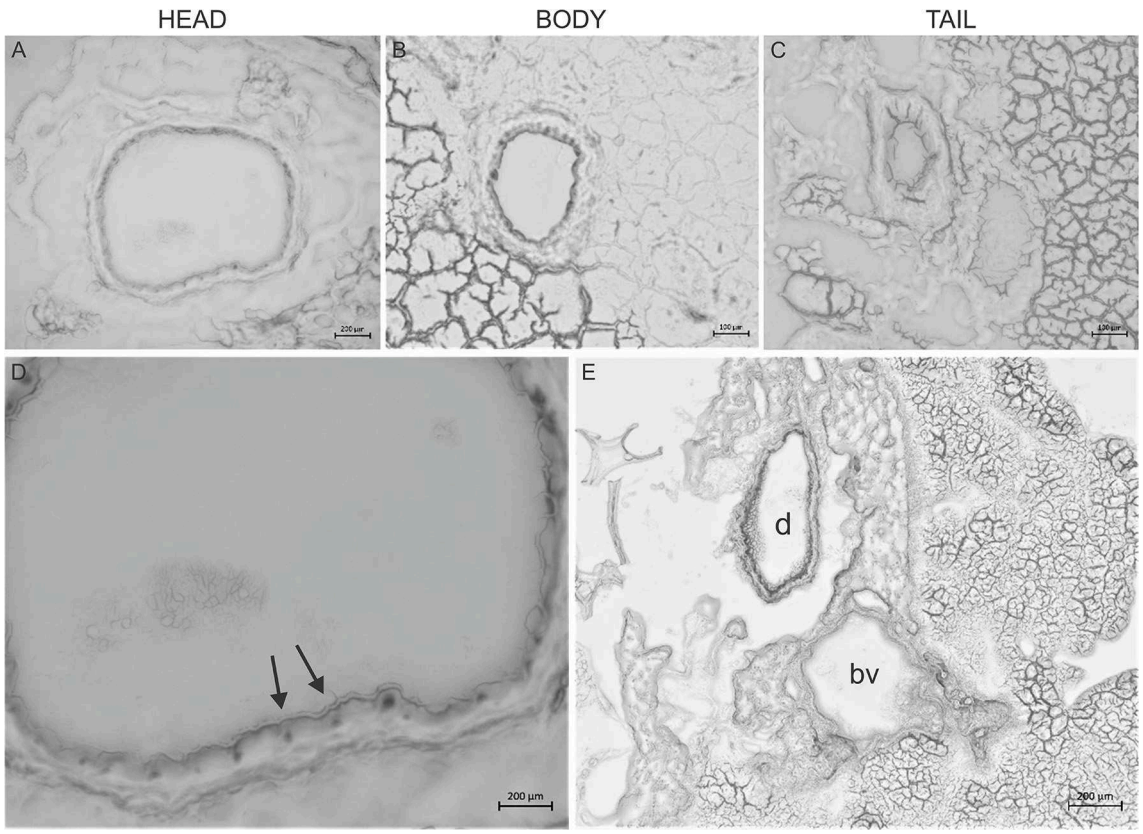

FIGURE 2 | Giemsa staining of the pancreas. Representative cryosections were cut from the head **(A)**, body **(B)**, and tail **(C)** of the pancreas. Giemsa stain causes dark coloring of the nuclei of inter-intralobular ducts in the head and body of the pancreas and slightly in the tail. **(D)** Magnified picture of **(A)**. Arrows indicate dark coloring of the nuclei. **(E)** Representative cryosection from the head of the pancreas shows that Giemsa stained the duct (d) but not the blood vessels (bv).

ice-cold ECS and transferred into a sterile Petri dish containing ice-cold ECS (**Figure 1A**). Higher magnification image of the gland shows the presence of an interlobular duct (**Figure 1B**). In the next step, the pancreas was cleaned from fat and connective tissue, and cut into small pieces (0.25–1.0 cm^3 in size) using surgical scissors. Individual pieces of agarose-injected pancreas were embedded in agarose (1.5–1.8%) (**Figure 1C**) and further sectioned either for immunohistochemistry (IHC) or for calcium imaging. For IHC, the isolated tissue was further embedded in cryomatrix and cut into 15 µm sections using a CM1800 cryostat (Leica Biosystems, Wetzlar, Germany). For calcium imaging, 140 µm thick sections were cut using a VT1000 vibratome (Leica Biosystems, Wetzlar, Germany) while the tissue was continuously buffered with ice-cold gassed ECS. Thirty to forty slices were prepared per animal and used immediately for staining.

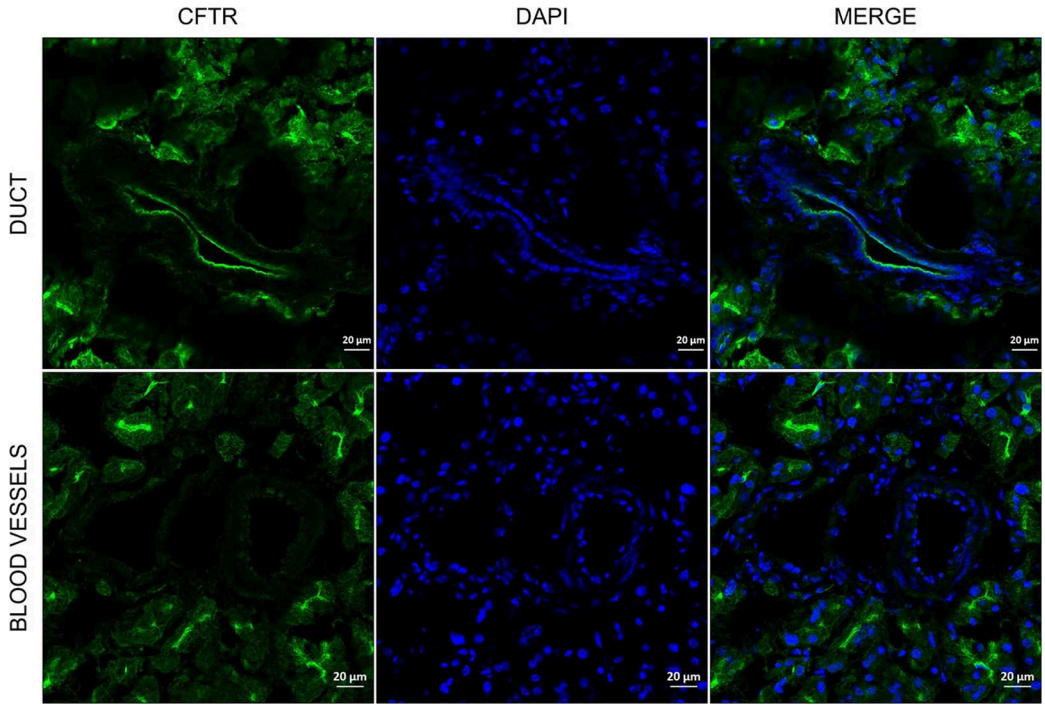

FIGURE 3 | Representative immunofluorescence staining of CFTR in agarose-injected mice pancreas. Pictures were taken at 20X magnification.

Immunohistochemistry

The cryosections were fixed in 4% (v/v) paraformaldehyde for 20 min at room temperature (RT) and washed in PBS 2–3 times. Slices were permeabilized with 0.05% TritonX-100 at RT for 30 min and blocked with the mixture of 1% (v/v) bovine serum albumin/Tris-buffered saline (BSA/TBS) and 10% (v/v) goat serum for 30 min. After the blocking step, slices were incubated with the CFTR rabbit polyclonal antibody (1:100 dilutions) at 4°C, overnight. After the incubation, slices were washed 2–3 times with PBS and incubated with Alexa fluor 488-conjugated goat anti-rabbit IgG secondary antibody (1:400 dilutions) for 3 h at RT. Nuclei were stained with DAPI (1:500 dilutions in BSA/TBS) for 15 min, followed by washing three times in PBS. Slices were mounted using Fluoromount and analyzed using a LSM 880 confocal laser scanning microscope (Carl Zeiss Technika Kft., Budaörs, Hungary). Pancreas slices were excited at 405 (Dapi) and 488 (Alexa fluor 488) nm and emissions were collected at 453 and 516 nm, respectively.

Giemsa Staining

Giemsa was diluted in low-melting-point agarose (1.5%) at a ratio of 1:10, then injected into the common bile duct of the mice as described in the Preparation of Pancreas Tissue Slices section. After the injection, the pancreas was removed cleaned and cut into three pieces (head, body, and tail). Each pieces of the pancreas were then embedded into cryomatrix and cut into 15 µm sections using a CM1800 cryostat (Leica Biosystems, Wetzlar, Germany) and Giemsa staining was analyzed using an Axio Scope.A1 light microscope (Carl Zeiss Technika Kft., Budaörs, Hungary).

Calcium Imaging

Ten to fifteen slices were incubated in dye-loading solution containing 6 µM of OGB-1, 0.03% Pluronic F-127 (w/v) and 0.12% dimethylsulphoxide (DMSO, v/v, dissolved in HEPES-buffered solution) for 50 min at RT on an orbital shaker (50 turns min^{-1}). Imaging was made within 12 h after staining. Following staining, slices were kept protected from light in a dye-free HEPES-buffered solution, which was exchanged every 2 h. Individual slices were transferred into the recording chamber of either a Leica TCS SP5 II inverted confocal system [Leica HCX PL APO CS 20x immersion objective (NA = 0.7)] or an upright Leica TCS SP5 II confocal system [Leica HCX APO L water immersion objective (20x, NA = 1.0)]. Slices were continuously perfused with gassed ECS at 37°C. OGB-1 was excited by an argon 488 nm laser and fluorescence detected by Leica HyD hybrid detector in the range of 500–650 nm. Eight-bit 512 × 512 pixels images at 1 frame per second were acquired. CDCA stimulation was achieved by manually exchanging delivery tubes of the perifusion system.

RESULTS

Visualization of Pancreatic Ducts in Freshly Prepared Slices

In order to investigate how deep, the agarose penetrates into the ductal tree, Giemsa dye was added to the low melting point agarose (1.5%) in 1:10 dilutions and injected into the

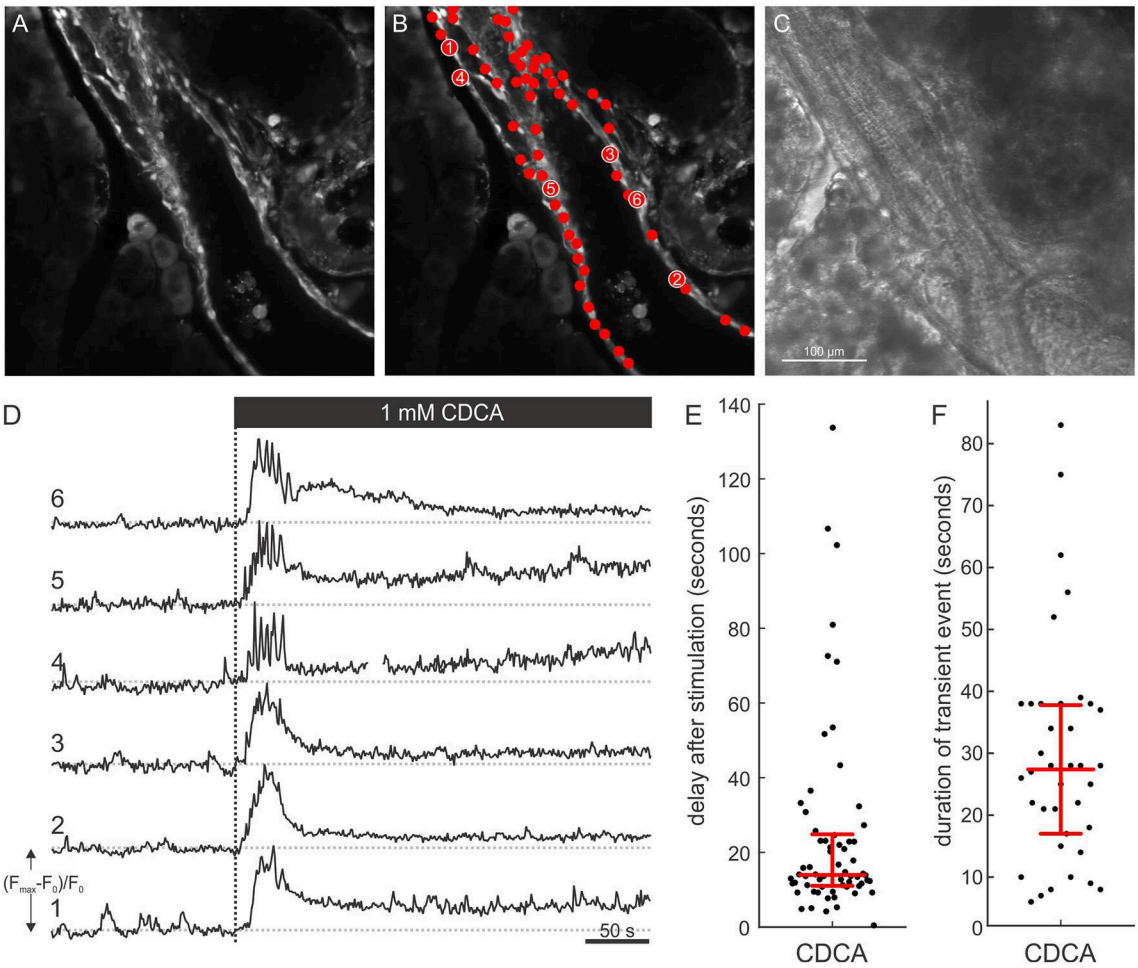

FIGURE 4 | $[Ca^{2+}]_i$ response in ductal cells after stimulation with 1 mM CDCA. **(A)** Confocal fluorescence image of a ductal structure and surrounding acinar tissue with selected regions of interest (ROI) denoting nuclei of individual PDECs. **(B)** Chenodeoxycholic acid (CDCA) induced $[Ca^{2+}]_i$ responses of individual cells corresponding to numbered ROIs in **(B)** (1–6). **(C)** Concurrent transmitted light image. **(D)** Dashed vertical line indicates the start of exposure to 1 mM CDCA. **(E,F)** Bee swarm plots with interquartile ranges and medians for delays of responses after stimulation with 1 mM CDCA ($n = 65$ cells from 4 slices) **(E)** and durations of transient $[Ca^{2+}]_i$ events ($n = 38$ cells from 4 slices) **(F)**.

main pancreatic duct, as described in section Materials and Methods. Freshly prepared pancreas slices of 15 µm thickness from the head, body, and the tail were examined under a stereomicroscope. **Figure 2** shows representative tissue slices with intact pancreas morphology and visible structures of exocrine and endocrine cells. Strong nuclei staining was detected in the intra- and inter-lobular ducts of the head (**Figures 2A,B**) and the body of the pancreas (**Figure 2C**), whereas only weak staining was found in the tail part (**Figure 2D**). Blood vessels were completely negative (**Figure 2E**), indicating that the injection affects only the ductal tree. Using CFTR immunostaining, we were able to identify more specifically the ductal cells in the tissue slices. Under normal conditions, CFTR channel is expressed at the apical membrane of the ductal cells. As shown on **Figure 3**, strong CFTR staining was detected at the apical membrane of PDECs and acini, whereas islet cells and blood vessels were completely negative for CFTR.

CDCA Stimulation Induced a Transient Change in Intracellular Calcium Concentration

To functionally characterize ductal-like structures, we resorted to confocal calcium imaging. Under non-stimulatory conditions, PDECs were brightly stained with OGB-1. Moreover, the dye accumulated in the nuclei producing a typical visual pattern of a mono-layered epithelium (**Figures 4A–C** and **Supplemental Video 1**). The tissue slice technique also enables simultaneous visualization of exocrine acinar cells and islets of Langerhans (**Supplemental Figure 1** and **Supplemental Video 1**). Moreover, calcium activity could be recorded from acinar cells in parallel with PDEC activity, whereas the islets of Langerhans did not respond to the stimulus used in this study (**Supplemental Figure 2**). We stimulated the PDECs using a square pulse-like protocol in which the tissue slices were initially perifused with ECS only, followed by

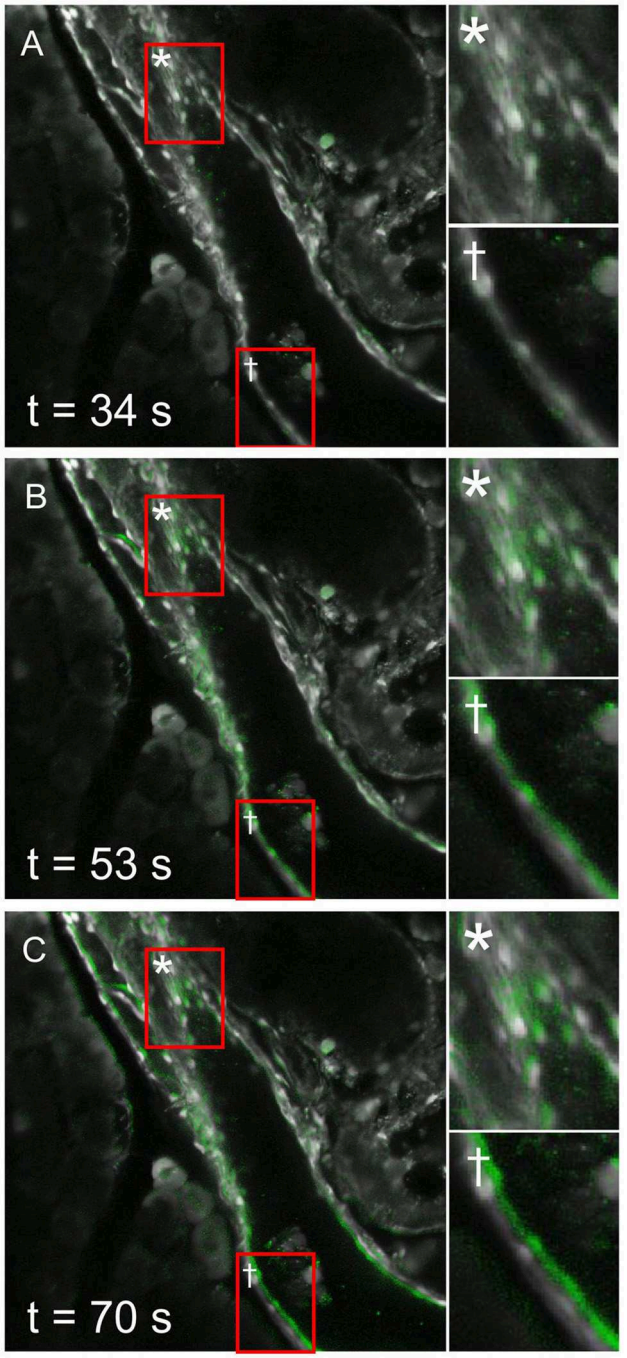

FIGURE 5 | Spatial displacement of ductal cells after stimulation with 1 mM CDCA. An intralobular duct is shown before **(A)** and during **(B,C)** the stimulation with chenodeoxycholic acid (CDCA). Constructs depicting early **(B)** and late **(C)** $[Ca^{2+}]_i$ response to CDCA display a background of cellular morphology in gray, and an overlay of calcium response in green (see Results section for detailed description). In some PDECs no spatial movement was detected (insets *), whereas in some cells noticeable spatial displacements were observed (insets †). Please note that in the PDECs that were displaced during CDCA response, change in $[Ca^{2+}]_i$ preceded the spatial displacement, therefore not interfering with the calcium response detection.

ECS containing 1 mM CDCA for 10 min. CDCA stimulation evoked a response that was detected in many cells within a single visual field (**Figure 4B**). Individual PDECs responded with a transient increase in $[Ca^{2+}]_i$, followed by a decrease in $[Ca^{2+}]_i$ to a sustained plateau (**Figure 4D**). The median response delay to CDCA stimulation was 14.0 s (Q1 = 11.0 s and Q3 = 24.8 s, **Figure 4E**) and the median duration of the transient change in $[Ca^{2+}]_i$ was 27.5 s (Q1 = 17.0 s and Q3 = 38.0 s, **Figure 4F**).

Coupled with the calcium response, a spatial displacement of PDECs was observed upon stimulation with CDCA (**Figure 5**). In order to exclude the possibility that the detected $[Ca^{2+}]_i$ signal in response to CDCA stimulation was an artifact of cell displacement, we meticulously characterized the movement and compared it with the $[Ca^{2+}]_i$ signal. The calcium response was calculated as $Fresp\,(t) = F(t) - F_0$, where $Fresp\,(t)$ presents the calculated calcium response at time t, F_0 the average of the first 100 frames under non-stimulatory conditions and $F\,(t)$ the calcium signal at time t. A construct was created in which the F_0 frame was displayed in grayscale and $Fresp\,(t)$ was overlaid in green (**Figure 5** and **Supplemental Video 2**). **Figure 5** shows this construct before CDCA stimulation (**Figure 5A**), as well as the immediate (**Figure 5B**) and late response to CDCA (**Figure 5C**). The initial increase in $[Ca^{2+}]_i$ was coupled with either no (**Figure 5B**, inset *) or minimal (**Figure 5B**, inset †) spatial movement. In contrast, later during the calcium response, some cells failed to display the spatial displacement (**Figure 5C**, inset *), whereas others profoundly changed their location (**Figure 5C**, inset †). The facts that (i) the $[Ca^{2+}]_i$ increase preceded the spatial displacement, and that (ii) $[Ca^{2+}]_i$ transients, similar to the ones in PDECs that did not displace, were recorded from all PDECs that underwent displacement, strongly substantiate that the observed $[Ca^{2+}]_i$ signals are not a motion artifact.

DISCUSSION

We successfully applied the tissue slice preparation technique to study PDECs. The main hallmark of the tissue slice approach, especially in contrast to the majority of studies that were done by isolating ducts using enzymes, is that the homotypic as well as heterotypic interactions are preserved. Histological and functional evaluations of the slices have shown that the slicing procedure did not damage the structure or the function of the tissue indicating that this technique represent an excellent *in situ* model in which the function and the cell-cell interactions of PDECs can be investigated.

For the study of pancreatic acini and islets, the thickness of the tissue slices is critical. The ideal thickness is 100–200 μm, depending on the use of the slice (Marciniak et al., 2014). For the functional cell imaging of PDECs, we found that a practically useful thickness of the slices is 140 μm, enabling the calcium dye to penetrate the cells and allowing for preservation of morphological tissue structure at the same time. Moreover, this thickness allowed for diffusion of gases

and nutrients into the tissue. Tissue slices could be maintained for >8 h in HEPES-buffered solution at RT, however, for even longer studies optimization of the culturing media and use of culture incubators might be needed. One of the critical steps in the preparation of the slices was the injection of agarose. Since pancreas is a "soft" type tissue, injection of agarose serves as a scaffold that stabilized the tissue during cutting. The scaffold effect was achieved by injecting low-melting point agarose at 37°C into the common bile duct, filling the ductal tree retrogradely. Our results have shown that agarose reaches the head and the body of the pancreas and to a smaller extent the tail. We found that the injection procedure did not affect the function or the structure of the ductal cells as confirmed by the histological and functional investigations. Preservation of the intact epithelium has also been confirmed by the fact that the presence of the epithelial-specific ion channel, CFTR, could be detected on the apical membrane of the ductal cells.

Normal calcium signaling plays a central role in the physiological regulation of HCO_3^- secretion by PDECs which is important for neutralization of protons secreted by acinar cells, as well as for keeping trypsinogen in an inactive form and washing it away. Pathologically changed calcium signals, through calcium overload of PEDCs, decreased ATP production due to mitochondrial damage, and impaired HCO_3^- secretion seem to importantly contribute to pathogenesis of acute and chronic pancreatitis (Lee and Muallem, 2008). The toxic calcium signals may be an interesting therapeutic target and thus models that enable studies of PDECs function in normal and pathological conditions are of great practical relevance (Hegyi and Petersen, 2013; Maléth and Hegyi, 2014). To the best of our knowledge, there is only one previous study that analyzed calcium signals in response to bile acids in PDECs. In guinea pig intra-interlobular ducts, low concentration of CDCA, i.e., 0.1 mM, elicited regenerative calcium oscillations that lasted 2–5 min and at this concentration, HCO_3^- secretion was significantly stimulated (Venglovecz et al., 2008). This concentration corresponds with concentrations of taurolithocholic acid sulfate (TLC-S) that elicited calcium responses in the majority of mouse acinar cells. Interestingly, the calcium response in acinar cells was qualitatively very similar to the one in guinea pig PDECs (Voronina et al., 2002). In contrast, 1 mM CDCA produced a transient increase in $[Ca^{2+}]_i$ lasting approximately 5 min, followed by a sustained plateau that returned to the baseline upon termination of stimulation. At this concentration, HCO_3^- secretion was strongly inhibited (Venglovecz et al., 2008). High concentration of TLC-S (0.5 mM) caused a qualitatively very similar response in $[Ca^{2+}]_i$ in mouse acinar cells (Voronina et al., 2002). An important difference in the calcium response between the primary tissue and the slice preparation is that the transient was approximately an order of magnitude shorter (i.e., lasting about 30 s) in the case of slices. Also, in contrast to the behavior in acinar cells, the calcium signals did not seem to be synchronized between different PDECs (Petersen and Findlay, 1987). It needs to be pointed out however, that during supraphysiologically high $[Ca^{2+}]_i$ also acinar cells may be uncoupled (Hegyi and Petersen, 2013). In future studies, the dose dependence of calcium responses in PDECs needs to be studied into more detail and the slice preparation offers the possibility to simultaneously study the responses of acinar cells. In addition, the specific composition of mouse bile should be taken into account and different bile acids tested for their potential to produce regenerative or sustained calcium responses (Sayin et al., 2013). This shall enable us to assess whether the observed quantitative differences are due to different methodological approaches or due to inter-species differences in responses to bile acids, depending on the relevance of a given bile acid in a given species. Most importantly, a more detailed description of normal and pathological calcium signals in mouse PDECs can help us better understand the etiopathogenesis of pancreatitis and find new therapeutic targets.

An especially interesting observation in this study was that following the CDCA stimulation, we recorded movement of PDECs, a property of PDECs not shown before (**Figure 5**). This active PDEC movement was not uniformly detected in all the cells, moreover it was preceded by the $[Ca^{2+}]_i$ increase, confirming that the recorded $[Ca^{2+}]_i$ signal was not an artifact of this movement. It is not clear what is the mechanism causing the movement of PDECs following CDCA stimulation. A change in osmolality of the local milieu due to the stimulated HCO_3^- secretion may result in an osmotically driven movement. However, we believe this not to be the case since (i) 1 mM CDCA more likely inhibits than stimulates HCO_3^- secretion (Venglovecz et al., 2008), and (ii) the shape of the PDECs as well as of the surrounding acinar cells remained unaffected. More likely, myoepithelial cells in the ducts could provide a mechanistic substrate for active contraction (Puchtler et al., 1975). Therefore, further experiments will be needed to resolve this issue.

In conclusion, we have successfully applied the tissue slice preparation in which the structure and function of PDECs are preserved. This model represents an *in situ* microenvironment that enables studying PDECs under both physiological and pathophysiological conditions and their interaction with the acinar or endocrine cells. This model also opens up the possibilities to investigate human pancreatic function in an intact, *in vivo*-like environment.

DATA AVAILABILITY

All datasets generated for this study are included in the manuscript and/or the **Supplementary Files**.

ETHICS STATEMENT

Animal experiments were conducted in compliance with the Guide for the Care and Use of Laboratory Animals (United States, Department of Health and Human Services, NIH publication No 85-23, revised 1985) and the experimental protocol was approved by the local Ethical Board of the University of Szeged, the National Scientific Ethical Committee on Animal Experimentation (Budapest, Hungary), and the Veterinary

administration of the Republic of Slovenia (permit number: U34401-12/2015/3).

AUTHOR CONTRIBUTIONS

EG was involved in all of the experiments and performed the Giemsa and CFTR staining. JD, AS, and VP performed the calcium imaging, analyzed and interpreted the data, and drafted and edited the manuscript. AÉ was involved in the Giemsa and CFTR staining. VV supervised the project and drafted the manuscript. All authors approved the final version of the manuscript.

FUNDING

This study was supported by the National Research, Development and Innovation Office (FK123982), the Economic Development and Innovation Operative Programme Grants (GINOP-2.3.2-15-2016-00015), the National Research, Development and Innovation Office, by the Ministry of Human Capacities (EFOP 3.6.2-16-2017-00006), by Bolyai Postdoctoral Fellowship of the Hungarian Academy of Sciences (HAS) to VV (00531/11/5), the HAS-USZ Momentum Grant (LP2014-10/2017) and UNKP-18-4 New National Excellence Program Of The Ministry Of Human Capacities, as well as by Slovenian Research Agency Programs I0-0029 and P3-0396, and projects N3-0048, J7-7226, J1-7009, and J3-9289.

SUPPLEMENTARY MATERIAL

The Supplementary Material for this article can be found online at: https://www.frontiersin.org/articles/10.3389/fphys.2019.00938/full#supplementary-material

Supplemental Video 1 | XYZ-stack of OGB-1 loaded acute tissue slice. Morphology of the intralobular duct can be followed, and surrounding acinar and islet cells can be observed. Please note that the structure of acinar cells, as well as an islet of Langerhans, can also be observed in the XYZ-stack.

Supplemental Video 2 | Video demonstrates construct of confocal time series images (see Results section for detailed description). CDCA stimulation from 3.07 s onwards. Background displays cellular morphology in gray, and an overlay of calcium response is depicted in green. See Results section for interpretation.

Supplemental Figure 1 | OGB-1 loaded acute tissue slice demonstrating that different cells types can be visualized simultaneously. The yellow stars depict exocrine acinar cells, the yellow dashed line depicts the border of a pancreatic duct, and the yellow dashed-dotted line depicts the border of an islet of Langerhans.

Supplemental Figure 2 | (A) OGB-1 loaded tissue slice. **(B)** On the same slice, PDECs responding to 1 mM CDCA (red) and spontaneously active acinar cells (blue) are depicted. Numbers correspond with calcium traces in **(C)**. **(C)** Calcium activity of PDECs during stimulation with 1 mM CDCA (red) and spontaneous activity of acinar cells within the slice shown in **(B)**. Numbers correspond with the labels in **(B)**.

REFERENCES

Argent Be, C. R. (1994). "Pancreatic ducts. Cellular mechanism and control of bicarbonate secretion," in *Physiology of the Gastrointestinal Tract*, ed L. Johnson (New York, NY: Raven Press), 1473–1497.

Argent, B. (2006). "Cell physiology of pancreatic ducts," in *Physiology of the Gastrointestinal Tract, 4th Edn,* ed L. Johnson (San Diego, CA: Elsevier), 1376–1396. doi: 10.1016/B978-012088394-3/50057-X

Argent, B. E., Arkle, S., Cullen, M. J., and Green, R. (1986). Morphological, biochemical and secretory studies on rat pancreatic ducts maintained in tissue culture. *Q. J. Exp. Physiol.* 71, 633–648. doi: 10.1113/expphysiol.1986.sp003023

Dolensek, J., Poherec, V., Rupnik, M. S., and Stozer, A. (2017). "Pancreas Physiology," in *Challenges in Pancreatic Pathology*, ed A. Seicean (Romania: IntechOpen), 19–52. doi: 10.5772/65895

Dolenšek, J., Stozer, A., Skelin Klemen, M., Miller, E. W., and Slak Rupnik, M. (2013). The relationship between membrane potential and calcium dynamics in glucose-stimulated beta cell syncytium in acute mouse pancreas tissue slices. *PLoS ONE* 8:e82374. doi: 10.1371/journal.pone.0082374

Enoki, R., Jakobs, T. C., and Koizumi, A. (2006). Horizontal slice preparation of the retina. *J. Vis. Exp.* e108. doi: 10.3791/108

Gilon, P., Jonas, J. C., and Henquin, J. C. (1994). Culture duration and conditions affect the oscillations of cytoplasmic calcium concentration induced by glucose in mouse pancreatic islets. *Diabetologia* 37, 1007–1014. doi: 10.1007/BF00400464

Graaf, I. A., Groothuis, G. M., and Olinga, P. (2007). Precision-cut tissue slices as a tool to predict metabolism of novel drugs. *Expert Opin. Drug Metab. Toxicol.* 3, 879–898. doi: 10.1517/17425255.3.6.879

Hegyi, P., Pandol, S., Venglovecz, V., and Rakonczay, Z. Jr. (2011). The acinar-ductal tango in the pathogenesis of acute pancreatitis. *Gut* 60, 544–552. doi: 10.1136/gut.2010.218461

Hegyi, P., and Petersen, O. H. (2013). The exocrine pancreas: the acinar-ductal tango in physiology and pathophysiology. *Rev. Physiol. Biochem. Pharmacol.* 165, 1–30. doi: 10.1007/112_2013_14

Hegyi, P., and Rakonczay, Z. (2010). Insufficiency of electrolyte and fluid secretion by pancreatic ductal cells leads to increased patient risk for pancreatitis. *Am. J. Gastroenterol.* 105, 2119–2120. doi: 10.1038/ajg.2010.191

Judák, L., Hegyi, P., Rakonczay, Z. Jr., Maleth, J., Gray, M. A., and Venglovecz, V. (2014). Ethanol and its non-oxidative metabolites profoundly inhibit CFTR function in pancreatic epithelial cells which is prevented by ATP supplementation. *Pflugers Arch.* 466, 549–562. doi: 10.1007/s00424-013-1333-x

Katona, M., Hegyi, P., Kui, B., Balla, Z., Rakonczay, Z. Jr., Razga, Z., et al. (2016). A novel, protective role of ursodeoxycholate in bile-induced pancreatic ductal injury. *Am. J. Physiol. Gastrointest. Liver Physiol.* 310, G193–G204. doi: 10.1152/ajpgi.00317.2015

Klemen, M. S., Dolensek, J., Stozer, A., and Rupnik, M. S. (2014). "Measuring exocytosis in endocrine tissue slices," in *Exocytosis Methods. Neuromethods*, ed P. Thorn (Totowa, NJ: Humana Press), 127–146. doi: 10.1007/978-1-62703-676-4_7

Lee, M. G., and Muallem, S. (2008). Pancreatitis: the neglected duct. *Gut* 57, 1037–1039. doi: 10.1136/gut.2008.150961

Liang, T., Dolai, S., Xie, L., Winter, E., Orabi, A. I., Karimian, N., et al. (2017). *Ex vivo* human pancreatic slice preparations offer a valuable model for studying pancreatic exocrine biology. *J. Biol. Chem.* 292, 5957–5969. doi: 10.1074/jbc.M117.777433

Maléth, J., and Hegyi, P. (2014). Calcium signaling in pancreatic ductal epithelial cells: an old friend and a nasty enemy. *Cell Calcium* 55, 337–345. doi: 10.1016/j.ceca.2014.02.004

Marciniak, A., Cohrs, C. M., Tsata, V., Chouinard, J. A., Selck, C., Stertmann, J., et al. (2014). Using pancreas tissue slices for in situ studies of islet of Langerhans and acinar cell biology. *Nat. Protoc.* 9, 2809–2822. doi: 10.1038/nprot.2014.195

Marciniak, A., Selck, C., Friedrich, B., and Speier, S. (2013). Mouse pancreas tissue slice culture facilitates long-term studies of exocrine and endocrine cell physiology *in situ*. *PLoS ONE* 8:e78706. doi: 10.1371/journal.pone.0078706

Moser, T., and Neher, E. (1997). Rapid exocytosis in single chromaffin cells recorded from mouse adrenal slices. *J. Neurosci.* 17, 2314–2323. doi: 10.1523/JNEUROSCI.17-07-02314.1997

Petersen, O. H., and Findlay, I. (1987). Electrophysiology of the pancreas. *Physiol. Rev.* 67, 1054–1116. doi: 10.1152/physrev.1987.67.3.1054

Puchtler, H., Waldrop, F. S., Meloan, S. N., and Branch, B. W. (1975). Myoid fibrils in epithelial cells: studies of intestine, biliary and pancreatic pathways, trachea, bronchi, and testis. *Histochemistry* 44, 105–118. doi: 10.1007/BF00494071

Sayin, S. I., Wahlstrom, A., Felin, J., Jantti, S., Marschall, H. U., Bamberg, K., et al. (2013). Gut microbiota regulates bile acid metabolism by reducing the levels of tauro-beta-muricholic acid, a naturally occurring FXR antagonist. *Cell Metab.* 17, 225–235. doi: 10.1016/j.cmet.2013.01.003

Scheele, G. A., Fukuoka, S. I., Kern, H. F., and Freedman, S. D. (1996). Pancreatic dysfunction in cystic fibrosis occurs as a result of impairments in luminal pH, apical trafficking of zymogen granule membranes, and solubilization of secretory enzymes. *Pancreas* 12, 1–9. doi: 10.1097/00006676-199601000-00001

Skrede, K. K., and Westgaard, R. H. (1971). The transverse hippocampal slice: a well-defined cortical structure maintained *in vitro*. *Brain Res.* 35, 589–593. doi: 10.1016/0006-8993(71)90508-7

Speier, S., and Rupnik, M. (2003). A novel approach to *in situ* characterization of pancreatic beta-cells. *Pflugers Arch.* 446, 553–558. doi: 10.1007/s00424-003-1097-9

Stožer, A., Dolenšek, J., and Rupnik, M. S. (2013a). Glucose-stimulated calcium dynamics in islets of langerhans in acute mouse pancreas tissue slices. *PLoS ONE* 8:e54638. doi: 10.1371/journal.pone.0054638

Stožer, A., Gosak, M., Dolensek, J., Perc, M., Marhl, M., Rupnik, M. S., et al. (2013b). Functional connectivity in islets of Langerhans from mouse pancreas tissue slices. *PLoS Comput. Biol.* 9:e1002923. doi: 10.1371/journal.pcbi.1002923

Venglovecz, V., Hegyi, P., Rakonczay, Z. Jr., Tiszlavicz, L., Nardi, A., Grunnet, M., et al. (2011). Pathophysiological relevance of apical large-conductance Ca2+-activated potassium channels in pancreatic duct epithelial cells. *Gut* 60, 361–369. doi: 10.1136/gut.2010.214213

Venglovecz, V., Pallagi, P., Kemeny, L. V., Balazs, A., Balla, Z., Becskehazi, E., et al. (2018). The importance of aquaporin 1 in pancreatitis and its relation to the CFTR Cl^- channel. *Front. Physiol.* 9:854. doi: 10.3389/fphys.2018.00854

Venglovecz, V., Rakonczay, Z. Jr., Ozsvari, B., Takacs, T., Lonovics, J., Varro, A., et al. (2008). Effects of bile acids on pancreatic ductal bicarbonate secretion in guinea pig. *Gut* 57, 1102–1112. doi: 10.1136/gut.2007.134361

Voronina, S., Longbottom, R., Sutton, R., Petersen, O. H., and Tepikin, A. (2002). Bile acids induce calcium signals in mouse pancreatic acinar cells: implications for bile-induced pancreatic pathology. *J. Physiol. (Lond).* 540, 49–55. doi: 10.1113/jphysiol.2002.017525

Conflict of Interest Statement: The authors declare that the research was conducted in the absence of any commercial or financial relationships that could be construed as a potential conflict of interest.

Co-author certification

I, myself as a corresponding author of the following publication(s) declare that the authors have no conflict of interest, and Attila Ébert Ph.D. candidate had significant contribution to the jointly published research(es). The results discussed in her thesis were not used and not intended to be used in any other qualification process for obtaining a PhD degree.

05.24.2024

Viktoria Venglovecz
Corresponding author

The publication(s) relevant to the applicant's thesis:

Gál E., Dolensek J., Stozer A., Pohorec V., Ébert A., Venglovecz V. A Novel in situ Approach to Studying Pancreatic Ducts in Mice. Front Physiol. 2019;10:938. doi: 10.3389/fphys.2019.00938.

MTMT number: 30769527